

Université de Montréal

**Une nouvelle approche pour l'identification des états
dynamiques de la parcellisation fonctionnelle cérébrale
individuelle**

par

Amal Boukhdhir

Département d'informatique et de recherche opérationnelle
Faculté des arts et des sciences

Thèse présentée en vue de l'obtention du grade de
Philosophiæ Doctor (Ph.D.)
en Informatique

July 28, 2021

Université de Montréal

Faculté des arts et des sciences

Cette thèse intitulée

Une nouvelle approche pour l'identification des états dynamiques de la parcellisation fonctionnelle cérébrale individuelle

présentée par

Amal Boukhdhir

a été évaluée par un jury composé des personnes suivantes :

Irina Rish

(président-rapporteur)

Max Mignotte

(directeur de recherche)

Pierre Bellec

(codirecteur)

Karim Jerbi

(membre du jury)

Catie Chang

(examineur externe)

Jacques Bélair

(représentant du doyen de la FESP)

Résumé

Les parcellations cérébrales sont appliquées en neuroimagerie pour aider les chercheurs à réduire la haute dimensionnalité des données d'IRM fonctionnelle. L'objectif principal est une meilleure compréhension de l'organisation fonctionnelle du cerveau tant chez les sujets sains que chez les sujets souffrant de troubles neurologiques, dont la maladie d'Alzheimer. Malgré la vague d'approches de parcellations précédentes, les mesures de performance doivent encore être améliorées pour générer des parcellations fiables, même avec de longues acquisitions. Autrement dit, une reproductibilité plus élevée qui permet aux chercheurs de reproduire des parcellations et de comparer leurs études. Il est également important de minimiser la perte d'informations entre les données compressées et les données brutes pour représenter avec précision l'organisation d'un cerveau individuel. Dans cette thèse, j'ai développé une nouvelle approche pour parcellaire le cerveau en reconfigurations spatiales distinctes appelées «états dynamiques de parcellations». J'ai utilisé une méthode d'agrégation de cluster simple DYPAC1.0 de parcelles basées sur des semences sur plusieurs fenêtres de temps. J'ai émis l'hypothèse que cette nouvelle façon de formaliser le problème de parcellisation améliorera les mesures de performance par rapport aux parcellations statiques. Le premier chapitre de ce document est une introduction générale au contexte des réseaux à grande échelle du cerveau humain. Je montre également l'importance des parcellations pour une meilleure compréhension du cerveau humain à l'aide de connectomes fonctionnels afin de prédire les schémas de progression de la maladie. Ensuite, j'explique pourquoi le problème de parcellisation cérébrale est difficile et les différentes questions de recherche ouvertes associées à ce domaine. Mes contributions à la recherche sont subdivisées en deux articles. Les deuxième et troisième chapitres sont consacrés au premier article principal et à son supplément publié dans Network Neuroscience Journal. Le quatrième chapitre représente le deuxième document en préparation. Le cinquième chapitre conclut mes contributions et ses implications dans le domaine de la neuroimagerie, ainsi que des orientations de recherche ouvertes. En un mot, la principale conclusion de ce travail est l'existence de reconfigurations spatiales distinctes dans tout le cerveau avec des scores de reproductibilité presque parfaits sur les données de test-retest (jusqu'à 0,9 coefficient de corrélation de Pearson). Un algorithme d'agrégation

de cluster simple et évolutif appelé DYPAC 1.0 est expliqué pour identifier ces reconfigurations ou «états dynamiques de parcellations» pour des sous-réseaux de départ spécifiques (deuxième chapitre). L'analyse de ces états a montré l'existence d'un répertoire plus riche «d'états dynamiques» dans le cas des cortex hétéromodaux (ex: cortex cingulaire postérieur et cortex cingulaire antérieur dorsal) par rapport aux cortex unimodaux (ex: cortex visuel). En outre, les résultats de l'analyse de reproductibilité ont montré que DYPAC 1.0 a de meilleurs résultats de reproductibilité (en termes de corrélation de Pearson) par rapport aux parcelles statiques (deuxième chapitre). Plusieurs analyses démontrent que DYPAC 1.0 est robuste au choix de ses paramètres (troisième chapitre). Ces résultats et l'évolutivité de DYPAC 1.0 ont motivé une analyse complète du niveau cérébral. Je présente DYPAC 2.0 comme une approche au niveau cérébral complet pour fragmenter le cerveau en «états dynamiques de parcellations». Des reconfigurations spatiales distinctes et se chevauchant ou «états dynamiques» sont identifiées pour différentes régions du cerveau (quatrième chapitre). Ces états ont des scores de compression prometteurs qui montrent une faible perte d'informations entre les cartes de stabilité d'état réduit et les données d'origine dans les cortex cérébraux, c'est-à-dire jusqu'à seulement 20% de perte de la variance expliquée. Cette thèse présente ainsi de nouvelles contributions dans le domaine de la parcellisation fonctionnelle qui pourraient avoir un impact sur la manière dont les chercheurs modélisent les interactions riches et dynamiques entre les réseaux cérébraux dans la santé et la maladie.

Mots clés Imagerie par résonance magnétique fonctionnelle, Analyse spatiale, Régions spécifiques au sujet, États dynamiques, Parcellisation du cerveau entier

Abstract

Brain parcellations are applied in neuroimaging to help researchers reduce the high dimensionality of the functional MRI data. The main objective is a better understanding of the brain functional organization in both healthy subjects and subjects having neurological disorders, including Alzheimer disease. Despite the flurry of previous parcellation approaches, the performance measures still need improvement to generate reliable parcellations even with long acquisitions. That is, a higher reproducibility that allows researchers to replicate parcellations and compare their studies. It is also important to minimize the information loss between the compressed data and the raw data to accurately represent the organization of an individual brain. In this thesis, I developed a new approach to parcellate the brain into distinct spatial reconfigurations called “dynamic states of parcellations”. I used a simple cluster aggregation method DYPAC1.0 of seed based parcels over multiple time windows. I hypothesized this new way to formalize the parcellation problem will improve performance measures over static parcellations. The first chapter of this document is a general context introduction to the human brain large scale networks. I also show the importance of parcellations for a better understanding of the human brain using functional connectomes in order to predict patterns of disease progression. Then, I explain why the brain parcellation problem is hard and the different open research questions associated with this field. My research contributions are subdivided into two papers. The second and the third chapters are dedicated to the first main paper and its supplementary published in Network Neuroscience Journal. The fourth chapter represents the second paper under preparation. The fifth chapter concludes my contributions and its implications in the neuroimaging field, along with open research directions. In a nutshell, the main finding of this work is the existence of distinct spatial reconfigurations throughout the brain with near perfect reproducibility scores across test-retest data (up to .9 Pearson correlation coefficient). A simple and scalable cluster aggregation algorithm called DYPAC 1.0 is explained to identify these reconfigurations or “dynamic states of parcellations” for specific seed subnetworks (second chapter). The analysis of these states showed the existence of a richer repertoire of “dynamic states” in the case of heteromodal cortices (e.g., posterior cingulate cortex and the dorsal anterior cingulate cortex) compared to unimodal cortices (e.g., visual cortex). Also, the reproducibility analysis

results showed that DYPAC 1.0 has better reproducibility results (in terms of Pearson correlation) compared to static parcels (second chapter). Several analyses demonstrate DYPAC 1.0 is robust to the choice of its parameters (third chapter). These findings and the scalability of DYPAC 1.0 motivated a full brain level analysis. I present DYPAC 2.0 as the full brain level approach to parcellate the brain into “dynamic states of parcellations”. Distinct and overlapping spatial reconfigurations or “dynamic states” are identified for different regions throughout the brain (fourth chapter). These states have promising compression scores that show low information loss between the reduced state stability maps and the original data throughout the cerebral cortices, i.e. up to only 20% loss in explained variance. This thesis thus presents new contributions in the functional parcellation field that may impact how researchers model the rich and dynamic interactions between brain networks in health and disease.

Keywords Functional magnetic resonance imaging, Spatial analysis, Subject specific regions, dynamic states, Whole brain parcellation

Contents

Résumé	3
Abstract	5
List of figures	12
List of abbreviations	16
Acknowledgments	18
Chapter 1. Introduction	19
1.1. Rationale	19
1.2. Resting state fMRI and its motivations	20
1.3. Human brain large scale networks	21
1.3.1. History of the brain anatomy	21
1.3.2. Anatomical brain boundaries are different from the functional brain boundaries	22
1.4. Brain regions changes their boundaries over time	23
1.5. Functional brain parcellations	24
1.5.1. Functional brain parcellation reduces the complex brain organization	24
1.5.2. Applications of functional brain parcellations	25
1.5.3. Anatomical parcellations	27
1.5.4. Brain networks are spatially distributed across the brain	28
1.5.5. There is no consensus regarding the number of clusters	29
1.5.6. The functional parcellation algorithms has a high dimensionality in time and space	30
1.6. Thesis objectives	30
1.6.1. First paper objectives	30
1.6.2. First paper supplementary objectives	31

1.6.3. Second paper objectives.....	31
Chapter 2. First Article.....	32
First Article. Unraveling reproducible dynamic states of individual brain functional parcellation	33
1. Introduction.....	34
2. Methods.....	36
2.1. Dataset and preprocessing	36
2.2. Individual dynamic states of parcellation.....	36
2.3. Choice of the studied subnetworks and their seed	40
2.4. Spatial reproducibility analysis	40
2.5. Fingerprinting experiment	41
2.6. States dwell time reproducibility analysis	41
2.7. Data records.....	42
3. Results.....	42
3.1. Temporal cluster analysis reveals "dynamic parcellation states" with highly homogeneous parcellations within a state, and highly dissimilar parcellations across states.....	42
3.2. Dynamic states of parcellations had better reproducibility than static parcellations using long acquisitions.....	45
3.3. Visual evaluation of dynamic states of parcellations within- and between-subjects.....	46
3.4. Dynamic states of parcellations are highly reproducible at the intra-subject level.....	50
3.5. Within-subject reproducibility of dynamic states of parcellations is substantially higher than between-subject reproducibility.....	50
3.6. Dynamic state stability maps can reliably identify subjects.....	53
3.7. Dynamic state dwell times were not reproducible across replications for the dACC and the PCC seeds.....	54
4. Discussion	56
5. Conclusion	62
References	63

Chapter 3. Supplementary materials of the first article	69
Second Article. Supplementary Materials: Unraveling reproducible dynamic states of individual brain functional parcellation	70
1. Introduction	71
2. Whole brain parcellations had no clear structured states	71
3. Dynamic states can be identified for spatially contiguous regions	73
4. Spatial similarity of the seed-based parcellations	76
5. The dynamic parcellation approach results are robust to its parameters	77
5.1. Reproducibility of our dynamic states of parcellations was insensitive to resolution, yet some spatial states were consistent for some subjects and variable for others	77
5.2. Dynamic states can be identified at different time scales.....	82
5.3. Subnetworks were multistate with a dominant primary state for different window lengths	83
5.4. Dynamic states reproducibility was insensitive to low cluster size thresholds.	84
5.5. The PCC and the dACC subnetworks were multistate and the PM-VIS was monostate for most subjects across different cluster size thresholds	85
5.6. Reproducibility of dynamic states of parcellations in the case of different smoothing kernels.....	87
5.7. The PCC and the dACC subnetworks were multistate for different smoothing kernels and the PM-VIS was mono-state for most subjects.....	87
5.8. The reproducibility of the dynamic states of parcellations was not sensitive to changes in the seeds coordinates	90
5.9. Within-subjects reproducibility was insensitive to the number of replications of the seed-based parcellations	90
6. Dynamic states suppressed differences within-sessions versus across days in the case of resting state functional MRI data.....	91
7. Different dynamic states had different temporal dynamics.....	92
8. Conclusion	93
Chapter 4. Second Article.....	95

Third Article. A scalable dynamic parcellation algorithm for the compression of individual fMRI data	96
1. Introduction.....	97
2. Methods.....	100
2.1. DYPAC2.0	100
2.1.1. Overview	100
2.1.2. First-level cluster analysis	100
2.1.3. Second-level cluster analysis	101
2.1.4. State trimming	101
2.1.5. Memory requirements.....	101
2.1.6. Processing time.....	101
2.1.7. Batch processing	102
2.1.8. Code implementation.....	102
2.2. Dataset and preprocessing	102
2.3. Functional MRI loss of information analysis after compression.....	104
2.4. Reproducibility analysis	104
3. Results.....	105
3.1. State stability maps led to better compression within-subject than between-subject	105
3.2. Within-subjects reproducibility was higher than between-subjects, with some overlap in distribution	108
3.3. Dynamic states of parcellations were reproducible for some regions in the brain and inconsistent for others across the full brain in the context of the movie data.....	109
3.3.1. Within-subject reproducibility	109
3.3.2. Between-subjects reproducibility	114
4. Discussion	118
5. Conclusion	121
6. Acknowledgment.....	121
Chapter 5. Discussion	122
5.1. Contributions.....	122
5.2. Conclusion.....	125

Supplementary Materials	126
.1. Supplement 1: The Dice score coefficient	126
.2. Supplement 2: The Adjusted Rand Index	126
.3. Supplement 3: The Hungarian algorithm	127
References	128

List of figures

1	Federal government expenditures and number of affected people with Alzheimer’s disease in U.S.A.....	20
2	The neuron theory suggested by Ramón y cajal.....	22
3	Evolution of the long distance pathways of the arcuate fasciculus.	23
4	Variability in boundaries of brain regions in longitudinal data.....	24
5	Between-subject variability in boundaries of cortical areas.	24
6	Generation of the functional connectome based on the functional parcellation.....	25
7	Graph theory metrics were biased by the choice of the functional parcellations.....	26
8	Using Brain Graph to map, track and predict patterns of disease propagation across the connectome.....	27
9	Anatomical parcellation of the cerebral cortex.....	28
10	Schematic linking between brain network topology and psychological function [36].....	29
1	Subject-specific dynamic parcellation approach (DYPAC).....	39
2	Dice similarity matrices of seed-based brain parcellations showed groups of highly homogeneous seed-based parcellations and other groups of dissimilar seed-based parcellations.....	43
3	Subnetworks were multistate with a dominant primary state. We included state dwell times for both sets of independent data.....	44
4	DYPAC dynamic states of parcellations outperformed static parcellations based on long acquisitions in terms of within-subjects reproducibility.....	45
5	PM-VIS dynamic state stability maps were similar across sets at the within-subject level and variable across states and subjects.....	47

6	dACC dynamic state stability maps were similar across sets at the within-subject level and variable across states and subjects.	48
7	PCC dynamic state stability maps were similar across sets at the within-subject level.	49
8	Within-subject reproducibility scores were higher than between-subject reproducibility scores for most dynamic states of parcellations.....	51
9	High spatial reproducibility of dynamic states of parcellations across subjects and seeds.....	52
10	The deterministic fingerprinting had higher accuracy than the fingerprinting by chance.....	53
11	The fingerprinting experiment showed high reliability of state stability maps in delineating subjects across seeds.....	55
12	Dwell time of dynamic states of parcellations was inconsistent across the two sets of independent data in the cases of the dACC and PCC seeds.....	56
1	Similarity between full brain parcellations.....	72
2	The spatially contiguous regions were overlapping with the spatially distributed parcels surrounding the seed in the state stability maps of the dACC seed.	73
3	The spatially contiguous regions were overlapping with the spatially distributed parcels surrounding the seed in the state stability maps of the PCC seed.....	75
4	Spatial similarity between seed-based parcellations in terms of Dice scores.....	76
5	Within-subject reproducibility of dynamic states was higher at the within-subject level than the between-subject level across scales.....	78
6	Primary states were overlapping across scales for some subjects in the case of the dACC seed.....	79
7	Secondary states were overlapping across scales for some subjects and states and variable across others in the case of the dACC seed.	80
8	Third dACC dynamic states were inconsistent across scales.....	81

9	Within-subject reproducibility scores were higher than between-subject reproducibility scores for most dynamic states of parcellations.....	82
10	The number of dynamic states and their dwell time was insensitive to different window lengths.....	83
11	Dynamic states reproducibility was insensitive to cluster size threshold.	85
12	The number of dynamic states and their dwell time was insensitive to different cluster size thresholds.....	86
13	The within- and between-subjects reproducibility of our dynamic states of parcellations were insensitive to the smoothing kernel size.....	87
14	The number of dynamic states and their dwell time was insensitive to the smoothing kernel.....	89
15	Within- and between-subjects reproducibility of our dynamic states of parcellations for 15 seeds per subnetwork.....	90
16	The within-subject reproducibility of our dynamic states of parcellations was insensitive to the number of replications of the seed-based k-Means parcellations.....	91
17	Dynamic states occurred with the same probability either across days or across sessions.....	92
18	Dynamic states of parcellations had different temporal dynamics.....	93
1	Subject-specific dynamic parcellation approach at the full brain level (DYPAC2.0).....	100
2	The functional MRI signal compression quality was higher within-subject than between-subjects.....	106
3	The state stability maps had lower information loss when used for functional MRI compression at the within-subject level compared to the between-subject level.....	107
4	Within-subjects reproducibility distribution was highly overlapping with the between-subjects reproducibility distribution in the case of movie data.....	108
5	Highly reproducible state stability maps across the training and the test data at the within-subjects level and across the whole brain.....	111

6	Averagely reproducible state stability maps across the training and the test data at the within-subjects level and across the whole brain in the context of movie data.....	112
7	Some state stability maps had low reproducibility across the training and the test data at the within-subjects level and across the whole brain.....	113
8	Highly reproducible state stability maps across the training and the test data at the between-subjects level and the movie data.....	115
9	Averagely reproducible state stability maps across the training and the test data at the between-subjects level in the context of movie data. . .	116
10	Some state stability maps had low reproducibility scores at the between-subject level.	117

List of abbreviations

fMRI	functional magnetic resonance imaging
BOLD	Blood oxygenation level dependent
MRI	Magnetic resonance imaging
HCP	Human connectome project
TR	Time resolution
MSC	Midnight scan club
DYPAC	Dynamic parcel aggregation with clustering
MNI	Montreal Neurological Institute
dACC	dorsal anterior cingulate cortex
PCC	Posterior cingulate cortex

PM-VIS	Posterior-medial visual region
MPFC	Medial prefrontal cortex
dAI	dorsal anterior insula
vAI	ventral anterior insula
TPJ	temporoparietal junction
ICA	Independent component analysis

Acknowledgments

During these five years of doctoral studies, I had the chance to work under the supervision of Pr. Max Mignotte and Pr. Pierre Bellec. I feel deeply grateful for both of them as I always felt their support and guidance. Their conversations not only provided for my a constant growing wisdom filled with much love and compassion and care. All this drove me to always want to provide the best of what I can do in my work. I would love also to express my gratitude to my laboratory colleagues for their infinite support and fun times: Aman, Yu, Yassin, Sebastien, Angela, Julie, Basile, Desiree, Shima, Sana, Lazhar, Aymen, Arnaud, Hanad. Outside academia, I would love to thank my friends who were there always standing by my side for emotional support: Khaoula, Amal, Cherifa and Rihem. Particular thanks to my parents and my sisters for their great support throughout these years and through my academic endeavor. To all my professors since the age of seven, I am so thankful for all your support and encouragements throughout my academic journey. I am also grateful for the government of Tunisia and the Montreal university to offer me the excellence scholarship and to Pr. Marouane kessentini for the advice that literally changed my life when he recommended me to apply for the scholarship itself. Thank you so much for everyone else for every single favor that contributed to this huge achievement. I am also grateful for myself to stand by my self during these years, to also allow myself to discover this outstanding medical imaging field. This experience upgraded who I am and how I perceived the world. It taught me better ways to deal with my self and others. I am so proud for both this achievement and this maturity. This amazing chapter is now over and it is opening doors for other exciting chapters throughout which I will continually try to build upon these steps ...

Chapter 1

Introduction

1.1. Rationale

Alzheimer disease result in the incurable degeneration of nerve cells and eventually leads to a debilitating condition called dementia. It is among the most worrisome health problems currently due to their rapid increase all over the world, with the aging of the population. The number of people affected by Alzheimer's dementia has indeed dramatically increased in U.S. since 2010, and is predicted to reach 13.4 million by 2050 (See Fig. 1). The costs associated with this upcoming epidemics are staggering, currently representing 184 billion and expected to reach 1.167 billions in 2050 [75]. Unfortunately, Alzheimer dementia is currently incurable, by contrast to all other top ten causes of death in the U.S. A key reason for the lack of effective treatment is that the diagnosis of Alzheimer is performed at a very advanced stage of the disease, where the neuronal tissues have been damaged beyond destroyed.

A major challenge for neurologists and clinical neuroscientists is therefore the early and reliable identification of Alzheimer disease, before the apparition of clinical symptoms. This challenge will likely only be addressed through unprecedented multidisciplinary research. Neuroimaging, and in particular functional magnetic resonance imaging (fMRI), is a promising tool to study the functional organization of the brain for an early, reliable diagnosis of Alzheimer disease. A key step to reach that objective is to parcellate the brain into functionally homogeneous networks, using fMRI data. This can be achieved for a particular patient, or by combining the data of many patients to derive a parcellation which describe common characteristics in a group.

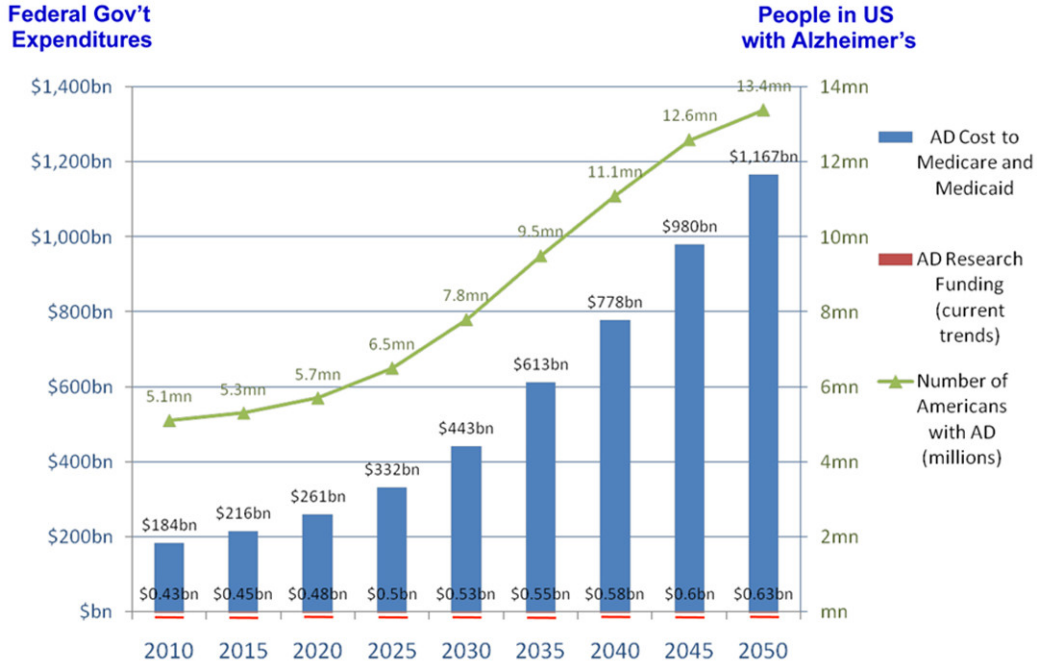


Fig. 1. Federal government expenditures and number of affected people with Alzheimer’s disease in U.S.A.

Sources: Alzheimer study group. A national Alzheimer strategic plan: The report of the Alzheimer study group; Alzheimer association. National Institute of health office of the budget [75].

The main outcome of my thesis will be new algorithms for brain parcellation at the individual using longitudinal functional MRI data. I believe these algorithms will be useful for the diagnosis of Alzheimer disease, and more generally for the study of neurological disorders.

1.2. Resting state fMRI and its motivations

Functional magnetic resonance imaging (fMRI) provides an indirect measure of neuronal activity, it acquires the blood-oxygen-level-dependent (BOLD) signal as an indirect measure of neuronal activity. This signal is a set of complex changes that reflect the oxygen demand and the blood flow at the proximity of neurons. The idea of fMRI is based on the relaxation of the hydrogen nuclei, by using specific fMRI sequences consisting of T2* weighted acquisitions that are sensitive to local distortions of the magnetic field. In fact, when a neuron is internally activated by a stimulus, it needs energy to restore its electrical and ionic concentration equilibrium. The mechanism that allows the generation of this energy is the glucose oxidative metabolism. This leads to the increase of the deoxyhemoglobin concentration (the hemoglobin without oxygen), a paramagnetic molecule, which creates distortions in the magnetic field and thus the perturbation of the hydrogen nuclei. So the

rationale behind the data acquired using fMRI stems from the idea that brain activity exists in areas where there are changes in the oxygen consumption.

Despite its inability to directly measure the neuronal activity, many researchers have studied the relationship between the fMRI recordings and the actual neuronal activity to provide an empirical assertion of the validity of the provided BOLD signal to measure the neuronal activity. For example, Logothetis et al. (2001) suggested that BOLD signal actually reflected the input and the local intracortical processing. Still, there is a need, in the future, for non-invasive neuroimaging techniques that are able to directly measure the activity of the nerve cells.

1.3. Human brain large scale networks

1.3.1. History of the brain anatomy

Before analyzing the brain function and dynamics, anatomists observed the brain organization at a structural level. One century before, Ramon y Cajal, a well-known anatomist at that time, proposed the neuron doctrine. He suggested that the nervous system was composed of neurons, which acted as independent functional entities. Cajal discussed both the specificity and diversity of nerve cells in his neuron theory (See Fig. 2). Neurons are individual cells that communicate information via junctions called synapses. Michio Kaku said: *"The human brain has 100 billion neurons, each neuron is connected to 10 thousand other neurons. Sitting on your shoulders is the most complicated object in the known universe"* [47]. The central nervous system is responsible for actions related to memory, cognition and behavior.

In the past, researchers looked at the human brain in detail to recognize the different morphology of nerve cells, physiologic and metabolic phenomena. Recent trends of modern research were rather oriented towards observing the large-scale architecture of the brain as an integrative system. The antagonist of Ramón y Cajal, Camillo Golgi defended, at that time, the reticulum theory in which he considered the brain as an ensemble of non-dependent entities that were interacting collectively to give rise to coordinated states at multiple scales. Small-scales go from neurons and their single paths, then it enlarges to more elaborated local networks. These local networks are themselves connected to other spatially distributed networks called large-scale networks. In the Nobel Lecture in 1906, Camillo Golgi said: *...far from being able to accept the idea of the individuality and independence of each nerve element, I never have reason, up to now, to give up the concept which I have always stressed, that nerve cells, instead of working individually, act together [...]. However,*

opposed to the popular tendency to individualize the elements, I cannot abandon the idea of a unitary action of the nervous system [...].

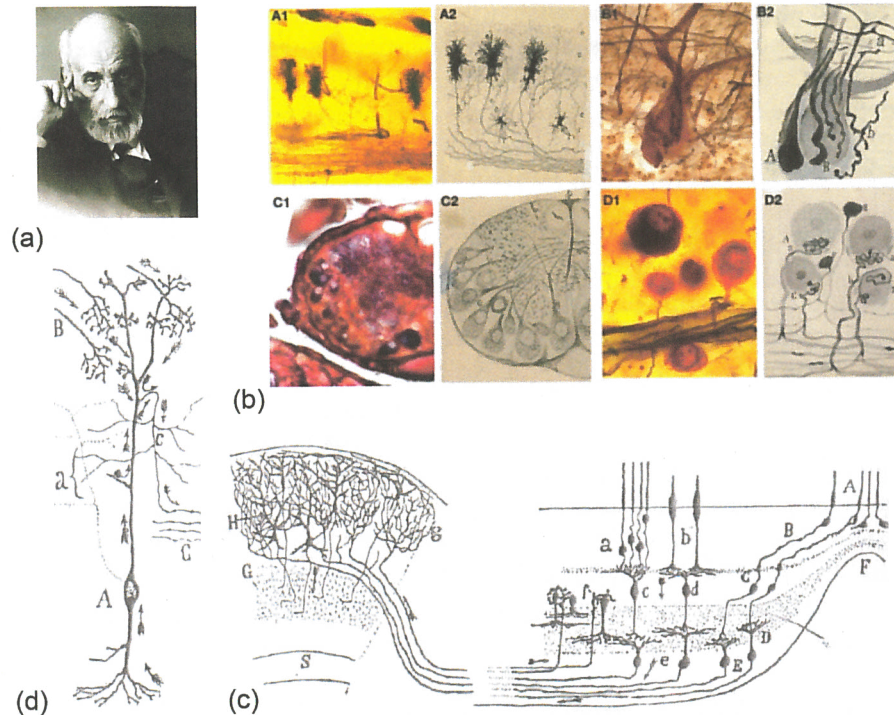


Fig. 2. The neuron theory suggested by Ramón y Cajal.

Santiago Ramón y Cajal gained the Nobel prize for his neuron theory more than a century ago. He explained the rules of space, time and material conservation and the morphological adaptation of neurons in the human brain (1906). (a) Recordings of the data by pen and ink drawings and their correspondent cells. (b-c) Cajal explained the way the retinal cone cells works (A in the figure) and passed via the synaptic junctions to the ganglion cells (C in the figure) and was projected after that to the axons (g in the figure) to end to the proximity of neurons (H in the figure)(c). Example of cells, the Shepherd's crook cell of the reptilian optic lobe had a specific characteristic compared to other nerve cells. In fact, its axon has a distinguished morphology since it do not emerge close to the cell body (A in this figure) (d) [36].

1.3.2. Anatomical brain boundaries are different from the functional brain boundaries

Studying the brain as a large-scale integrative system was crucial for brain functions such as cognition and behavior.

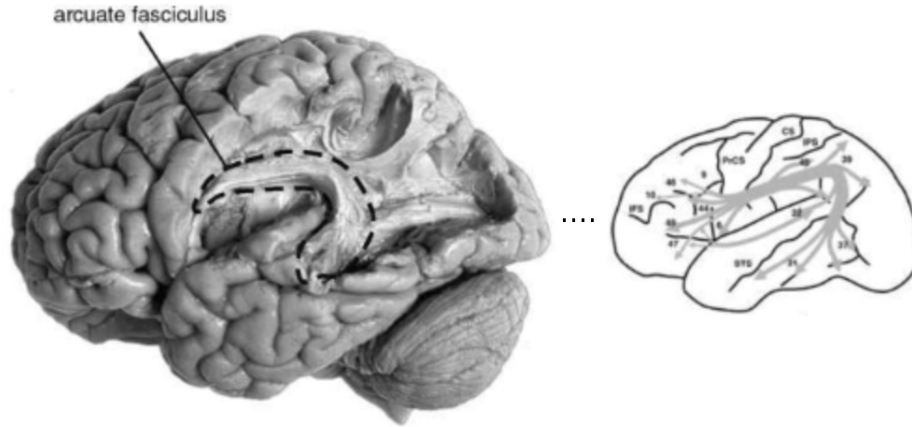


Fig. 3. Evolution of the long distance pathways of the arcuate fasciculus.

The left hand image illustrated an anatomical preparation showing the arcuate fasciculus in the left cerebral hemisphere of the human brain. The right hand image illustrated the connectivity in the arcuate fasciculus. It showed the large-scale aspect of brain networks. It also illustrated the fact that the boundaries of functional connectivity were not restricted to the boundaries of anatomy [71] .

These large-scale aspects of functional networks needed to be considered when subdividing the functional organization into regions based on a functional; parcellation approach. Fig. 3 showed an example of the large-scale network of the arcuate fasciculus. In this thesis, we were interested to develop new parcellation algorithms and our main objective was to reduce the complex functional MRI into neurobiologically meaningful brain regions.

1.4. Brain regions changes their boundaries over time

Brain functional organization variability represented one of the most challenging issues for more than two decades in neuroscience research both at the within- and the between-subject level (See Fig. 4 and Fig. 5). There were two major factors at the origin of changes in the structural and functional structure of the cerebral cortex, at the individual level. These factors were the age and the learning processes. Learning contributed to acquiring cognitive reserves that enhanced functional performances of the brain. These factors resulted in changes in the boundaries of anatomical and functional regions. There was a difference in the anatomical boundaries of regions for one subject both at the temporal and the between subject level. Anatomical differences were also reflected in the differences associated with the functional organization of the human brain [36]. This could be noticed, in reality, by differences at the level of intelligence or reasoning between individuals.

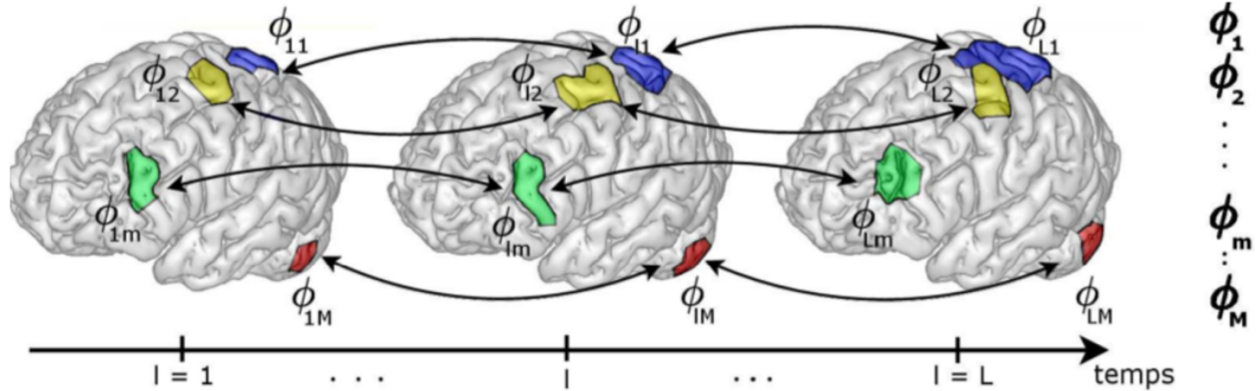


Fig. 4. Variability in boundaries of brain regions in longitudinal data. We observed changes in the boundaries of brain regions over time [14].

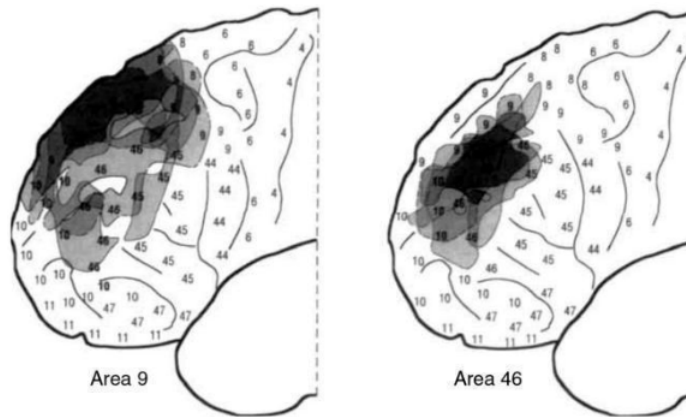


Fig. 5. Between-subject variability in boundaries of cortical areas. We observed five superimposed left-hemisphere reconstructions of the cortical areas 9 and 46 based on their cytoarchitectonic profile. The outlines of the two areas in individual brains were marked by lines, and their overlap was indicated by the level of shading. The cortical territory occupied by area 9 or area 46 in all five individual brains was filled in black [71].

1.5. Functional brain parcellations

1.5.1. Functional brain parcellation reduces the complex brain organization

Functional MRI parcellation aimed to simplify the complex organization of the brain voxels by grouping them into regions/parcels. Each voxel represented a set of neurons in the brain. A region or parcel represented a set of spatially connected voxels with functionally homogeneous time series (i.e., these voxels correspond to neurons that interact together to communicate pieces of information associated with a cognitive task). Spatially distributed regions/parcels represented a cluster. The parcellation problem could be seen as a compromise between redundancy minimization and segregation maximization. To minimize redundancy,

all voxels associated with functionally homogeneous time series were grouped together in the same parcel. To maximize segregation, only representative voxels of a specific/unique functional pattern were grouped together within a parcel.

1.5.2. Applications of functional brain parcellations

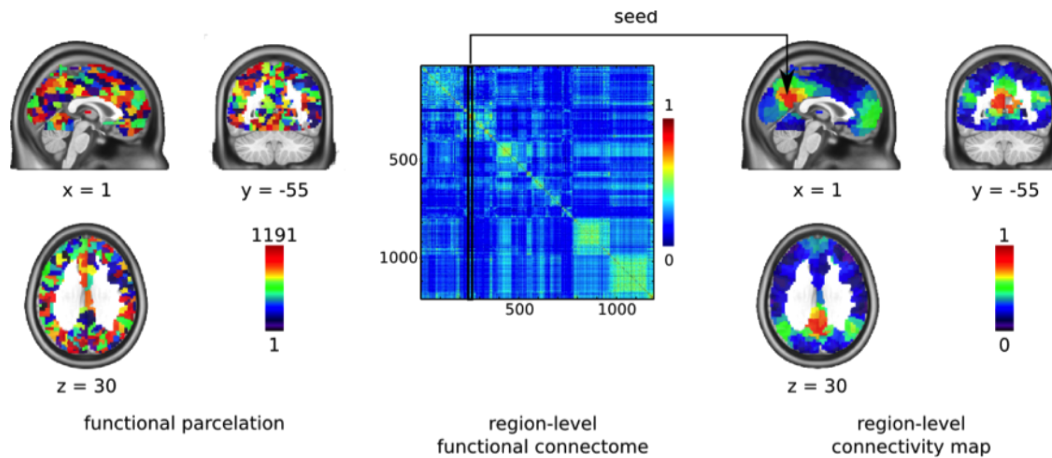


Fig. 6. Generation of the functional connectome based on the functional parcellation.

The functional connectome was the matrix that contained the correlations (e.g., Pearson correlation) between each pair of regions (i.e., here 1191 regions/parcels). The average time series of all the voxels included in one seed region was computed and correlated to the average time series from other regions in the brain. The map of a seed region (or region of interest) was shown in the right hand side [15].

Prior to the analysis of functional MRI data, researchers applied functional parcellation as a dimensionality reduction. For instance, graph theory approaches used brain parcels as nodes in the graph to represent human brain networks [72]. These networks were then analyzed for a better understanding of the brain dynamics. Additionally, generating connectomes based on brain parcellations was widely investigated (See Fig. 6). Recently, the connectomics theory represented a promising area of research since it helped neuroscientists to have a better understanding of brain functional networks [36]. For instance, the connectomics and graph-theory provided an attractive framework for mapping, tracking and predicting patterns related to brain disorders (See Fig. 8 [36, p.28]). Another different recent application of functional parcellations was the construction of subtypes [31]. The main objective of functional subtypes was the amelioration of the accuracy of the prediction of a neurological disease; e.g. Alzheimer disease.

Previous studies reported the choice of brain parcellations had a clear bias between network measures for different brain parcellations depending on how well these brain regions

were actually representative of the functional brain networks (See Fig. 7). This suggested a cautious choice of brain parcellations was required to avoid such bias.

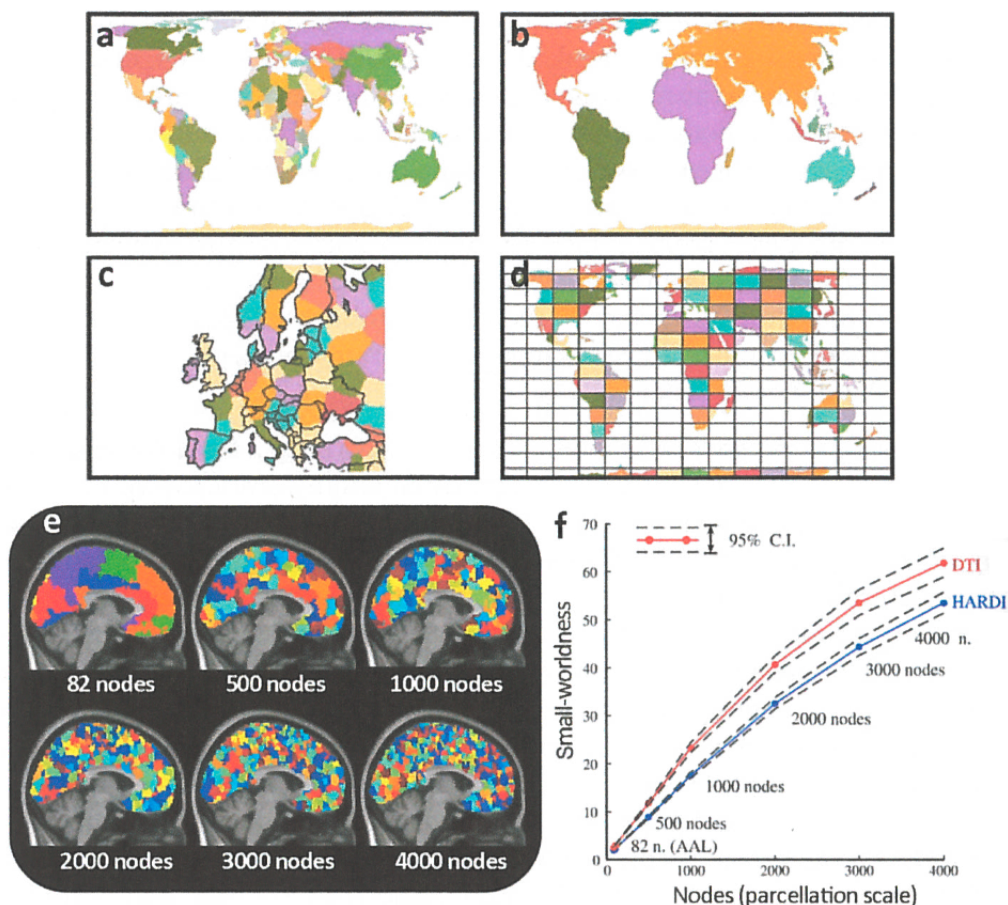


Fig. 7. Graph theory metrics were biased by the choice of the functional parcellations.

An analogy to the brain networks (a-d) illustrated the parcellation applied on a geographical map to show that the choice of erroneous boundaries lead to wrong identification of country localization. Likewise, the brain parcellation map included multiscale features. Large-scale features were, for instance, oceans and fine-grained features were cities. (e) showed parcellations at different resolutions. Each brain network was constructed based on a parcellation (f) demonstrating the effect of the different number of regions (nodes) on a graph-theory metric called small worldness [36, p.76].

The development of computational models of large-scale network dynamics allowed the simulation of the functional architecture of the brain. For instance, recently functional connectomics emerged as a promising theory for representing, in a helpful way, the functional patterns [72]. Once the architecture was established, the development of statistical techniques and models for the inference of differences between patterns of functional connectivity at the individual-level, as well as, the group level could be performed. Pathology

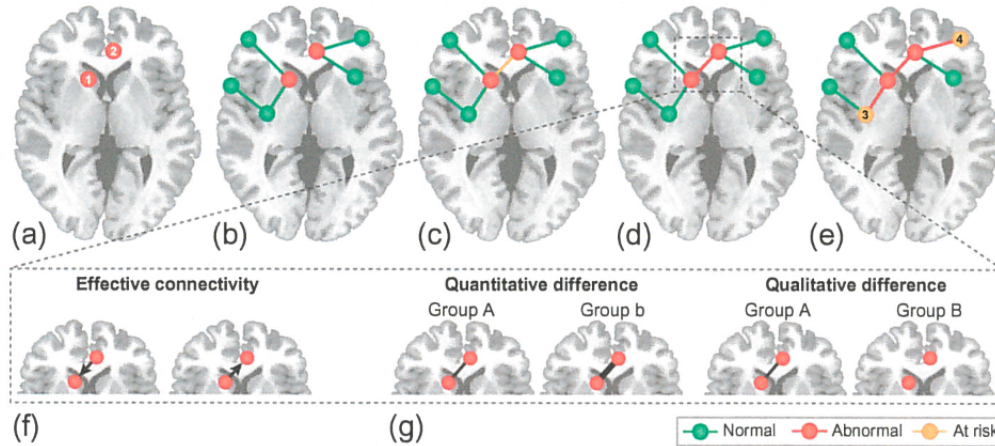


Fig. 8. Using Brain Graph to map, track and predict patterns of disease propagation across the connectome.

(a) Most studies related to the diagnosis of brain disorders compare differences between brain regions for one or a group of suspect patients and a control group for some regions of the cerebral cortex based on some measures. Here, regions 1 and 2 show abnormality in the patient group. This comparison between brain regions helps in identifying abnormalities localization. Then, (b-e) the mapping of brain connectivity allows us to understand the context of the abnormal regions and the abnormal connexions with other regions suggesting that these regions are subject to pathological processes [36, p.28].

in the brain could be associated with changes at the brain organization; i.e. regions shape and size and connections between regions. These analysis had to be done at different levels for the identification of the level of impairment and prospects of recovery following the therapeutic intervention [36, p.28] (See Fig. 8). Another application by [31] was the prediction of schizophrenia based on functional subtypes to ameliorate the accuracy of the detection of heterogeneity in functional patterns between patients and controls. Overall, functional brain parcellations represented the cornerstone of several neuroimaging applications to help reduce and understand the functional complex brain organization. This allowed researchers to make several discoveries towards the identification and the prevention of neurological diseases.

1.5.3. Anatomical parcellations

Earlier approaches in neuroscience, researchers focused on parcellating the human brain into regions to understand its organization. Although many anatomists proposed different parcellations, there existed no consensus related to anatomical regions. The underlying heterogeneity was mainly due to differences in the morphology of cortical regions at the intra- and between-subjects level added to the subjectivity of anatomists (See Fig. 9). Thus, the parcellation could be considered as an ill-defined problem for which there existed many

possible solutions. Another limitation of anatomical parcellations was the failure to parcellate several regions in the brain including the precuneus and neighboring posterior cingulate.

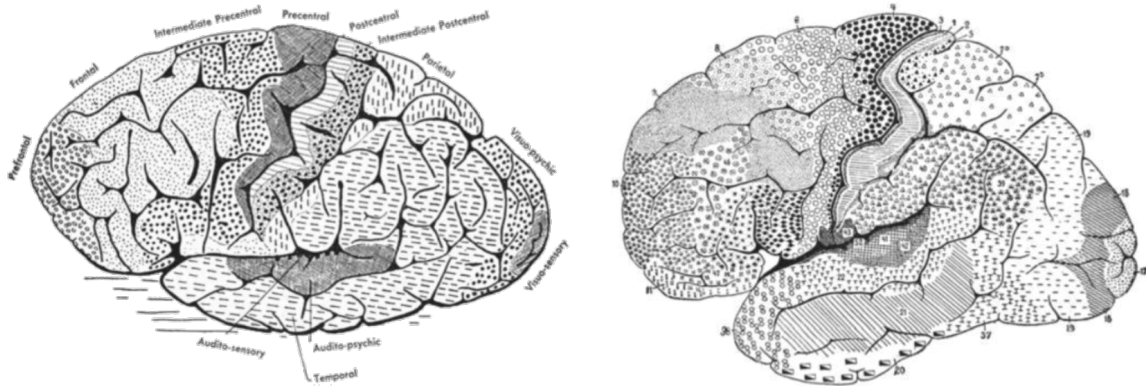


Fig. 9. Anatomical parcellation of the cerebral cortex.

The left hand image corresponded to Alfred Campbell subdivision into 14 regions and the right hand image was the Korbinian Brodmann subdivision into 44 regions [71].

1.5.4. Brain networks are spatially distributed across the brain

Many recent approaches relied on spatial contiguity of voxels to generate parcels. Although this hypothesis was valid for many regions of the brain corresponding to contiguous voxels, there existed spatially distributed voxels that were interrelated via indirect connexions [71]. In 1909, Brodmann argues: *One cannot think of their taking place in any other way than through an infinitely complex and involved interaction and cooperation of numerous elementary activities [...] we are dealing with a physiological process extending widely over the whole cortical surface and not a localised function within a specific region* [71]. Imposing the commonly used spatial constraints, uniformly, for all cortical regions did not correspond to the reality of the cerebral cortex.

Previous studies demonstrated that anatomical and functional subdivisions were consistent [58]. However, BOLD correlations did not necessarily reflect the anatomical connectivity. Some functional fMRI parcellation approaches identified, only, functional parcels corresponding to fine-scales (i.e; functional sub-networks resulted from local nerve cells interactions) such that large numbers of these functional parcels could match anatomical parcels. These coarse parcellations were insufficient to capture rich interactions between large scale networks [58, 45]. It was also not representative for cognitive functions [36]. Fig. 10 illustrated the schematic linking between brain network topology and psychological function. It suggested the existence of both fine scale and multiscale properties of brain networks.

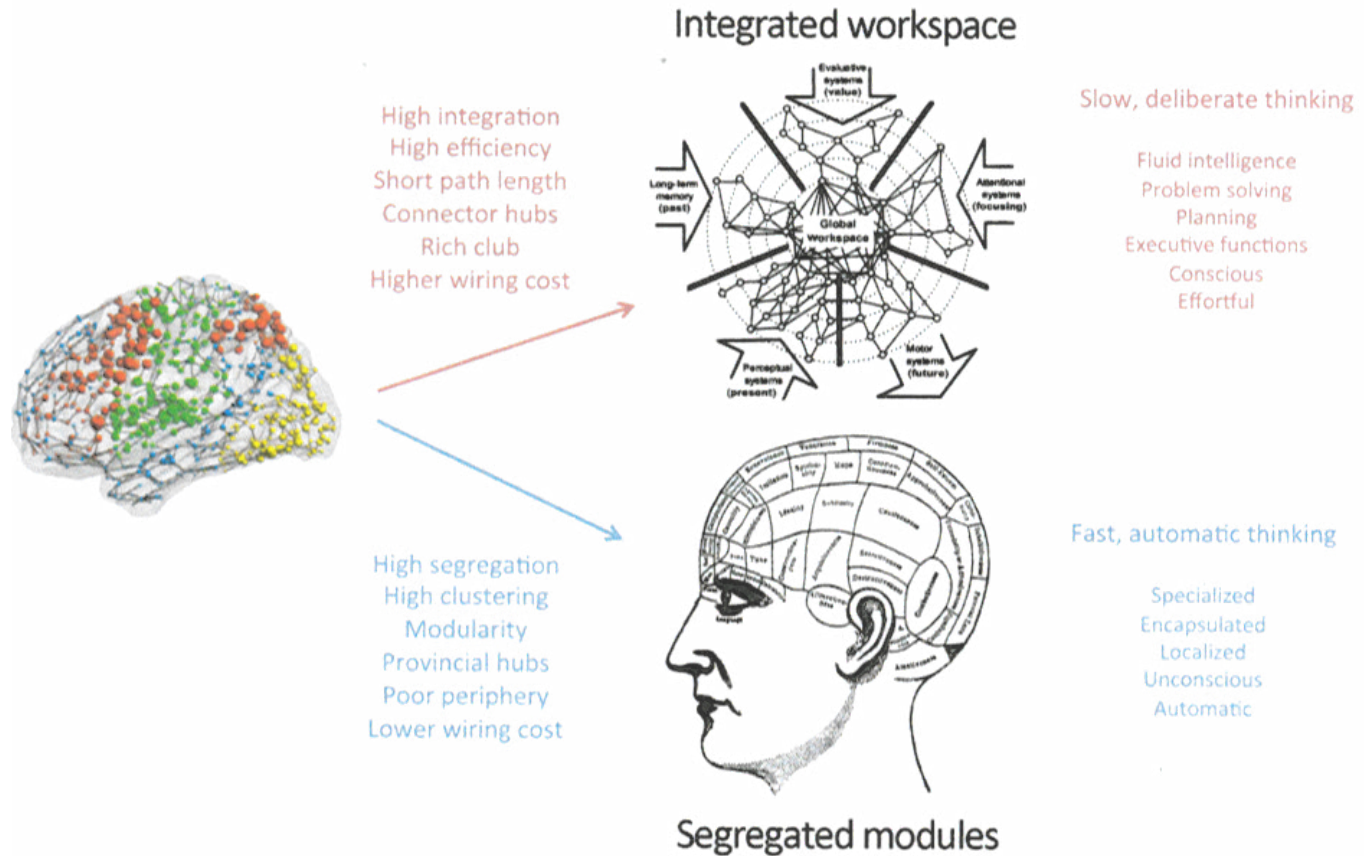


Fig. 10. Schematic linking between brain network topology and psychological function [36].

Depending on the psychological function, there existed some regions in the brain that were involved either at the locally connected regions or the distributed regions throughout the brain.

1.5.5. There is no consensus regarding the number of clusters

Due to the lack of theoretical directives and a ground truth to guide the choice of the number of clusters, researchers estimated a range for meaningful values ranging between [5 .. 10 000] (e.g., [74]). Another more interesting way was to choose the number of clusters according to performance measures. For example, the number of clusters was chosen based on maximizing the stability contrast measure (derived from the silhouette criterion on the within and between cluster variance). The impact of the number of clusters on the significance in differences between groups measured for each connexion between parcels. Experimental results showed that performance measures (i.e., sensitivity and specificity) were high and consistent across scales inferior to 25. Surprisingly, in the case of schizophrenia, the highest significance was found in the case of the basal ganglia for 55 parcels [13]. Other studies reported that the choice of the number of clusters was a tradeoff between complexity of the

reduced brain representation and analytic performance. That is, a higher number of clusters had better analytic performances at the expense of higher complexity [66].

1.5.6. The functional parcellation algorithms has a high dimensionality in time and space

The dimensionality of functional fMRI data is a challenging issue in functional MRI parcellations. Recently, neuroimaging datasets had a dramatic increase in size. This increase included either the number of scanned runs, the scans durations, the resolution of the acquired data or the number of subjects. Up to date, one of the most massive online datasets were the Human Connectome Project (HCP) [42], and the cneuromod dataset [28]. These datasets had up to 20 TB of disk space. For instance, these data were acquired for 1200 subjects in the case of HCP for two hours each. cneuromod dataset had up to X hours per subject for six subjects. Additionally, cneuromod and HCP had the same scanning protocol with 2 millimeters spatial resolution instead of the commonly scanning 3 or 4 millimeters and a fast temporal resolution TR (TR=1.49s in the case of cneuromod dataset). Therefore, scalable parcellation algorithms were highly needed to reduce the dimensionality of these fMRI 'Big Data' [77]. In parallel with the high demand in intensive computational resources, there existed several grid computing servers adapting to this high demand. For instance, compute canada had many servers with hundreds of computing cores available. These nodes had at least 125G available memory [?]. Still, the scalability of neuroimaging algorithms including the functional parcellation algorithms facilitates the replication of experiments on different datasets and different computing environments from different researchers. Up to date, this replication is still challenging for many state of the art functional parcellations and thus, urgent scalable solutions for reducing the processing time and the memory demands of neuroimaging Big Data processing.

1.6. Thesis objectives

1.6.1. First paper objectives

The first contribution of this thesis was the development of a new method that captured reproducible dynamic states of parcellations at the individual level. These dynamic states represented the spatial brain reconfigurations over time in the resting state condition. This is very important in the context of ignoring the substantial dynamic reorganization of the human brain by previous static parcellation approaches. Additionally, our results suggested these static approaches were incorrectly averaging well defined and distinct dynamic states. This brought important caution for any work based on static atlases.

Paper accepted in Network Neuroscience journal: Boukhdhir, A., Zhang, Y., Mignotte, M., Bellec, P. 2020. Unraveling reproducible dynamic states of individual brain functional parcellation. Network Neuroscience journal.

1.6.2. First paper supplementary objectives

The second contribution of this thesis represented the supplementary materials of our first published paper. We investigated different research questions associated with our proposed dynamic parcellation approach. First, we validated our hypothesis regarding the inexistence of a clear structured state in the whole brain parcellation. This is important because it motivated us to the seed-based parcellations as a cornerstone of our dynamic parcellation approach. Second, we showed it was possible to extend the dynamic parcellation algorithm by considering both the spatially connected dynamic states and the spatially distributed dynamic states. Third, we replicated all the experiments of chapter 2 (the main paper) with different parameters to verify the robustness of our dynamic parcellation algorithm. Fourth, we investigated the dynamic states reproducibility scores both at the within-session and between sessions effect. This allowed us to know whether the acquisitions of functional MRI data across days impacted the reproducibility of the dynamic states. Fifth, we quantified the synchrony between the different states of parcellations. That allowed us to know whether two different states were involved at the same time or not in a resting state condition.

1.6.3. Second paper objectives

The third contribution of this thesis is the extension of the seed-based dynamic parcellation approach at the full brain level. To validate the goodness of the dynamic parcellations, we aimed to test the compression of the functional MRI signal at the within-subject level over the between subject level. We also aimed to quantify the reproducibility of the full brain dynamic states and compare it at the within-subjects level over the between subjects level. We used longitudinal functional MRI acquisitions in the context of movie data.

Paper in preparation: Boukhdhir, A., Boyle, J., Pensard, B., Mignotte, M., Bellec, P. Dynamic states of parcellations are subject-specific at the full brain level.

Chapter 2

First Article

First Article.

Unraveling reproducible dynamic states of individual brain functional parcellation

by

Amal Boukhdhir¹, Yu Zhang², Max Mignotte³, and Pierre Bellec⁴

- (¹) Centre de recherche de l'institut universitaire de gériatrie de Montréal, Montréal, Québec, Canada
Département d'informatique et de recherche opérationnelle, Université de Montréal, Montréal, Québec, Canada
- (²) Centre de recherche de l'institut universitaire de gériatrie de Montréal, Montréal, Québec, Canada
- (³) Département d'informatique et de recherche opérationnelle, Université de Montréal, Montréal, Québec, Canada
- (⁴) Département de psychologie, Université de Montréal, Montréal, Québec, Canada

This article was submitted in Network Neuroscience.

ABSTRACT. Data-driven parcellations are widely used for exploring the functional organization of the brain, and also for reducing the high dimensionality of fMRI data. Despite the flurry of methods proposed in the literature, functional brain parcellations are not highly reproducible at the level of individual subjects, even with very long acquisitions. Some brain areas are also more difficult to parcellate than others, with association heteromodal cortices being the most challenging. An important limitation of classical parcellations is that they are static, i.e. they neglect dynamic reconfigurations of brain networks. In this paper, we proposed a new method to identify dynamic states of parcellations, which we hypothesized would improve reproducibility over static parcellation approaches. For a series of seed voxels in the brain, we applied a cluster analysis to regroup short (3 minutes) time windows into “states” with highly similar seed parcels. We splitted individual time series of the Midnight scan club sample into two independent sets of 2.5 hours (test and retest). We found that average within-state parcellations, called stability maps, were highly reproducible (over .9 test-retest spatial correlation in many instances) and subject specific (fingerprinting accuracy over 70 percent on average) between test and retest. Consistent with our hypothesis, seeds in heteromodal cortices (posterior and anterior cingulate) showed a richer repertoire of states than unimodal (visual) cortex. Taken together, our results indicate that static functional parcellations are incorrectly averaging well-defined and distinct dynamic states of brain parcellations. This work calls to revisit previous methods based on static parcellations, which includes the majority of published network analyses of fMRI data. Our method may, thus, impact how researchers model the rich interactions between brain networks in health and disease.

Keywords: data-driven brain parcellation, dynamic states of parcellation, seed-based parcellation, spatial reproducibility, within-subject reproducibility, between-subject reproducibility

1. Introduction

Brain parcellation is a tool for understanding the functional organization of the human cerebral cortex, and also to reduce the dimensionality of fMRI data. Parcellations are notably heavily used to characterize brain network properties. A brain parcellation was defined as the entire subdivision of the brain into clusters (or spatially distributed parcels/regions). A good parcellation should typically satisfy two conflicting objectives. The first objective is to be reproducible enough to allow for replication and comparison across studies. The second objective is to be flexible enough to accurately represent the organization of an individual brain. Simultaneously achieving these two objectives is challenging, in part due to inter-subject variability [19, 73, 61], which is also associated with measures of cognitive performance [16]. In addition, it has also become apparent that brain functional connectivity substantially reorganizes dynamically [79] according to different cognitive states [67]. Our main objective in this work was to develop a new method to capture reproducible dynamic states of parcellations at the individual level. These dynamic states represent the spatial brain reconfigurations over time in the resting

state condition.

A proliferation of approaches also exist in the literature to study the dynamics of functional connectivity. These studies confirmed the spatio-temporal reconfiguration of the brain networks [43, 1, 4] and associated it to dynamics of cognitive processing or mental states dictated by tasks [9, 37, 20, 64, 54]. The co-activation patterns [24, 55], spatial independent component analysis [69] were among the most widely applied techniques to consider brain dynamics (see [25] for a review). These dynamic analyses of the brain, using for instance sliding window correlation, have demonstrated better results compared to stationary approaches in the detection of neurological disease [65, 44]. Other findings confirmed the interaction between brain networks for different task states [81, 19, 23]. For instance, Braga and Buckner discovered that the default mode network could be reliably subdivided into parallel networks within the same individual [19]. Chen and colleagues modeled these states switching processes of resting state brain activities using a hidden markov model [24]. Therefore, neuroscientists mentioned there is a need to have neuroimaging tools to identify how brain parcels reconfigure spatially in the case of highly cognitive regions over time and to evaluate the variability of brain parcels across time and across individuals [54]. Even though dynamic functional connectivity is well studied, to the best of our knowledge, the only parcellation approach that considered dynamic changes of parcels was suggested by Salehi and colleagues. These authors demonstrated that the brain functional parcellations are not spatially fixed, but reconfigure with task conditions [67, 68]. These reconfigurations were used to reliably predict different task conditions. Still, this approach only suggested a brain parcellation per task condition, and it neglected brain parcel reconfigurations across short time durations, within each task. Dynamic brain parcellation, thus represents a promising area of research to further investigate brain dynamics.

In this paper, we build upon the findings of Salehi and colleagues [67, 68], and we propose a novel approach to extract different dynamic states of functional parcellations at the individual level. We define a dynamic state of parcellation as the spatial reconfiguration of a given brain network that occurs for short time durations in the resting state condition. We hypothesize the existence of homogeneous modes of spatial reconfigurations, or dynamic states of parcellations, at the level of these short time windows and we propose a dynamic cluster analysis for their identification. Our approach is based on aggregating sliding-window parcellations for a given region to obtain stability maps of the different dynamic states of parcellations. We generate these dynamic states for the ten subjects of the Midnight scan club (MSC) resting-state dataset and we aim to study similarities and variations within-state (across replication sets), across states (within-subject), and across subjects.

We also aim to evaluate the reliability of the generated states maps in a "fingerprinting" experiment, i.e. matching state maps generated from the same subjects within a group.

2. Methods

2.1. Dataset and preprocessing

The resting-state MSC dataset includes ten healthy subjects (female=5, male=5, their age ranges between 24-34 years old [39]). Informed consent was obtained from all participants. The study was approved by the Washington university school of medicine human studies committee and institutional review board [39]. Each subject underwent a total of five hours of resting state functional MRI data, with a series of 30 minutes contiguous acquisitions, beginning at midnight for ten consecutive days. In each session, subjects visually fixated on a white crosshair presented against a black background. All functional imaging was performed using a gradient-echo EPI sequence (TR = 2.2s, TE = 27 ms, flip angle = 90°, voxel size = 4mm × 4mm × 4mm, 36 slices) on a Siemens TRIO 3T MRI scanner. An EyeLink 1000 eye-tracking system allowed continuous monitoring of the eyes of the subjects in order to check for periods of prolonged eye closure, potentially indicating sleep. Only one subject (MSC08) demonstrated prolonged eye closures. For details about the data acquisition parameters see [39]. The MSC dataset was preprocessed and analyzed using the NeuroImaging Analysis Kitexecuted within a Ubuntu 16.0.4 Singularity container, running GNU Octave version 4.2.1, and the MINC toolkit version 1.9.15. The first five volumes of each run were suppressed to allow the magnetisation and reach equilibrium. Time series were normalized to the zero mean and unit variance. Each fMRI session was corrected for interslice difference in acquisition time and the parameters of a rigid-body motion was estimated for each time frame. The "scrubbing" method of [63], was used to remove the volumes with excessive motion (frame displacement greater than 0.5). No session was excluded due to excessive motion. Each session had at least 420 volumes after scrubbing, across all subjects, and with a maximum of 810 volumes available. Also, the nuisance parameters were regressed out from the time series at each voxel i.e., slow time drifts, average signals in conservative masks of the white matter and the lateral ventricles, as well as the first principal components of the six rigid-body motion parameters and their squares. The fMRI volumes were spatially smoothed with a 6 mm isotropic Gaussian blurring kernel. A more detailed description of the preprocessing pipeline can be found on the NIAK [12].

2.2. Individual dynamic states of parcellation

We developed an algorithm which identifies dynamic states of brain parcellation at the individual level called Dynamic Parcel Aggregation with Clustering (DYPAC). The

algorithm is composed of four steps as illustrated in Fig. 1. In the first step (Fig. 1A), we select a series of sliding time windows from individual fMRI time series ($W=100$ time points, with $O=10$ time points of overlap, starting from the first time point), and we generate parcellations for the whole cerebral cortex using a k-Means clustering algorithm (number of clusters = 12) [62]. We select fMRI time windows from several runs, such that some time series may combine signals from separate runs. The motivation behind this parcellation step is the identification of brain regions with similar temporal activity for a given time window. We choose the k-Means for its linear complexity and simplicity to run; i.e. no need for many parameters to tune [56, 7]. Our algorithm is parallelized based on the multiprocessing library to run computations on multiple cores. We also used k-Means using scikit-learn implementation [62] to generate parcellations and used the k-Means++ method to choose initial cluster centers in a strategic way in order to speed-up convergence. Although the k-Means algorithm has the drawback of falling into local minima, the k-Means++ initialization helps overcome this limitation with a better exploration of the parcellation solution search space. We also replicate the k-Means parcellations (repetition = 5) for each window with different initializations of the random number generator. This helps identify consistent solutions across different local minima. All the replicated solutions with different seeds are pooled with the set of k-Means parcellations. That is, we simply used all the K-Means based parcellations from different sliding windows as an input for the similarity matrix of the Hierarchical clustering. The total number of K-Means parcellations used in the similarity matrix equals the number of sliding windows multiplied by the number of replications. This result is multiplied by the number of sessions (e.g. if the number of replications=5, number of sliding windows=10, number of sessions=2 then the total number of k-Means parcellations = 100).

In the second step (Fig. 1B), we identify for a particular seed voxel which parcel this voxel is associated with. We thus obtain a binary representation called seed-based parcellation. This step may contribute to the success of our approach, since it allows us to simplify the complexity of the full brain parcellation problem by focusing on the functional activity of one region of interest.

In the third step (Fig. 1C), we calculate the pairwise similarity of all seed-based parcellations generated from different sliding windows. A seed-based parcellation was defined as the subdivision of the entire subnetwork, associated with a given seed, into spatial clusters (i.e., spatially distributed regions/parcels). This similarity is measured with the so-called Dice similarity score. Then, we apply the Hierarchical clustering (here, with the average linkage method) on the Dice-similarity matrix to group seed-based parcellations into dynamic clusters or ‘states’, according to an empirical similarity threshold. This threshold

constrains the clustering of seed-based parcellations by requiring a minimum Dice similarity (here, 0.3) between these parcellations in the same dynamic state, which will in turn infer the number of states in a data-driven way. Given the previously mentioned settings, we hypothesize that some dynamic states of parcellations only appeared in few sliding windows, i.e. inferior to 10% of the total number of available seed-based parcellations. These states might be associated with spurious or non-reproducible spatial brain reconfigurations. Then, we apply another threshold which filtered the identified states based on their number of seed-based parcellations in order to keep only those with more than 10% of the total number of seed-based parcellations. This second threshold will remove noisy states in order to keep reproducible patterns over time. There should be a trade-off between the similarity threshold imposed on the Dice similarity matrix and the threshold that constrains the number of seed-based parcellations in a given state. In other words, a higher Dice score threshold allows to obtain smaller states (i.e., the higher the Dice score, the lower the number of seed-based parcellations of a given state) and thus, it requires a smaller number of seed-based parcellations threshold. This allows us to avoid missing the most interesting states.

In the last step (Fig. 1D), we averaged all seed-based parcellations for a given cluster to get its state stability map. This provides a probability of each voxel to be assigned to a given state as a measure of the stability of voxels with respect to their membership in a particular area. Stability maps represent the spatial signature of each dynamic state of brain parcellations, and the final outcome of the algorithm.

Our method generates dynamic states of parcellations as functionally distributed subnetworks across the brain or local subnetworks surrounding the seed. We also suggest a simple conversion to split subnetworks into multiple spatially contiguous/connected regions instead of spatially distributed parcels. This can be useful in the context of graph theory by considering contiguous regions as nodes in the graph. To this end, we apply a constraint that separates out connected components and assigns to each region a unique state label, using the Nilearn function implementation. We set the minimum region size in volume required to keep after extraction to 50 voxels. This removes small or spurious regions.

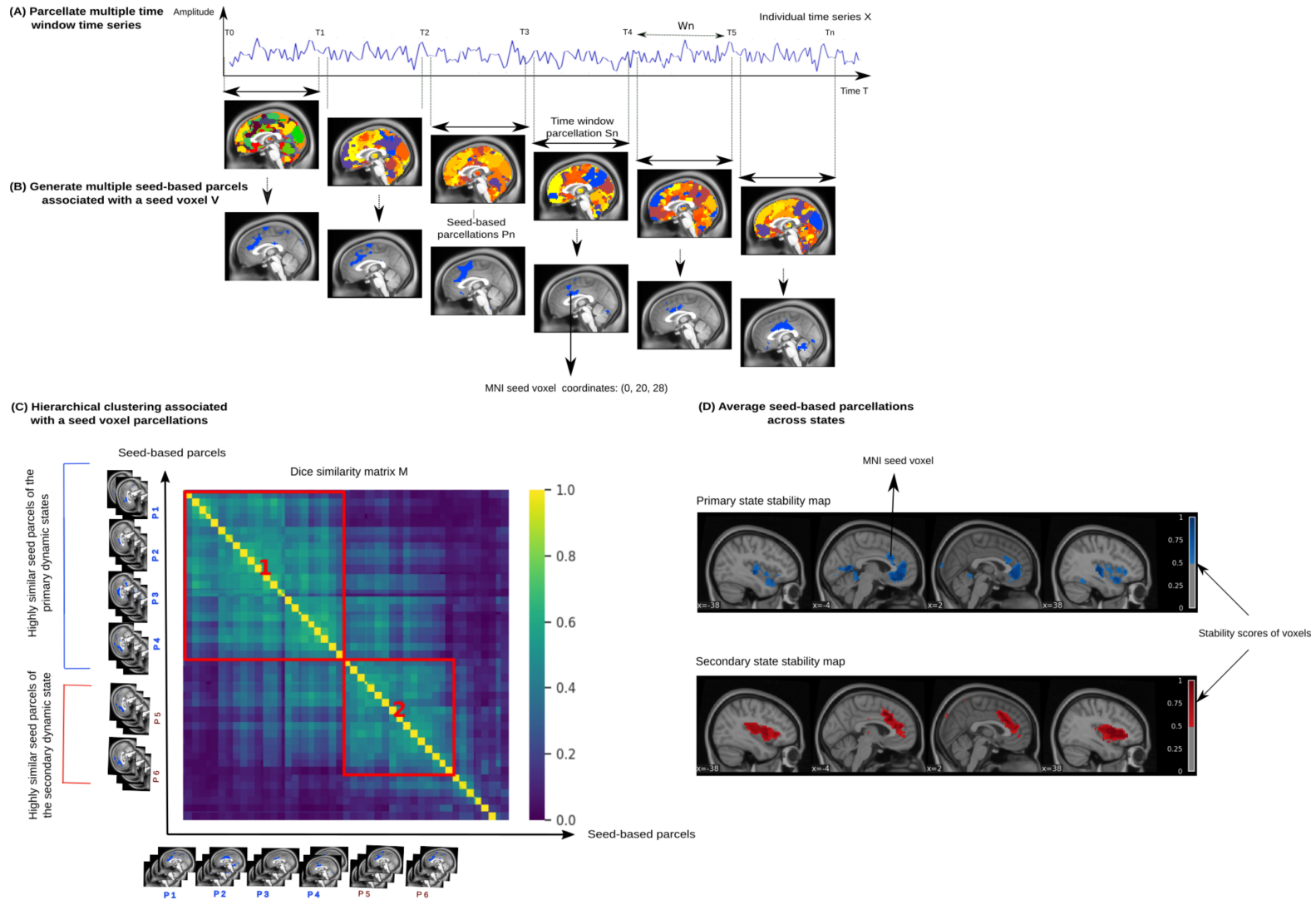


Fig. 1. Subject-specific dynamic parcellation approach (DYPAC).

(A) we generate multiple short time window parcellations for the whole cerebral cortex per subject. (B) Then, we identify the parcel associated with a particular seed-voxel. (C) We calculate the pairwise similarity of these seed-based parcellations based on the Dice similarity score. We apply a Hierarchical clustering on this similarity matrix to group these parcellations into a set of clusters (or dynamic states of parcellations) according to a threshold imposed on the Dice similarity matrix, as well as the number of sliding windows included in the state. (D) For each cluster and each seed, we average all of its seed-based parcellations to obtain the final dynamic state stability maps.

2.3. Choice of the studied subnetworks and their seed

To generate seed-based parcellations, we studied seed voxels from three regions of the MIST parcellation. We picked MNI coordinates (0, -76, 10), (0, 20, 28) and (3, -43, 37) as the respective medoids of the ROIs 90, 6 and 42 corresponding to the posterior medial visual subnetwork (PM-VIS), the dorsal anterior cingulate cortex (dACC) and the posterior cingulate cortex (PCC) subnetworks in the MIST atlas [76]. The choice of seeds was driven by the properties of the networks in the literature. We first chose a seed from an area with the least functional variability [38]: PM-VIS, a core visual area [39]. In the case of the dACC, this region played a prominent role within the salience network, which is involved in many functions including response selection, conflict resolution and cognitive control and it is among the most highly dissimilar networks across subjects [38, 3, 60]. Finally, the PCC is considered as a hub node in the default mode subnetwork. Previous findings reported it as a highly heterogeneous network and suggested it may play a direct role in regulating the focus of attention, memory retrieval, conscious awareness and future planning. Also, functional interaction between the nodes of the salience seed and those of the default mode, including the PCC, during moral reasoning is reported in previous studies [26, 46].

2.4. Spatial reproducibility analysis

To evaluate the quality of the dynamic states of parcellations, we conducted two quantitative analyses. First, we compared the performances of the DYPAC algorithm with a static parcellation algorithm; i.e. the k-Means algorithm. This allowed us to compare the goodness of our dynamic states of parcellations with an existing static state of the art parcellations. Second, we conducted a quantitative consistency analysis at the within-subject level. This allowed us to identify, for a given subject, similarities and variations in the spatial reconfigurations across states and seeds. We conducted a reproducibility analysis for the two analyses.

In both analyses, we half-split the Midnight scan club dataset into two equally sized sets of five independent sessions (of a total of 2.5 hours each) per subject. Each half (about 2.5 hours per subject) was used to replicate several seed-based parcellations that we called replication sets. Then, we generated dynamic states of parcellations based on our proposed approach (See Fig. 1). We sorted the states by decreasing dwell time for the first replication set (i.e. the cumulative durations of all sliding windows associated with a given state, relative to the total duration of the scan). Accordingly, we labeled the states of the first replication set into primary state, secondary state, tertiary state, etc. Prior to comparing our state stability maps, we matched the first set maps to maps from the second set using the Hungarian method [51] which used the Pearson correlation for the spatial matching between state stability maps. The Hungarian method was applied to the within-subject and

between-subjects analysis. A high correlation reflected a strong linear relationship between states maps and is indicative of consistent spatial regions from the two sets of independent data. We replicated these consistency analyses across all states and all subjects of the Midnight scan club dataset. We run both our DYPAC algorithm and the k-Means algorithm 15 times per set with different random seeds due to the stochastic aspect of the k-Means algorithm. This allowed us to verify the sensitivity of both algorithms to local minima.

2.5. Fingerprinting experiment

We finally evaluated the individual specificity of our dynamic states of parcellations by attempting to match dynamic states maps generated from data acquired on the same subjects, when these maps are mixed with maps generated from other subjects. To this end, we cross-correlated a given state stability map with all state stability maps from all subjects. The state stability maps were generated from the split half sets of the Midnight scan club dataset and all these maps were pooled altogether in the fingerprinting. For a given map, we looked for the map that matched the closest map from the pool of all maps. Each seed subnetwork was analyzed separately. A fingerprinting was successful when maximal correlation was observed between a pair of two state stability maps originating from the same subject, otherwise it was considered as a failure. We repeated this experiment for all state maps across all subjects and seeds. We denoted this procedure by the deterministic fingerprinting. We computed the accuracy score as the number of correct states matching over the total number of matched maps. A high accuracy score revealed that state stability maps were reliable to differentiate subjects based on their specific spatial brain reconfigurations. Inversely, a low accuracy score was associated with state stability maps which were either very similar across subjects or unreliable within subjects.

To correct for the different number of identified states for each subject, we run a fingerprinting by chance experiment. To do that, we selected a state map, arbitrarily for each subject. Second, we selected another second state map arbitrarily from the pool of state stability maps of all subjects. If these two maps belonged to the same subject, then the fingerprinting was successful, otherwise it was considered a failure. We repeated this process 1000 times. We computed the accuracy of the fingerprinting by chance and compared it to the deterministic fingerprinting.

2.6. States dwell time reproducibility analysis

We aimed to get a better understanding of the dwell time reproducibility over time of the dynamic states; i.e., the proportion of the total number of sliding windows that were associated with a given state. To this end, we performed a spatial matching of states between

two sets of independent sessions in terms of the Pearson correlation and we reported their associated dwell times in Fig. 12. This matching was based on the Hungarian method. Therefore, only the dwell times associated with spatially reproducible states were included.

2.7. Data records

Scripts used in this study are available on Github ¹. The generation of state stability maps can be executed online via a Jupyter notebook via the binder platform. We have also made available online all the state stability maps for the ten subjects of the MSC dataset on the neurovault website ².

3. Results

3.1. Temporal cluster analysis reveals "dynamic parcellation states" with highly homogeneous parcellations within a state, and highly dissimilar parcellations across states

We first aimed to assess whether homogeneous parcellations can be extracted from short time windows of about 3 minutes duration. We replicated seed-based parcellations on 220 sliding-windows for this purpose. These time windows were extracted from a pool of time samples, generated by randomly concatenating five sessions of imaging data for the Midnight scan club sample, resulting in a total of 2.5 hours of fMRI signals per subject.

For a given seed voxel in the brain, we observed pairs of seed-based parcellations with high homogeneity across different time windows: Dice coefficients between pairs of seed-based parcellations were larger than 0.8, or 0.9 for some seeds and subjects, see Fig. 2. We reported the Dice coefficients distributions for the identified states across the studied subnetworks (see Supplementary Material 4). By contrast, many pairs of seed-based parcellations associated with different sliding windows had very low Dice scores, close to zero, despite being associated with the same seed. For example, in the similarity matrix of subject MSC02, bright colors were associated with some highly homogeneous seed-based parcellations across the diagonal, while the remaining pairs of seed-based parcellations were associated with low Dice scores (blue color). This observation motivated us to develop a "dynamic cluster analysis", grouping seed-based parcellations on sliding windows into a number of homogeneous "dynamic states of parcellations", for a given seed voxel. This approach allowed us to disentangle different dynamic states of parcellations based on the variability of their spatial distribution over time, specifically for a given brain subnetwork.

¹<https://github.com/SIMEXP/dynamic-states-parcellations>

²<https://identifiers.org/neurovault.collection:6642>

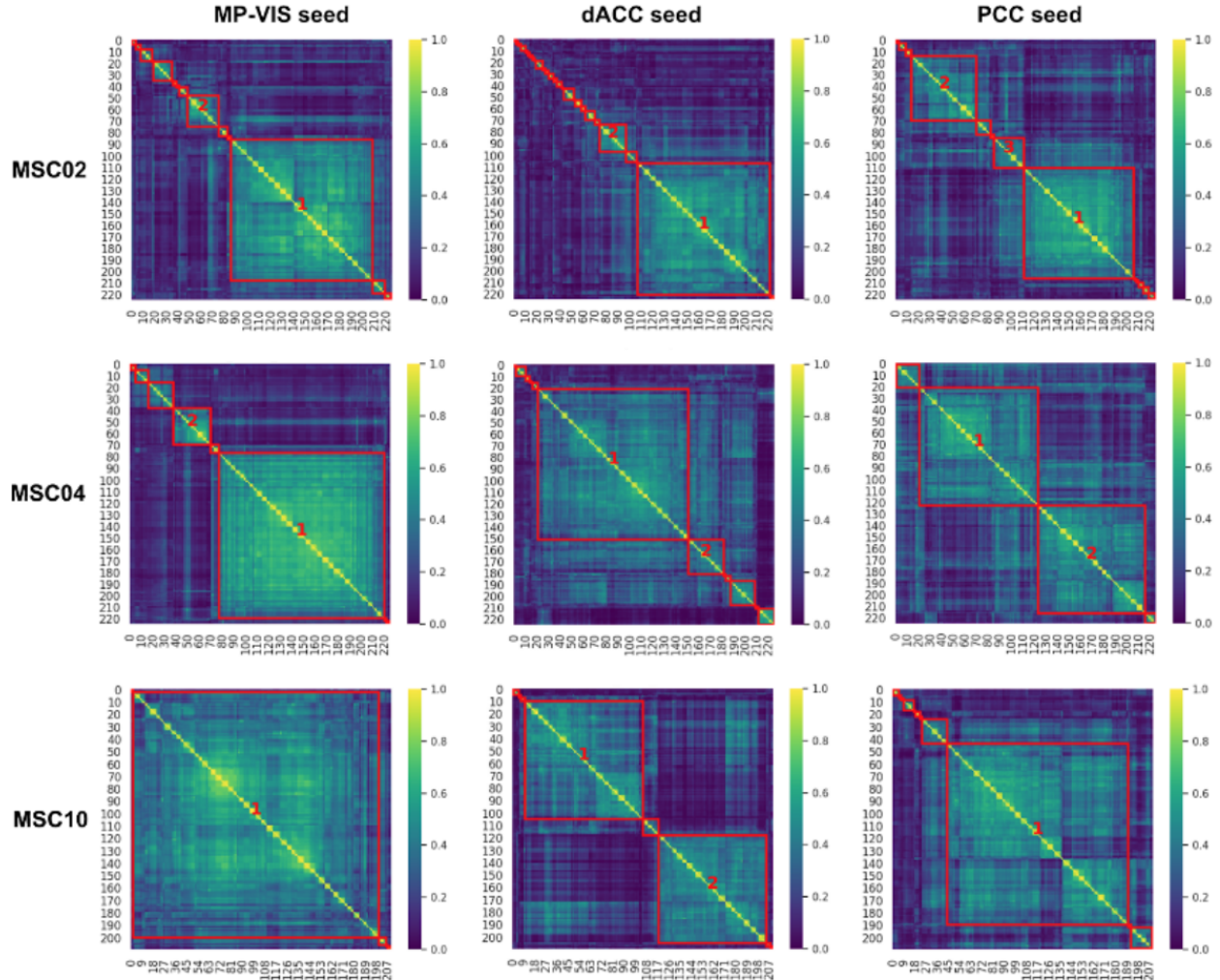


Fig. 2. Dice similarity matrices of seed-based brain parcellations showed groups of highly homogeneous seed-based parcellations and other groups of dissimilar seed-based parcellations.

Each element in the similarity matrix represented the Dice score between a pair of seed-based parcellations. This matrix was calculated, separately for each subject and each seed voxel. Three subjects of the MSC dataset and three seeds were investigated, i.e. the Posterior Medial Visual subnetwork (PM-VIS), the dorsal Anterior Cingulate (dACC) and the Posterior Cingulate Cortex (PCC).

Moreover, our findings suggested the existence of different temporal dynamics for most of the different states either associated with the same seed or different seeds (See Supplementary Materials 7).

Each dynamic state was characterized by its dwell time relative to the total scan duration, i.e. the proportion of the total number of sliding windows that were associated with a given state. We applied two criteria to decide on the number of states for a seed

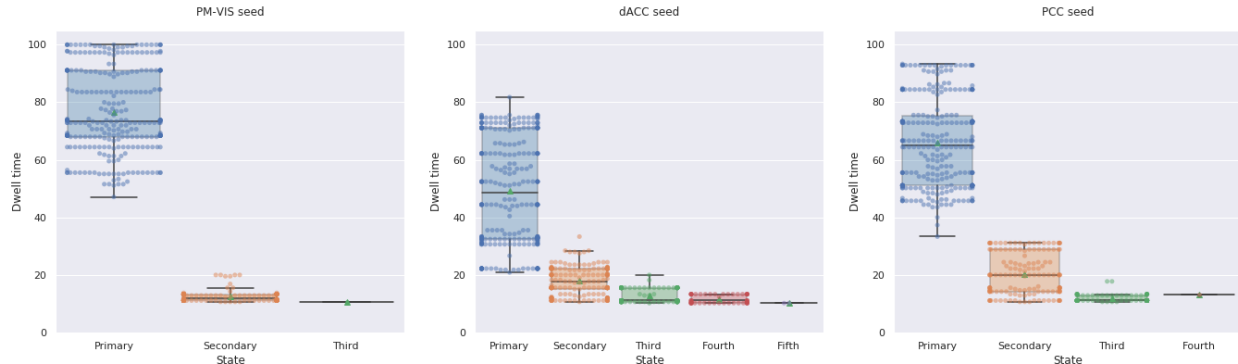


Fig. 3. Subnetworks were multistate with a dominant primary state. We included state dwell times for both sets of independent data.

Three seed subnetworks were investigated including the PM-VIS, the dACC and the PCC subnetworks across ten subjects of the Midnight scan club dataset. The number of replications of seed-based parcellations per sliding window = 5. We reported dwell times from 30 replications of the DYPAC algorithm.

voxel: 1) seed-based parcellations within a state had to exhibit a minimal average level of Dice similarity; i.e. $\text{Dice} > 0.3$, and 2) the dwell time of a given dynamic state needed to be substantial, i.e. larger than 10%. For example, using these two criteria for the PCC seed and subject MSC02, three separate dynamic states of parcellations were identified, and together these dynamic states of parcellations added to about 75% dwell time of all available sliding-windows, see Fig. 2.

For a better understanding of the dwell time distribution across dynamic states, we showed its distribution across the ten subjects of the Midnight scan club dataset and the DYPAC algorithm. The results showed the existence of a dominant state for the three studied subnetworks. For instance, the primary states of the PM-VIS had a median dwell time of 73% over only 11% median dwell time in the case of its secondary states. Similarly, the primary states of the PCC had a median dwell time of 63% over only 20% median dwell time in the case of its secondary states. Moreover, the dACC and the PCC subnetworks were multistate with up to five states in the case of the dACC seed and up to four states in the case of the PCC seed. Less states were observed in the case of PM-VIS with very low dwell time, i.e. 10%. Therefore, the PM-VIS was monostate for most subjects even though some subjects had multistate maps with a dominant primary state (See Fig. 3).

Taken together, these results showed that resting-state brain parcellations fall into a number of highly homogeneous and distinct states over time, at an individual level. We also investigated the impact of different parameters of our DYPAC algorithm on the states dwell time including the window length (Supplementary Material 5.3), the cluster size threshold

(Supplementary Material 5.5) and the smoothing kernel size (Supplementary Material 5.6). Our findings were consistent across different parameters.

3.2. Dynamic states of parcellations had better reproducibility than static parcellations using long acquisitions

We aimed to compare the performance of the DYPAC algorithm to the performance of the k-Means algorithm. DYPAC aggregated seed-based parcellations on short time windows (of about 3 minutes duration) while the k-Means used long time series (about 2.5 hours of resting state functional MRI signal). We compared the within-subject reproducibility of DYPAC stability maps with the k-Means parcellations for three seed voxels associated with the PM-VIS, the dACC and the PCC subnetworks. Our results showed that most DYPAC parcellations outperformed the k-Means parcellations (with long time series) in terms of reproducibility. Particularly, the reproducibility scores of the Dypac primary states outperformed the k-Means parcellations across seeds. For instance, the dACC seed and the DYPAC primary states had a median Pearson correlation of 0.84 over a median correlation of 0.76 in the case of the k-Means parcellations. Similarly, the PCC seed and the DYPAC primary states had a median correlation of 0.93 over a median correlation of 0.63 in the case of the k-Means parcellations (See Fig. 4).

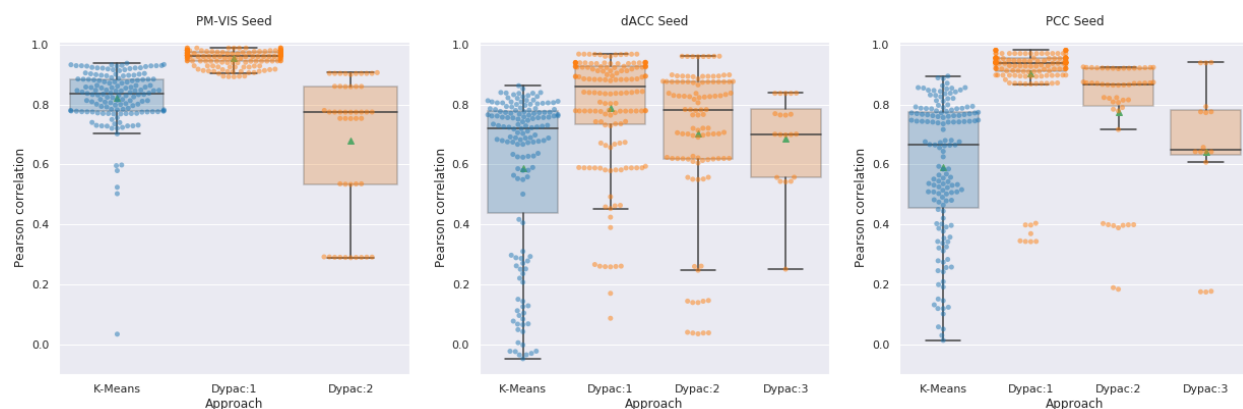


Fig. 4. DYPAC dynamic states of parcellations outperformed static parcellations based on long acquisitions in terms of within-subjects reproducibility.

The within-subject reproducibility scores were computed between the two sets of five independent sessions. Both our DYPAC parcellations and the k-Means parcellations used a total of 2.5 hours per set. Each algorithm was replicated 15 times per set with different seeds. The box plots represented the distribution of within-subject Pearson correlation scores. Dypac:1, Dypac:2 and Dypac:3 denoted the primary, secondary and third states of our DYPAC algorithm. The green dots represented the mean Pearson correlation score for each distribution. We studied three seed voxels from the PM-VIS, the dACC and the PCC subnetworks. Ten subjects of the Midnight scan club dataset were investigated.

Also, DYPAC secondary states had better reproducibility scores compared to the k-Means parcellations reproducibility in the cases of the dACC and the PCC seeds. For instance, the dACC seed and the DYPAC secondary states had a median correlation of 0.79 over a median correlation of 0.76 in the case of the k-Means parcellations. Likewise, the PCC seed and the DYPAC secondary states had a median correlation of 0.84 over a median correlation of 0.63 in the case of the k-Means parcellations (See Fig. 4).

3.3. Visual evaluation of dynamic states of parcellations within- and between-subjects

To assess the reproducibility of parcellations, the DYPAC dynamic parcellation method was applied on independent datasets for each subject, each dataset was composed of five sessions (for a total duration of 2.5 hours of data per subject) available in the MSC sample. We looked at the spatial reconfigurations of dynamic states of parcellations and tried to identify similarities and variations within-state (across replication sets, within-subject), across states (within-subject), and across subjects. We also added an extension for our method to consider spatially contiguous regions, which lead to similar conclusions as distributed parcellations (see Supplementary Material 3).

At the within-state level, we observed a high consistency between the dynamic states of the two replication sets, for all seeds and subjects. For instance, in subject MSC04 and the PM-VIS seed, the primary state maps showed high consistency in the left anterior insula (AI) region (Fig. 5, X=-38) and the supragenual anterior cingulate cortex (sACC) region (Fig. 5, X=-4). Similarly, the secondary state map of subject MSC02 and the dACC seed had consistent dACC region (Fig. 6, X=-4) and left AI region (Fig. 6, X=-38). Finally, the primary and the tertiary state maps of subject MSC02 and the PCC seed, had respectively consistent TPJ (Fig. 7, X=-38) and MPFC (Fig. 7, X=2) across the two replication sets.

Across states, there existed different spatial reconfigurations within the same subject, especially in the cases of the dACC and PCC seeds. We observed some differences locally, at the level of a region surrounding the seed. For example, the region around the dACC seed was circumscribed and anterior in the primary state of subject MSC02, while the region shifted to the posterior direction in the secondary state (Fig. 6, X=-4). We also observed differences involving multiple regions distributed throughout the brain. Using again the example of subject MSC02 and the dACC seed, the entire AI was involved in the primary state, while the secondary state included only the dorsal anterior insula region (dAI) and the ventral anterior insula (vAI) regions (Fig. 6, X=-38). Similar local and distributed variations were observed with the PCC seed, which had up to three states in the case of

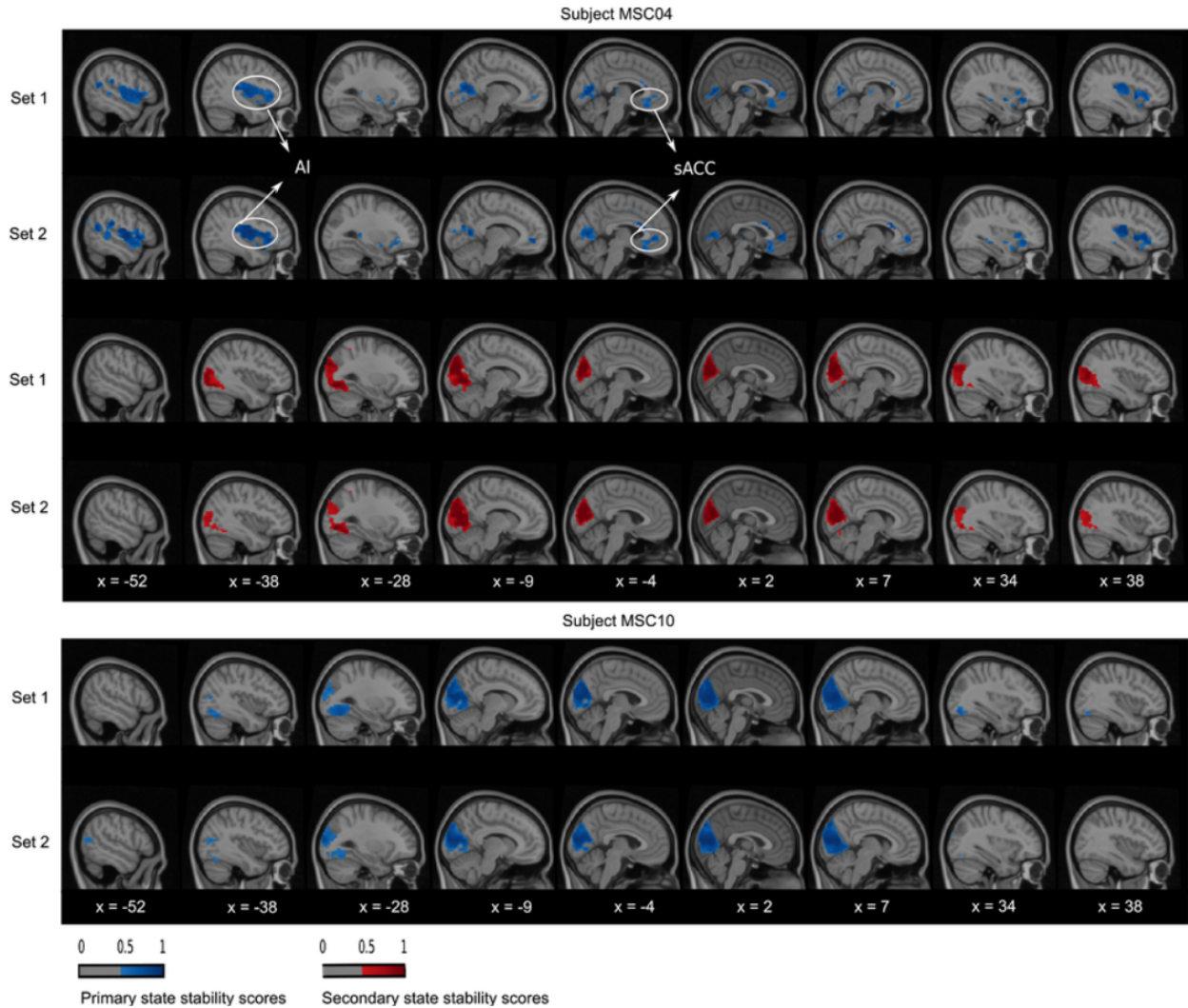


Fig. 5. PM-VIS dynamic state stability maps were similar across sets at the within-subject level and variable across states and subjects.

A complete matching between states was applied using the Hungarian method by maximizing the Pearson correlation between maps. The primary and secondary states were represented in, respectively, blue and red colors. A threshold was applied to keep only stability scores over 0.5.

subject MSC02 (Fig. 7). The primary state had a cortical region following the boundaries of PCC (Fig. 7, X=-4), along with distributed regions in the cerebellum (Fig. 7, X=38) and the left-temporoparietal junction (TPJ) (Fig. 7, X=-38). By contrast, the tertiary state included the PCC core (Fig. 7, X=-4) along the MPFC (X=2). Finally, the secondary state involved almost exclusively an extensive PCC region (Fig. 7, X=-4).

At the inter-subject level, we found some overlapping in regions as well as completely inconsistent regions between subjects in their state spatial maps. As an example of overlapping

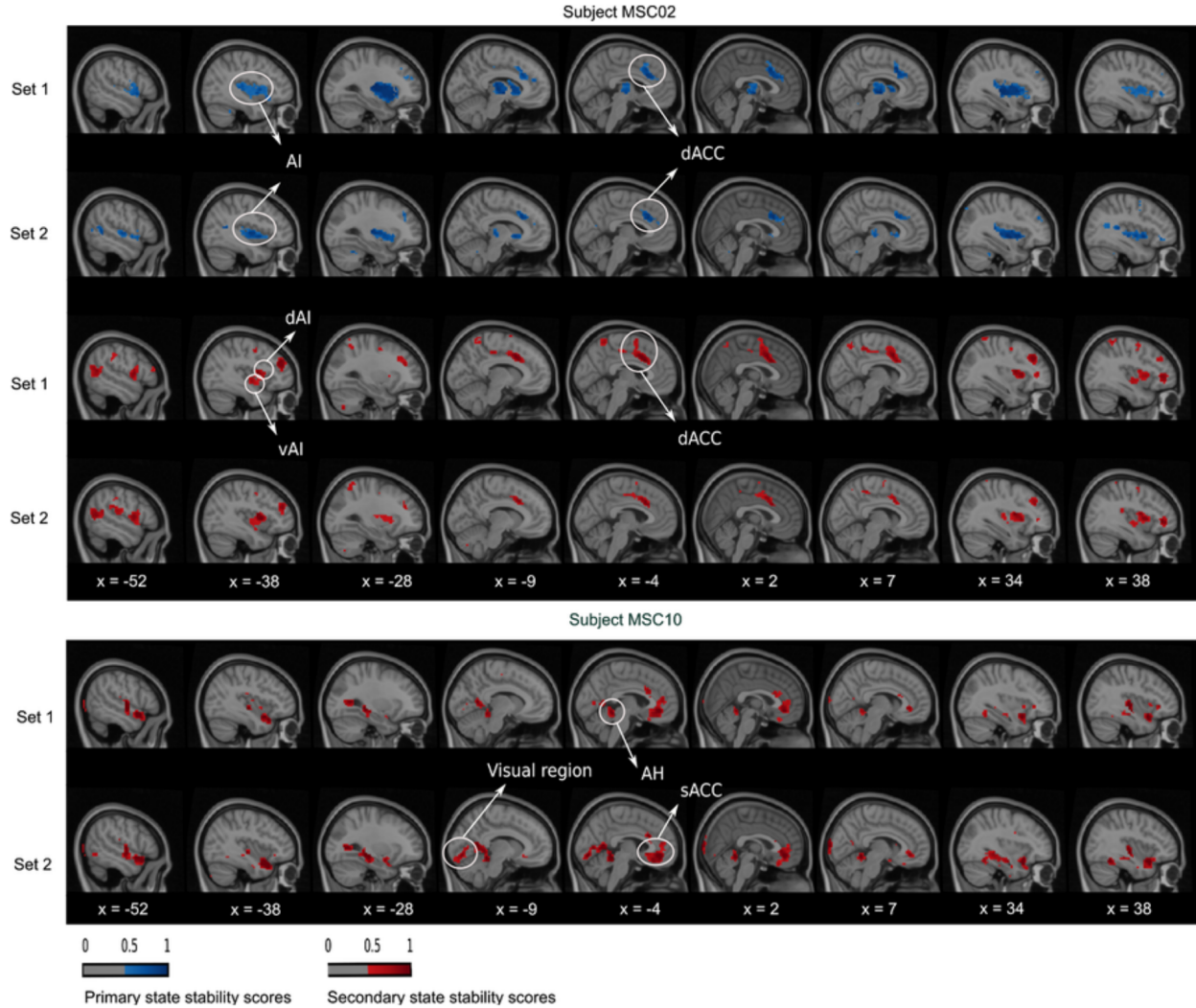


Fig. 6. dACC dynamic state stability maps were similar across sets at the within-subject level and variable across states and subjects.

A complete matching between states was applied using the Hungarian method by maximizing the Pearson correlation between pairwise maps. The primary and secondary states were represented in, respectively, blue and red colors. A threshold was applied to keep only stability scores over 0.5.

regions, we found that the PM-VIS seed was characterized by highly similar visual cortex regions for all subjects (Fig. 5). Only subject MSC04 had an inconsistent primary state map that differed from other subjects maps. Here, we observed that the PM-VIS seed involved AI regions (Fig. 5, X=-38) and sACC regions (Fig. 5, X=-4). It was worth mentioning that no spatial matching was applied between state maps of two different subjects in Fig. 5, 6 and 7. Unlike the PM-VIS seed, the dACC and the PCC seeds had both overlapping and non-overlapping regions when we compared their state maps across subjects. As an example, we found some overlapping regions in the primary states of subjects MSC02 and MSC10 and the dACC seed (Fig. 6), e.g. overlapping AI region (Fig. 6, X=-38) and dACC region (Fig. 6,

X=-4). For the same dACC seed, some subjects had non-overlapping regions such as the secondary states of subject MSC02 and subject MSC10 (Fig. 6). In the secondary state of subject MSC02, the dACC region (Fig. 6, X=-4) occurred as a dominant region along with AI regions (Fig. 6, X=-38). However, the secondary state of subject MSC10 was particularly characterized by the existence of the visual region (Fig. 6, X=-9), the anterior hippocampus (AH) and the sACC (Fig. 6, X=-4).

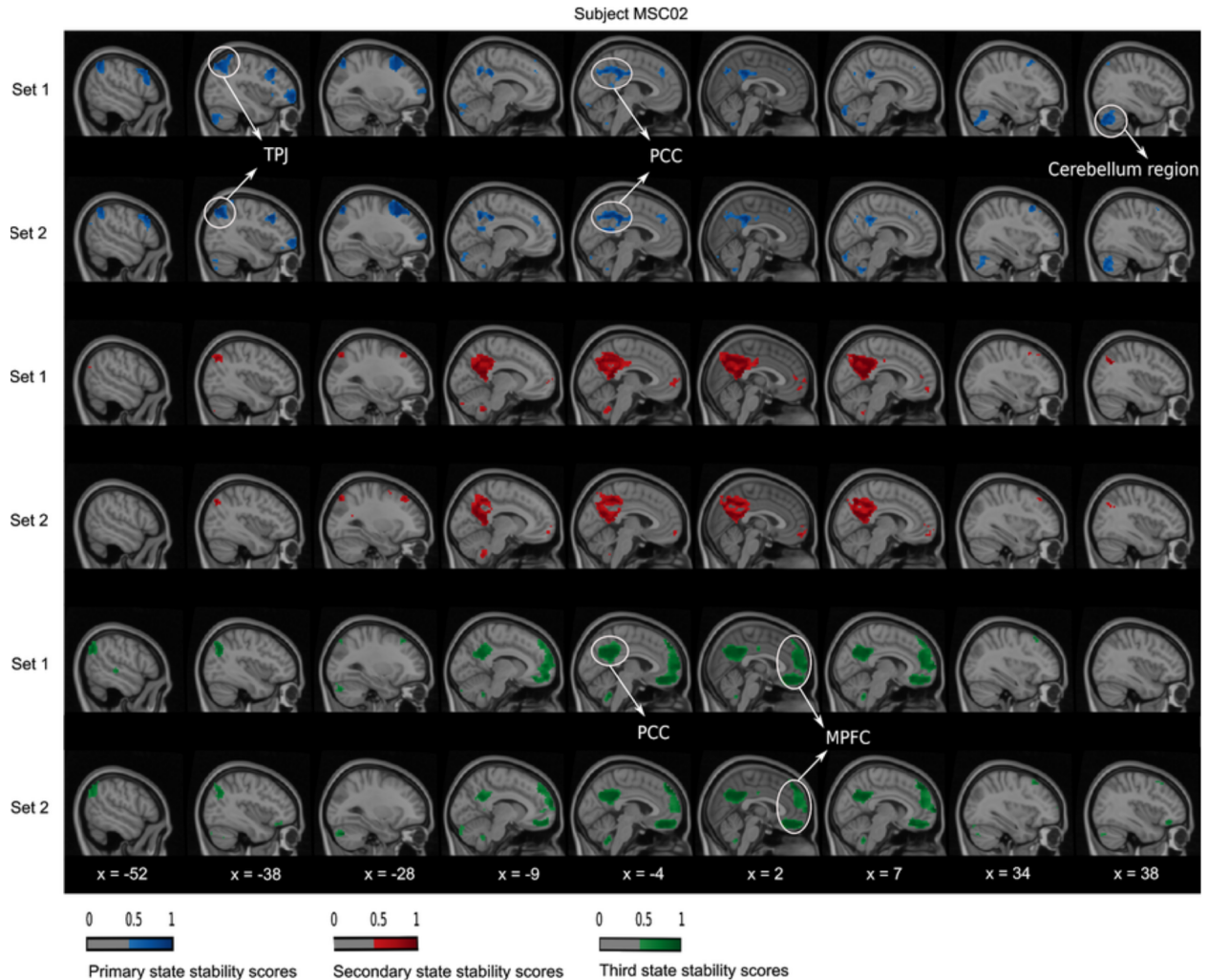


Fig. 7. PCC dynamic state stability maps were similar across sets at the within-subject level.

A complete matching between states was applied using the Hungarian method by maximizing the Pearson correlation between pairwise maps. The primary and secondary states were represented in, respectively, blue and red colors. A threshold was applied to keep only stability scores over 0.5.

3.4. Dynamic states of parcellations are highly reproducible at the intra-subject level

We quantified the reproducibility of our dynamic states of parcellations at the within-subject level. First, we computed the within-subject consistency by means of a spatial similarity measure (i.e. Pearson correlation) between state stability maps associated with two sets of five sessions per subject. Each value in the stability map represented the probability of a voxel to belong to the cluster of a given seed. In these maps, we observed high within-subject reproducibility scores across states and seeds. For instance, most subjects had a reproducibility score that exceeded 0.8 in terms of the Pearson correlation across seeds in the cases of primary and secondary states. Although the third state rarely occurred, it had a high reproducibility score with more than 0.75 reproducibility score, e.g. for the dACC seed, both subjects MSC3 and MSC8 had, respectively, 0.78 and 0.75 Pearson correlation scores. Similarly, in the case of the PCC seed, subject MSC2 had a 0.9 correlation score. The PM-VIS seed was characterized by the highest reproducibility scores compared to the dACC and the PCC with more than 0.9. Except subject MSC04, all subjects had only one highly reproducible state (see Fig. 9). From one set, some states did not have a matched map from the second set and had, therefore a zero correlation score. For example, in the case of the PM-VIS seed and the primary state, subject MSC02 did not have a state in the replication sample that matched the primary state of the discovery sample (see Fig. 9).

3.5. Within-subject reproducibility of dynamic states of parcellations is substantially higher than between-subject reproducibility

In this section, our purpose was to contrast the dynamic states reproducibility within and between subjects. To this end, we cross-correlated their state stability maps as a measure of reproducibility and compared the results at the between- and within-subject levels, where the measures were derived from all the state maps simultaneously (i.e. pooling primary, secondary, etc). Our results showed that within-subject reproducibility scores outperformed the between-subject reproducibility scores with almost two disjoint distributions of correlation scores for all dynamic states and seeds, see Fig. 8. For example, the between-subject PCC-related scores did not exceed 0.78 while most within-subject reproducibility scores exceeded 0.8. Similar findings were observed in the case of the dACC. Only a few cases of the within-subject reproducibility scores fell within the distribution of between-subject reproducibility. We also investigated the impact of different parameters of our DYPAC algorithm on the reproducibility of the dynamic states. We compared the results with different clusters; i.e. number of clusters in 12, 50 (see Supplementary Material 5.1), different window lengths in 30,

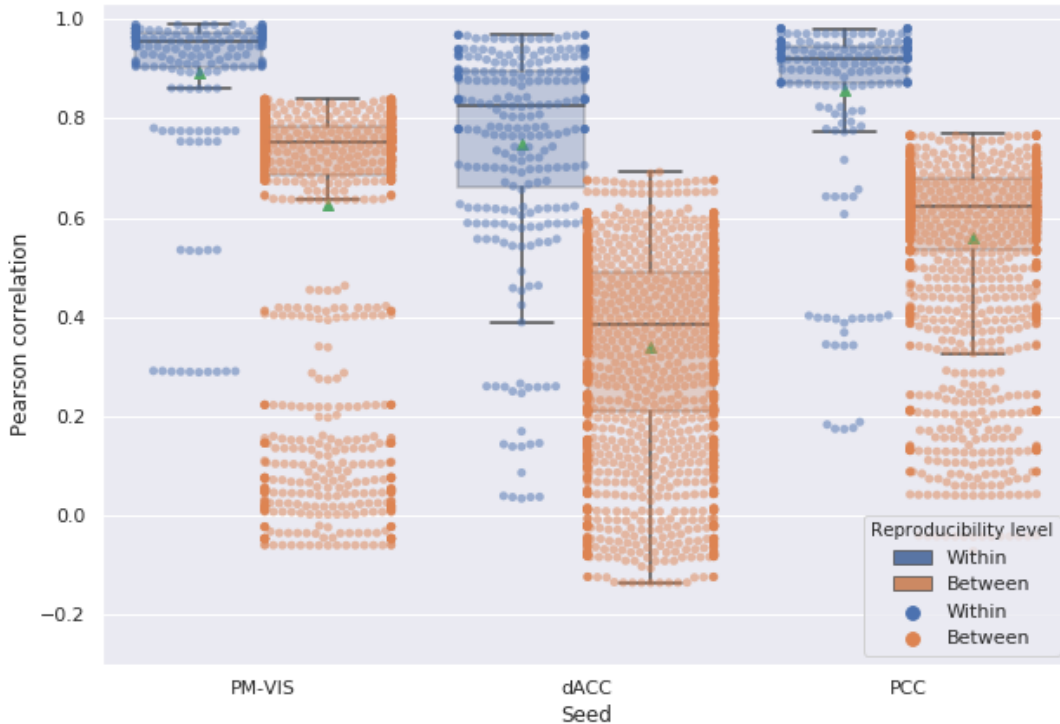


Fig. 8. Within-subject reproducibility scores were higher than between-subject reproducibility scores for most dynamic states of parcellations.

The DYPAC algorithm was replicated 15 times with different seeds for each half of the data set. Number of replications of seed-based parcellations = 5. The green dots represented the mean of the Pearson correlation. We studied the PM-VIS, the dACC and the PCC seeds.

50, 100, 200 (see Supplementary Material 5.2), different cluster size thresholds in 5%, 10%, 20% (see Supplementary Material 5.4), different smoothing kernels in 4mm, 6mm, 8mm (see Supplementary Material 5.6), 15 different seed voxel coordinates from the visual network, the dACC and PCC subnetworks (see Supplementary Material 5.8) and, finally, different number of replications of seed-based parcellations with random seeds; i.e. number of replications in 1,5,30 (see Supplementary Material 5.9). Our conclusions on the reproducibility of the dynamic states of parcellations were valid for different parameters of the algorithm. That is, the within-subject reproducibility analysis robustly outperformed the inter-subject reproducibility across all ranges of parameters that were investigated. Moreover, differences in the distributions of within-subject reproducibility related to parameter changes were only subtle.

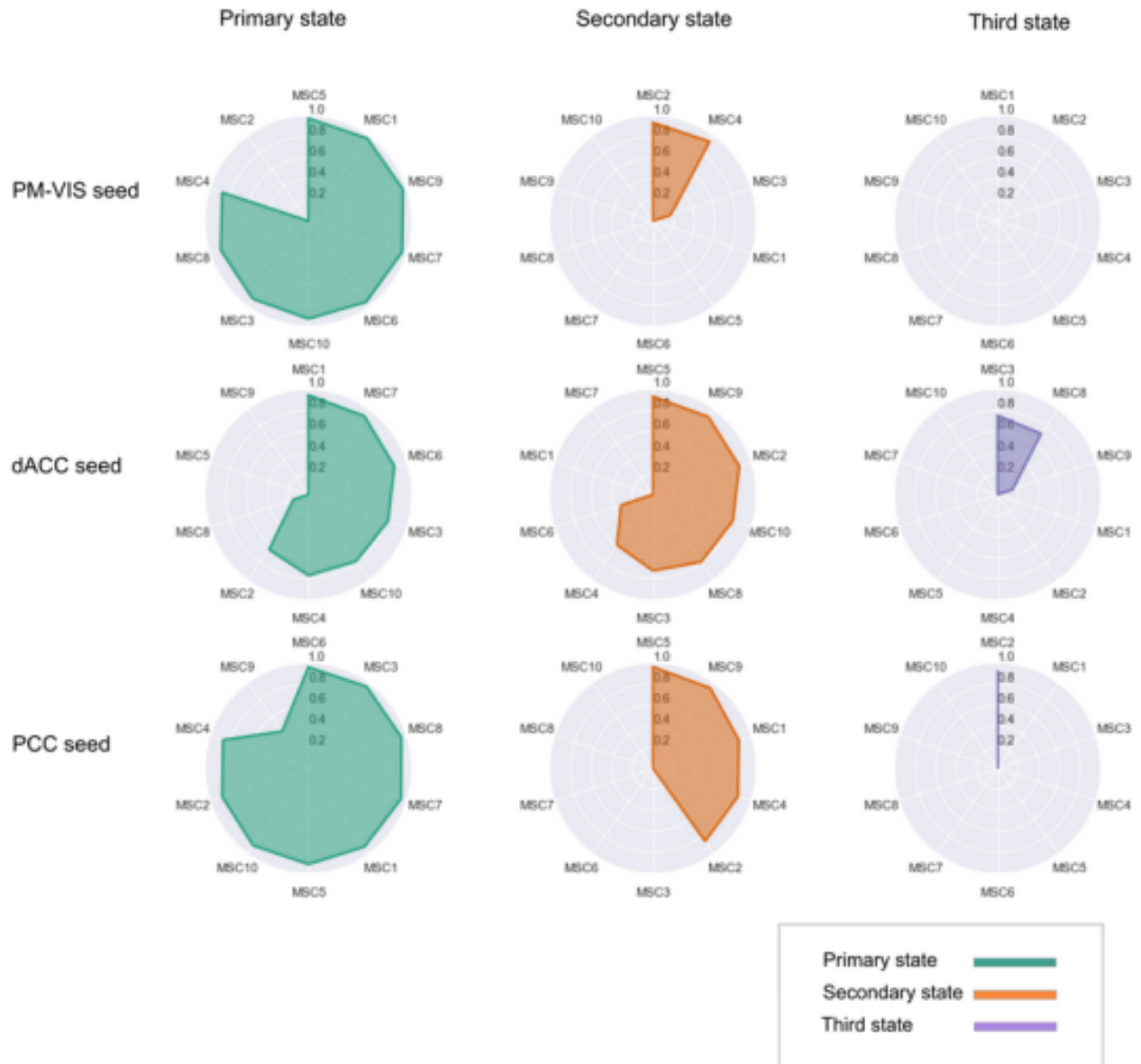


Fig. 9. High spatial reproducibility of dynamic states of parcellations across subjects and seeds.

Most subjects had two dynamic states of parcellations and the highest reproducibility score was found for the primary states of three subnetworks including the PM-VIS, the dACC and the PCC seeds. These reproducibility scores represented the similarity between state stability maps associated with two sets of data for each subject. Each set included five independent sessions. A complete matching between states was applied using the Hungarian method by maximizing the Pearson correlation between pairwise maps. States were sorted and labeled (i.e., primary state, secondary state, third state, etc.) based on their dwell time such that the primary state had the highest dwell time. Ten subjects of the MSC dataset were investigated, i.e. MSC1, MSC2, MSC3, etc.

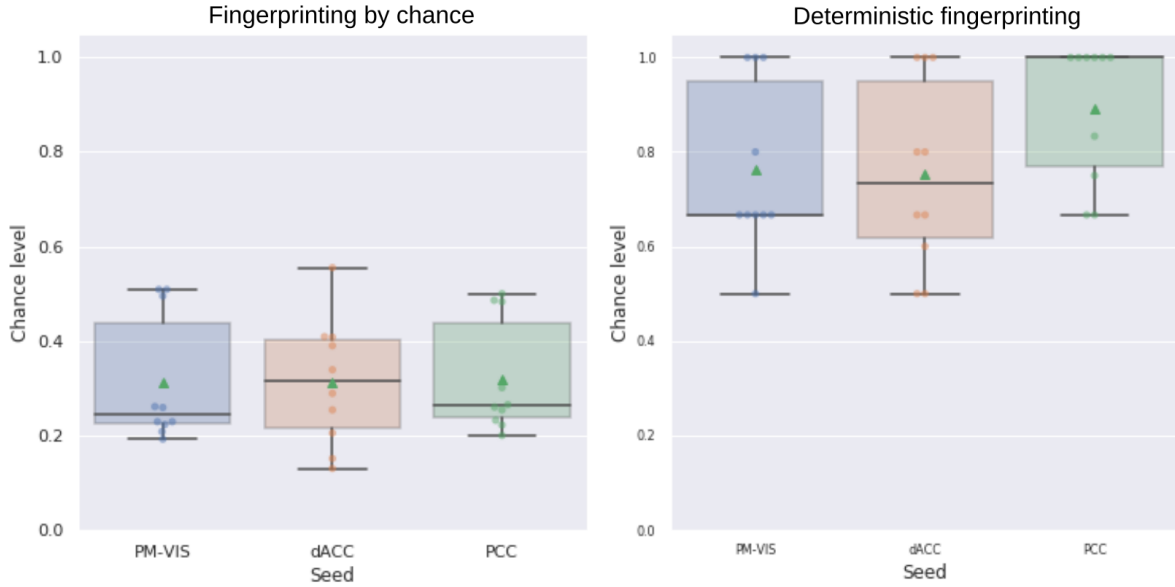


Fig. 10. The deterministic fingerprinting had higher accuracy than the fingerprinting by chance.

The accuracy of the fingerprinting represented the ratio of the successful fingerprinting over the total number of matchings both in the cases of the deterministic fingerprinting and the fingerprinting by chance. The state stability maps were generated from the split half sets of the Midnight scan club dataset and all these maps were pooled altogether in the fingerprinting. For a given map, we looked for the map that matched the closest map from the pool of all maps. In the case of a successful fingerprinting, the matched maps belonged to the same subject. The PM-VIS, dACC and PCC seeds were analyzed separately. Ten subjects of the Midnight scan club dataset were included.

3.6. Dynamic state stability maps can reliably identify subjects

We evaluated the reliability of our dynamic state stability maps in identifying a particular subject among a pool of subjects using the fingerprinting experiment. Due to differences in the number of states per subject, we set up a fingerprinting by chance experiment as a baseline to verify the impact of these differences on the accuracy of the fingerprinting. We evaluated the accuracy of the fingerprinting by chance, and we compared it to the deterministic fingerprinting. Our results showed poor accuracy in the case of the fingerprinting by chance with an average accuracy score of 0.3 compared to the deterministic fingerprinting for which the average accuracy varied between 0.72 and 0.9 across seeds (See Fig. 10). These results showed a low impact of the differences in the number of states on the deterministic fingerprinting and, thus its accuracy scores were reliable.

The results of the deterministic fingerprinting experiment showed high accuracy results across seeds, with more than 0.72 average accuracy scores. This confirmed that many subjects were successfully fingerprinted based on one of their state maps. The highest accuracy results were associated with the PCC seed with an average accuracy of 0.9 across states. Also, the dACC state maps had a high average accuracy score of 0.72. Similarly, the PM-VIS had an average accuracy of 0.78. In the case of a failure, two state stability maps were highly correlated but their maps were not associated with the same subject. Most failures were associated with the PM-VIS and the dACC. Overall, these findings confirmed that our dynamic state stability maps were reliable in the delineation of subjects (See Fig. 10).

We further reported the Pearson correlation scores associated with the deterministic fingerprinting experiment. The distribution of correlation scores across subjects allowed us to quantify the spatial similarity across subjects. Most importantly, failed fingerprinting allowed us to have a better understanding of the degree to which state maps were similar across subjects. Our results showed that the successfully matched maps had high Pearson correlation scores. For instance, the dACC and the PCC seeds had, respectively 0.8 and 0.9 Pearson correlation scores. In the case of failures, the lowest scores were associated with the PM-VIS seed with a 0.5 median correlation, while the highest scores were associated with the PCC seed with a 0.7 median correlation (See Fig. 11). The high Pearson correlation scores in the case of failures; correlation > 0.6 , may be associated with spatially similar maps across subjects. Here, the PCC had the highest spatially similar state maps between subjects. Overall, the high accuracy and the high correlation measures confirmed the reliability of the fingerprinting in identifying a given subject based on his dynamic state map.

3.7. Dynamic state dwell times were not reproducible across replications for the dACC and the PCC seeds

We aimed to get a better understanding of the dwell time reproducibility over time. To this end, we performed a spatial matching of states between two sets of independent sessions in terms of the Pearson correlation. This matching was based on the Hungarian method. Therefore, only the dwell times associated with spatially reproducible states were included. Our results showed an inconsistency between states dwell time for most states between the two sets in the cases of the dACC and the PCC seeds. For instance, the primary state and the dACC seed had 43% median dwell times for the first set over 22% median dwell times for the second set. Similarly, the PCC and the secondary states had 23% median dwell times for the first set over 17% median dwell times for the second set. Unlike the dACC and the PCC seeds, the dwell times of the PM-VIS had higher reproducibility across the

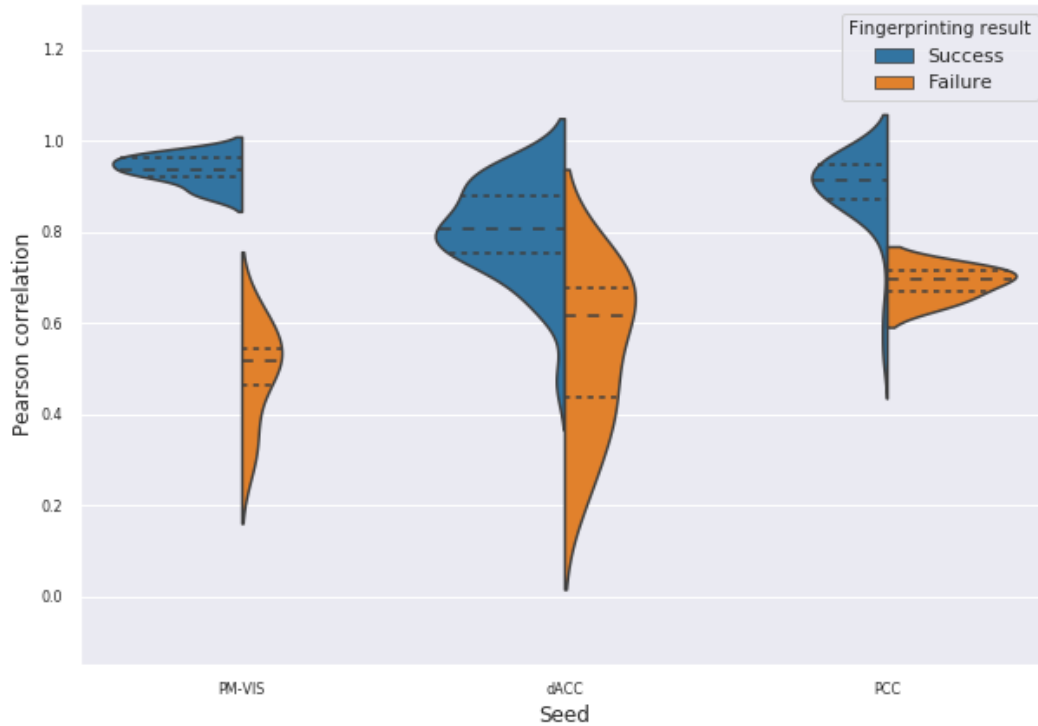


Fig. 11. The fingerprinting experiment showed high reliability of state stability maps in delineating subjects across seeds.

We showed the correlation scores for the deterministic fingerprinting experiment results. The spatial similarity was computed between pairs of state stability maps in terms of Pearson correlation. If the correlated maps were associated with the same subject, it was considered a success fingerprinting (blue color). Otherwise, the correlated maps were associated with different subjects. This was considered a failure (orange color). We studied three seeds from three subnetworks including the PM-VIS, the dACC and the PCC. Ten subjects of the Midnight scan club dataset were included.

two sets. For instance, the primary state and the PM-VIS seed had 62% dwell times for the first set over 64% dwell times for the second set (See Fig. 12). Overall, the dynamic states dwell times were not reproducible across the two sets of independent data for the dACC and the PCC subnetworks. The PM-VIS showed higher levels of consistency between dwell times of the two sets.

We also observed that some states might have a high dwell time but no matching in the second set. For instance, in the case of subject MSC09 and the dACC seed, there existed five states with the following dwell times for the first set: 31.11%, 12%, 11.11%, 10.66%, 10.22%. However, this subject had only two states in the second set with the following dwell times

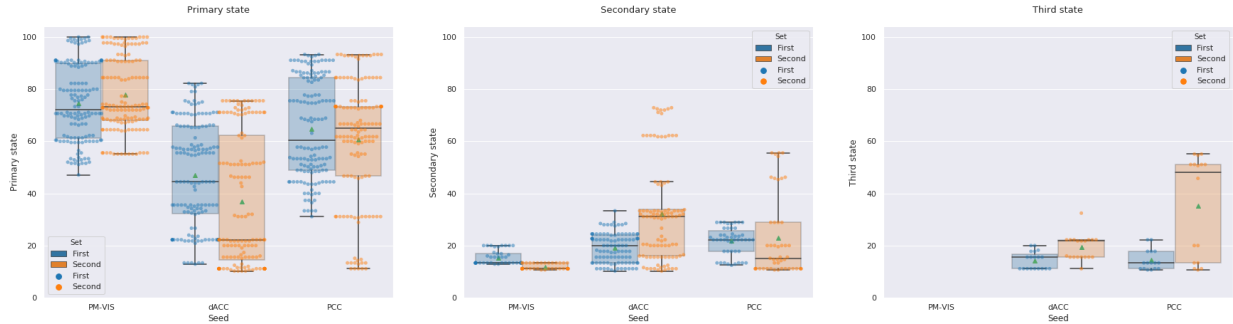


Fig. 12. Dwell time of dynamic states of parcellations was inconsistent across the two sets of independent data in the cases of the dACC and PCC seeds.

The dwell time across states was computed by summing durations of time-windows per state from two sets of five independent sessions for each subject. Three seeds were investigated including the PM-VIS, the dACC and the PCC. The seed-based parcellations number = 5. The number of replications of the DYPAC algorithm = 30. The seed-based parcellations were clustered into 12 clusters. The smoothing kernel = 6 mm, the cluster size threshold = 10%, the Dice threshold = 0.3. Number of timepoints in the window length = 100. All the ten subjects of the Midnight scan club dataset were included. Green dots represented the mean of the dwell time value.

22.22% and 13.33%. After the spatial matching, the matched primary states had 11.11% and 22.22% dwell times for the first and second set, while the secondary state had 10.22% and 13.33% for the first and second sets, respectively.

4. Discussion

In this paper, our overall objective was the identification of dynamic states of brain parcellations in individual resting state fMRI data. Our first main finding was the existence of highly similar spatial parcellations extracted from short time windows, sometimes separated by several days. This led us to propose a dynamic cluster analysis to extract dynamic states of parcellations. These dynamic states were markedly different in terms of the brain regions involved, despite being derived from the same seed region and the same subject. We also found that dynamic states of parcellations were subject-specific, highly reproducible, and are reliable enough to successfully differentiate subjects in a fingerprinting experiment with high accuracy.

In the literature of brain parcellation, the only approach that had consistent findings with our approach was published by Salehi and colleagues [67, 68]. We both suggested an approach that contradicts the notion of a fixed functional parcellation of the brain. The main difference with our work is that Salehi and colleagues generated a different parcellation for different cognitive states in a series of task datasets (i.e. motor task, working memory, rest,

etc.), while in our approach we identified different dynamic states of parcellations in short windows of a single cognitive state (resting state). Our results on dynamic brain parcellation is in line with several studies which showed that brain connectivity is highly dynamic, with recurring spatiotemporal patterns of brain subnetworks [43, 1, 4, 33, 50] both in the case of spatially distributed regions or even in the case of spatially contiguous regions (see Supplementary Material 3). For instance, Irajiloo and colleagues demonstrated the existence of spatial fluid interactions between intra- and inter-networks relationships, emphasizing the dynamic interplay between segregation and integration [44]. Researchers raised the need for new computational methods to reveal robust, interpretable reconfigurations in the complex and high-dimensional feature space of dynamic fMRI data [25]. Such methods would allow a better understanding of the individual differences in internal state changes over short time scales [25]. In the brain parcellation literature, our approach is, to our knowledge, the first attempt to shed light on this dynamic brain organization at fine temporal scale (in the order of few minutes) and at a voxel level (i.e. without reducing the dimensionality in a fine-grain parcellation).

To evaluate the quality of our dynamic states of parcellations, we relied mainly on a reproducibility analysis. We found that our reproducibility scores markedly outperformed static brain parcellation scores [49]. For instance, the reproducibility scores observed in the case of our visual dynamic states of parcellations were near perfect (with an average correlation scores of 0.95), while static visual parcels using about 2.5 hours of data had 0.85 correlation score in average (See Fig. 3). Moreover, visual static brain parcels reported previously in the literature did not reach near perfect similarity scores (with an average Dice score of 0.85) [49]. Such high reproducibility scores were also observed for all three seeds such that dynamic states scores outperformed static parcels scores (See Fig. 4). Another important consideration was that parcels reproducibility depended on the spatial location in the brain in the case of static parcellations, while we observed the same ranges of values for the three seeds. For instance, static parcellations reproducibility ranged between 0.7 and 0.85 average Dice scores in the cases of temporal and visual cortices regions, respectively [49]. Interestingly, our spatial correlation similarity measure exceeded 0.85 for the three seeds for the primary states, and exceeded 0.7 correlation score for secondary and third states for almost all subjects and seeds (See Fig. 4). Recent attempts towards better reproducibility scores of static connectivity measures relied on long fMRI acquisitions [39]. Even though similarity measures were improved (with 10 minutes and 50 minutes of data, authors got, respectively 0.6 and 0.7 average Dice scores), these measures plateaued after 40 minutes of acquired signal with a maximum average of 0.7 Dice score across the ten subjects of MSC dataset. Using long acquisitions of functional MRI data, the comparison of the k-Means parcellations with our dynamic states confirmed that a

dynamic approach of the parcellation problem resulted in improved reproducibility (See Fig. 4). Moreover, higher Dice scores were observed for pairs of seed-based parcellations as extracted from a few minutes (3 minutes) of fMRI data within a given dynamic state (see Supplementary Material 4). Overall, many studies have aimed to derive static brain parcellation approaches either at the group or the individual level (See [5] and [34] for a review) and yet, no technique had highly reproducible individual parcels. This leads to the conclusion that human brain parcellation is a hard ill-posed problem [5]. Our results demonstrated that the main limitation associated with static brain parcellation approaches is neither the quality of employed clustering algorithms, the quality of fMRI data in specific brain regions nor the duration of fMRI acquisitions. The main issue was the incorrect formalization of functional brain parcellation as a static problem, which did not take into consideration the dynamic organization of the brain. Specifically, we showed here that a very basic clustering algorithm, k-Means, leads to highly reproducible parcellation maps when applied on short fMRI time series (a few minutes) with a dynamic approach.

Another important consideration was the comparison of the reproducibility scores within and between subjects. Previous studies reported that within-subject similarity of dynamic states of parcellations was substantially higher than inter-subject similarity [49]. Our quantitative and qualitative evaluation were consistent with these findings (See Fig. 4, 5, 6, 7 and Supplementary Material 5) and we suggest that dynamic states of parcellations captured some of the variability between subjects. To further evaluate the reliability of these dynamic state stability maps in identifying a particular subject from a pool of ten subjects from the Midnight scan club dataset, we implemented a fingerprinting experiment. Even though the fingerprinting failed in a few samples, results on the ten subjects of the MSC dataset showed high scores with 0.6 and 0.7 average accuracy scores for the PCC and the dACC seeds, respectively (See Fig. 11). Due to the small sample size, in the MSC dataset, investigating and validating our results on larger samples in the future, needs to be considered. Researchers already demonstrated the variability in functional connectivity profiles as a reliable fingerprinting to identify subjects from a large group [35]. Our state stability maps were derived from binary cluster maps that eliminated a huge amount of the fine details present in a connectivity map. Despite such dramatic dimensionality reduction in dynamic state maps, it preserved enough relevant information to reliably delineate subjects, especially in the case of highly cognitive networks (i.e., the PCC subnetwork). Our PCC and PM-VIS accuracy scores actually outperformed the accuracy scores of connectivity maps-based fingerprinting in some networks (DMN and the salience), as reported in [8], but this observation may also reflect the fact that we used much longer individual fMRI time series and less subjects.

In the context of our DYPAC algorithm, we showed that the reproducibility of the dynamic states of parcellations were robust to the choice of different parameters (See Supplementary Materials 5). Still, it is important to mention that the number of clusters k is a critical parameter, and can be used to uncover the pseudo-hierarchy of brain subnetworks. Here, we simply checked that “states” could be identified at two different resolutions (i.e., 12 and 50), but it remains to be tested how the number of states vary with resolution, and whether dynamic parcellation follows a pseudo-hierarchical organization as was previously described by static parcellations [76].

Added to the spatial reproducibility analysis, our temporal analysis showed that the dwell times of dynamic parcellations were inconsistent across the two sets of independent data. This may either indicate algorithmic variability in the estimation of dwell times, maybe linked to our choice of threshold on inter-parcel similarity to define states, or physiological variability where a given subject expresses markedly different states over long time scales. We believe the latter to be more plausible, but further validation of this hypothesis would require data which directly manipulate cognitive states across replication states, e.g. using tasks, and is outside of the scope of the present paper. We note however, that the high variability of dwell times across replication sets is probably the factor that drives the "glass ceiling" in reproducibility of static methods: even the definition of what is the primary state can change over long time scales, so averaging across states is not sufficient to stabilize parcel estimates.

Another important aspect of the evaluation of the dynamic states of parcellations was their neurobiological validity. In the absence of brain organization ground truth, current parcellation work capitalized on replication, robustness and convergence as criterias for biological validity. However, the observed variations in the shape and position in the spatial patterns across individuals suggest that these patterns are likely to be associated with physiological or cognitive processes [34]. As pointed out in the previous section, our quantitative results support the neurobiological validity of our dynamic states of parcellations. Qualitatively, we observed that many regions from the dynamic states of parcellations relate to previous literature when studying subnetwork dynamics. For instance, the regions of the dACC state stability maps overlapped with the salience network regions as reported by [3] including the insula and the anterior cingulate cortex (i.e., sACC). Consistently with previous research, we frequently observed the AI and the dACC either in the primary or the secondary states of parcellations. These regions were among the most frequently activated regions in functional neuroimaging research [21, 80]. In some dynamic states of parcellations, we observed a high stability around the motor and premotor regions of the dACC maps (See Fig. 6). This may be explained by the existence of a functional

coupling between the AI and the dACC that facilitates a rapid access to the motor system [3]. Similarly to the dACC seed, we also observed that the PCC is multistate. In the literature, researchers observed a high spatial heterogeneity in the PCC [53, 57], but in our case dynamic states were observed from a single seed and subject. Dynamic states of parcellation of the PCC seed identified, mainly ventromedial prefrontal cortex regions (i.e., including the MPFC), the superior parietal cortex regions and the precuneus. Leech and Sharp surveyed the different studies that investigated the variations in PCC activity with arousal state and its interactions with other brain networks. Authors suggested that the high heterogeneity of the PCC activity was attributed to its important role in regulating the balance between internal and external attentional focus [53]. While higher order seeds revealed multistate maps including the dACC and the PCC seeds, our results showed the PM-VIS was also multistate for some subjects (e.g. subject MSC04) even though most subjects had a monostate PM-VIS subnetwork. Consistently to resting state functional connectivity studies, the visual cortex was considered as a unimodal system since it had a maximal distance along the principal gradient between the visual and the DMN which was considered as a highly heteromodal network (Margulies et al., 2016). Overall, these qualitative observations support our hypothesis that dynamic states are driven by biological validity rather than methodological effects [34].

In addition to biological meaningful brain parcels, researchers hypothesized the existence of some non-meaningful parcels that may occur due to physiological sources or other non-neural effects such as head motion [25, 53]. For the scope of this paper, we did not characterize these sources and we consider this an important follow up question to be studied for more seed regions. However, with the proposed method, a large number of time windows were not associated with a state, if no robust parcel configuration was identified. This feature of the method may help to mitigate the influence of confounding effects on dynamic brain parcellations. However, sources of physiological noise with highly consistent spatial distribution, such as cardiac noise and motion artifacts, may still lead to robust spatial parcellation states. We also showed there was no sessions effect on the identified dynamic states (See Supplementary Material 6).

The main conclusion of this work is that stable brain parcellations emerge from a dynamic analysis considering short time windows, which challenges the notion of a fixed, static brain parcellation estimated from very long time series [39]. But this observation was restricted to a few seed regions in the brain, and an important point of discussion is whether the DYPAC algorithm could be generalized to the full brain ? The core generation of brain parcellations was a simple k-Means algorithm applied on full brain data, and we trust that our conclusions extend beyond the handful of seeds which we considered. We notably

confirmed that our conclusions generalize to many neighboring voxels around selected seed regions, see Supplementary Material 5.8. One way of conceptualizing k-Means as a sparse spatial decomposition: each brain voxel is associated with only one brain parcel, which naturally leads to parcels (or seed-based parcellation) that include only a small portion of the brain (for a large number of clusters k). Similarly, our dynamic analysis can be conceptualized as a sparse temporal decomposition: for each brain voxel, only a subset of time points are associated with a single brain parcellation (or seed-based parcellation), and many time points are associated with no brain parcellations at all. The DYPAC algorithm is, thus a double sparse space-time decomposition technique, which focuses only on temporally recurring and highly spatially similar brain parcels. DYPAC could, in theory, be applied on the brain parcels associated with all brain voxels simultaneously, represented as a basis of one-hot spatial encoding vectors, although the memory cost of the hierarchical clustering step would become prohibitive. We are working on a modified DYPAC algorithm using k-Means both for parcellations generation and aggregation, which scales to the full brain even at high spatial and temporal resolutions. We would like to emphasize at this stage that the idea of applying a space-time decomposition to fMRI data is old, at least as old as spatial independent component analysis, ICA [59] which identified brain networks as a temporal mixture of spatially independent components, including noise. This approach was extensively applied for more than two decades in fMRI research (see survey of [11]). Some more recent space-time decomposition of fMRI data explicitly included a spatial sparsity constraint [29]. Based on a visual comparison of our dynamic states of parcellations and ICA spatial maps, we identified overlapping patterns especially in the case of the visual and the default mode network including the PCC/precuneus, the MPFC regions and regions of the dorsal attentional subnetwork [10, 30, 84]. A major limitation of the ICA technique was the variability of functional resting state signal at the individual level added to its random initialization [10, 30, 84]. An intriguing possibility is that dynamic states of parcellations would converge towards some similar spatial patterns as those identified by ICA, although with superior spatial stability. This possibility will need to be further investigated. Such observation would create a bridge between traditional cluster analysis and space-time decomposition techniques such as ICA, even though the underlying formalism is quite different.

The existence of dynamic states of parcellation could have important implications for graph-based analysis of brain networks. In such circumstances, building brain graphs using these parcels remains a challenging question. As discussed in the preceding paragraph, a full-brain extension of DYPAC would, in practice, be a new flavor of space-time decomposition of fMRI data which may result in improved characterization of brain graphs compared to either static clustering-based parcels or ICA techniques. Unlike traditional static brain parcellation, and like an ICA, our dynamic states of parcellations have spatial overlap (if they associate

with different states of the same voxel). Such types of decompositions are straightforward to apply in a graph-based analysis, as indeed many graph analysis of fMRI data have relied on ICA decomposition to define nodes [83]. The key difference between static parcellations and space-time decomposition is how fMRI data are embedded in the parcels. For static parcellation, the embedding is univariate in nature, as each parcel is treated separately: an average time series is generated for each parcel, or a principal component analysis is applied to the time series inside the parcel [34]. For space-time decomposition, the embedding is multivariate in nature, as the parcels (or spatial modes of decomposition) are treated jointly using a multivariate regression analysis to fit a full brain activity volume at each time point [22]. When applied to traditional static parcellations generated by a cluster analysis, this regression step is equivalent to extracting the average time series per parcel. However, in the presence of overlap between brain parcels the regression solution is different. In this paper, the implementation of DYPAC is a proof of concept and it is restricted to a seed brain region, thus, it is not directly applicable to generate full brain graphs. As mentioned earlier, we are working on a full brain extension of DYPAC. In this case, we intend in the future to assess the practical advantages of DYPAC to study fMRI graph analysis.

5. Conclusion

To summarize, we show that a simple clustering technique such as k-Means can lead to highly reproducible functional parcellation associated with a particular brain seed, even when applied on short fMRI time series (a few minutes). We proposed a method to identify the main states of these dynamic parcellations, and showed that their spatial distributions were subject specific. The main limitation of previous work on functional brain parcellation may be due to the over simplified static parcellation approaches. This limitation may be biasing all neuroimaging analyses that rely on static parcellation as a dimensionality reduction step, including many graph-based neuroimaging analyses. Therefore, we urge the neuroimaging scientific community to replace static brain parcellations by dynamic parcellation approaches, in order to properly capture the rich interactions between brain subnetworks. Dynamic parcellations may thus impact widely applications of brain connectivity in health and disease.

References

- [1]
- [2]
- [3] Salience network.
- [4] E. A. Allen, E. Damaraju, S. M. Plis, E. B. Erhardt, T. Eichele, and V. D. Calhoun. Tracking whole-brain connectivity dynamics in the resting state. *Cereb. Cortex*, 24(3):663–676, Mar 2014.
- [5] S. Arslan, S. I. Ktena, A. Makropoulos, E. C. Robinson, D. Rueckert, and S. Parisot. Human brain mapping: A systematic comparison of parcellation methods for the human cerebral cortex. *Neuroimage*, 170:5–30, 04 2018.
- [6] Salim Arslan and Daniel Rueckert. Multi-level parcellation of the cerebral cortex using resting-state fmri. In *International Conference on Medical Image Computing and Computer-Assisted Intervention*, pages 47–54. Springer, 2015.
- [7] David Arthur and Sergei Vassilvitskii. How slow is the k-means method? In *Proceedings of the Twenty-Second Annual Symposium on Computational Geometry, SCG '06*, page 144–153, New York, NY, USA, 2006. Association for Computing Machinery.
- [8] A. Badhwar, Y. Collin-Verreault, D. Lussier, H. Sharmarke, P. Orban, S. Urchs, I. Chouinard, J. Vogel, O. Potvin, S. Duchesne, and P. Bellec. A dataset of long-term consistency values of resting-state fMRI connectivity maps in a single individual derived at multiple sites and vendors using the Canadian Dementia Imaging Protocol. *Data Brief*, 31:105699, Aug 2020.
- [9] D. S. Bassett, N. F. Wymbs, M. A. Porter, P. J. Mucha, J. M. Carlson, and S. T. Grafton. Dynamic reconfiguration of human brain networks during learning. *Proc. Natl. Acad. Sci. U.S.A.*, 108(18):7641–7646, May 2011.
- [10] C. F. Beckmann, M. DeLuca, J. T. Devlin, and S. M. Smith. Investigations into resting-state connectivity using independent component analysis. *Philos. Trans. R. Soc. Lond., B, Biol. Sci.*, 360(1457):1001–1013, May 2005.
- [11] Christian F. Beckmann. Modelling with independent components. *NeuroImage*, 62(2):891 – 901, 2012. 20 YEARS OF fMRI.
- [12] P. Bellec, S. Lavoie-Courchesne, P. Dickinson, J. P. Lerch, A. P. Zijdenbos, and A. C. Evans. The pipeline system for Octave and Matlab (PSOM): a lightweight scripting framework and execution engine for scientific workflows. *Front Neuroinform*, 6:7, 2012.
- [13] Pierre Bellec, Y Benhajali, Felix Carbonell, C Dansereau, G Albouy, M Pelland, C Craddock, O Collignon, J Doyon, E Stip, et al. Multiscale statistical testing for connectome-wide association studies in fmri. *arXiv preprint arXiv*, 2014.

- [14] Pierre Bellec, Vincent Perlbarg, Saâd Jbabdi, Mélanie Pélégrini-Issac, Jean-Luc Anton, Julien Doyon, and Habib Benali. Identification of large-scale networks in the brain using fmri. *Neuroimage*, 29(4):1231–1243, 2006.
- [15] Pierre Bellec, Pedro Rosa-Neto, Oliver C Lyttelton, Habib Benali, and Alan C Evans. Multi-level bootstrap analysis of stable clusters in resting-state fmri. *Neuroimage*, 51(3):1126–1139, 2010.
- [16] R. F. Betzel, M. A. Bertolero, E. M. Gordon, C. Gratton, N. U. F. Dosenbach, and D. S. Bassett. The community structure of functional brain networks exhibits scale-specific patterns of inter- and intra-subject variability. *Neuroimage*, 202:115990, 11 2019.
- [17] Woolrich M. W. Glasser M. F. Robinson E. C. Beckmann C. F. Van Essen D. C. Harrison S. J. Bijsterbosch, J. D. and S. M. Smith. The relationship between spatial configuration and functional connectivity of brain regions. 2018.
- [18] Amal Boukhdhir, Yu Zhang, Max Mignotte, and Pierre Bellec. Unraveling reproducible dynamic states of individual brain functional parcellation. *Network Neuroscience journal*, 2020.
- [19] R. M. Braga and R. L. Buckner. Parallel Interdigitated Distributed Networks within the Individual Estimated by Intrinsic Functional Connectivity. *Neuron*, 95(2):457–471, Jul 2017.
- [20] U. Braun, A. Schfer, D. S. Bassett, F. Rausch, J. I. Schweiger, E. Bilek, S. Erk, N. Romanczuk-Seiferth, O. Grimm, L. S. Geiger, L. Haddad, K. Otto, S. Mohnke, A. Heinz, M. Zink, H. Walter, E. Schwarz, A. Meyer-Lindenberg, and H. Tost. Dynamic brain network reconfiguration as a potential schizophrenia genetic risk mechanism modulated by NMDA receptor function. *Proc. Natl. Acad. Sci. U.S.A.*, 113(44):12568–12573, 11 2016.
- [21] B. R. Buchsbaum, S. Greer, W. L. Chang, and K. F. Berman. Meta-analysis of neuroimaging studies of the Wisconsin card-sorting task and component processes. *Hum Brain Mapp*, 25(1):35–45, May 2005.
- [22] V. D. Calhoun, T. Adali, G. D. Pearlson, and J. J. Pekar. Spatial and temporal independent component analysis of functional mri data containing a pair of task-related waveforms. *Hum Brain Mapp*, 13(1):43–53, May 2001.
- [23] J. Casorso, X. Kong, W. Chi, D. Van De Ville, B. T. T. Yeo, and R. Li?geois. Dynamic mode decomposition of resting-state and task fMRI. *Neuroimage*, 194:42–54, 07 2019.
- [24] J. E. Chen, C. Chang, M. D. Greicius, and G. H. Glover. Introducing co-activation pattern metrics to quantify spontaneous brain network dynamics. *Neuroimage*, 111:476–488, May 2015.
- [25] J. E. Chen, M. Rubinov, and C. Chang. Methods and Considerations for Dynamic Analysis of Functional MR Imaging Data. *Neuroimaging Clin. N. Am.*, 27(4):547–560, Nov 2017.
- [26] W. Chiong, S. M. Wilson, M. D’Esposito, A. S. Kayser, S. N. Grossman, P. Poorzand, W. W. Seeley, B. L. Miller, and K. P. Rankin. The salience network causally influences default mode network activity during moral reasoning. *Brain*, 136(Pt 6):1929–1941, Jun 2013.
- [27] Wolf D. H. Power J. D. Roalf D. R. Baum G. L. Ruparel K. Shinohara R. T. Elliott M. A. Eickhoff S. B. Davatzikos C. Gur R. C. Gur R. E. Bassett D. S. Ciric, R. and T. D. Satterthwaite. Benchmarking of participant-level confound regression strategies for the control of motion artifact in studies of functional connectivity. *NeuroImage*, (154):174–187, March 2017.
- [28] cneuromod. cneuromod, 2018-2020. <https://www.cneuromod.ca/>, Accessed on July 29, 2020.
- [29] K. Dadi, G. Varoquaux, A. Machlouzarides-Shalit, K. J. Gorgolewski, D. Wassermann, B. Thirion, and A. Mensch. Fine-grain atlases of functional modes for fMRI analysis. *Neuroimage*, 221:117126, Jul 2020.
- [30] J. S. Damoiseaux, S. A. Rombouts, F. Barkhof, P. Scheltens, C. J. Stam, S. M. Smith, and C. F. Beckmann. Consistent resting-state networks across healthy subjects. *Proc. Natl. Acad. Sci. U.S.A.*, 103(37):13848–13853, Sep 2006.

- [31] christian Dansereau, Pierre Orban, and Pierre Bellec. Functional subtypes for prediction in schizophrenia. 2016.
- [32] Lee R. Dice. Measures of the amount of ecologic association between species. *Ecology*, 26(3):297–302, 1945.
- [33] P. Donnelly-Kehoe, V. M. Saenger, N. Lisofsky, S. Kohn, M. L. Kringelbach, J. Schwarzbach, U. Lindenberger, and G. Deco. Reliable local dynamics in the brain across sessions are revealed by whole-brain modeling of resting state activity. *Hum Brain Mapp*, 40(10):2967–2980, 07 2019.
- [34] S. B. Eickhoff, B. T. T. Yeo, and S. Genon. Imaging-based parcellations of the human brain. *Nat. Rev. Neurosci.*, 19(11):672–686, 11 2018.
- [35] E. S. Finn, X. Shen, D. Scheinost, M. D. Rosenberg, J. Huang, M. M. Chun, X. Papademetris, and R. T. Constable. Functional connectome fingerprinting: identifying individuals using patterns of brain connectivity. *Nat. Neurosci.*, 18(11):1664–1671, Nov 2015.
- [36] Alex Fornito, Andrew Zalesky, and Edward Bullmore. *Fundamentals of Brain Network Analysis*. Academic Press, 2016.
- [37] J. Gonzalez-Castillo, C. W. Hoy, D. A. Handwerker, M. E. Robinson, L. C. Buchanan, Z. S. Saad, and P. A. Bandettini. Tracking ongoing cognition in individuals using brief, whole-brain functional connectivity patterns. *Proc. Natl. Acad. Sci. U.S.A.*, 112(28):8762–8767, Jul 2015.
- [38] E. M. Gordon, T. O. Laumann, B. Adeyemo, J. F. Huckins, W. M. Kelley, and S. E. Petersen. Generation and Evaluation of a Cortical Area Parcellation from Resting-State Correlations. *Cereb. Cortex*, 26(1):288–303, Jan 2016.
- [39] E. M. Gordon, T. O. Laumann, B. Adeyemo, and S. E. Petersen. Individual Variability of the System-Level Organization of the Human Brain. *Cereb. Cortex*, 27(1):386–399, 01 2017.
- [40] Liang Han, Neil K Savalia, Micaela Y Chan, Phillip F Agres, Anupama S Nair, and Gagan S Wig. Functional parcellation of the cerebral cortex across the human adult lifespan. *Cerebral Cortex*, 28(12):4403–4423, 10 2018.
- [41] Samuel J. Harrison, Janine D. Bijsterbosch, Andrew R. Segerdahl, Sean P. Fitzgibbon, Seyedeh-Rezvan Farahibozorg, Eugene P. Duff, Stephen M. Smith, and Mark W. Woolrich. Modelling subject variability in the spatial and temporal characteristics of functional modes. *NeuroImage*, 222:117226, 2020.
- [42] HCP. Hcp data releases, 2012-2015. <http://www.humanconnectome.org/>, Accessed on July 12, 2016.
- [43] R Matthew Hutchison, Thilo Womelsdorf, Elena A Allen, Peter A Bandettini, Vince D Calhoun, Maurizio Corbetta, Stefania Della Penna, Jeff H Duyn, Gary H Glover, Javier Gonzalez-Castillo, et al. Dynamic functional connectivity: promise, issues, and interpretations. *Neuroimage*, 80:360–378, 2013.
- [44] A. Iraj, T. P. Deramus, N. Lewis, M. Yaesoubi, J. M. Stephen, E. Erhardt, A. Belger, J. M. Ford, S. McEwen, D. H. Mathalon, B. A. Mueller, G. D. Pearlson, S. G. Potkin, A. Preda, J. A. Turner, J. G. Vaidya, T. G. M. van Erp, and V. D. Calhoun. The spatial chronnectome reveals a dynamic interplay between functional segregation and integration. *Hum Brain Mapp*, 40(10):3058–3077, 07 2019.
- [45] Estrid Jakobsen, Joachim Boettger, Pierre Bellec, Stefan Geyer, Rudolf Ruebsamen, Michael Petrides, and Daniel S Margulies. Subdivision of broca’s region based on individual-level functional connectivity. *European Journal of Neuroscience*, 43(4):561–571, 2016.
- [46] S. R. Jilka, G. Scott, T. Ham, A. Pickering, V. Bonnelle, R. M. Braga, R. Leech, and D. J. Sharp. Damage to the Salience Network and interactions with the Default Mode Network. *J. Neurosci.*, 34(33):10798–10807, Aug 2014.
- [47] Michio Kaku. *The future of the mind: The scientific quest to understand, enhance, and empower the mind*. Doubleday, 2014.

- [48] S. Katyal, Clint Greene, and D. Ress. High-resolution functional magnetic resonance imaging methods for human midbrain. *Journal of visualized experiments : JoVE*, 63:e3746, 2012.
- [49] R. Kong, J. Li, C. Orban, M. R. Sabuncu, H. Liu, A. Schaefer, N. Sun, X. N. Zuo, A. J. Holmes, S. B. Eickhoff, and B. T. T. Yeo. Spatial Topography of Individual-Specific Cortical Networks Predicts Human Cognition, Personality, and Emotion. *Cereb. Cortex*, 29(6):2533–2551, 06 2019.
- [50] O. Korhonen, H. Saarimaki, E. Glerean, M. Sams, and J. Saramaki. Consistency of Regions of Interest as nodes of fMRI functional brain networks. *Netw Neurosci*, 1(3):254–274, Oct 2017.
- [51] H. Kuhn. The hungarian method for the assignment problem. *Naval Research Logistic Quarterly*, 2, 05 2012.
- [52] C. Lanczos. Evaluation of Noisy Data. *Journal of the Society for Industrial and Applied Mathematics Series B Numerical Analysis*, (1):76–85, 1964.
- [53] R. Leech and D. J. Sharp. The role of the posterior cingulate cortex in cognition and disease. *Brain*, 137(Pt 1):12–32, Jan 2014.
- [54] J. Liu, X. Liao, M. Xia, and Y. He. Chronnectome fingerprinting: Identifying individuals and predicting higher cognitive functions using dynamic brain connectivity patterns. *Hum Brain Mapp*, 39(2):902–915, 02 2018.
- [55] X. Liu and J. H. Duyn. Time-varying functional network information extracted from brief instances of spontaneous brain activity. *Proc. Natl. Acad. Sci. U.S.A.*, 110(11):4392–4397, Mar 2013.
- [56] J. MacQueen. Some methods for classification and analysis of multivariate observations. In *Proceedings of the Fifth Berkeley Symposium on Mathematical Statistics and Probability, Volume 1: Statistics*, pages 281–297, Berkeley, Calif., 1967. University of California Press.
- [57] D. S. Margulies, S. S. Ghosh, A. Goulas, M. Falkiewicz, J. M. Huntenburg, G. Langs, G. Bezgin, S. B. Eickhoff, F. X. Castellanos, M. Petrides, E. Jefferies, and J. Smallwood. Situating the default-mode network along a principal gradient of macroscale cortical organization. *Proc. Natl. Acad. Sci. U.S.A.*, 113(44):12574–12579, 11 2016.
- [58] Daniel S Margulies, Justin L Vincent, Clare Kelly, Gabriele Lohmann, Lucina Q Uddin, Bharat B Biswal, Arno Villringer, F Xavier Castellanos, Michael P Milham, and Michael Petrides. Precuneus shares intrinsic functional architecture in humans and monkeys. *Proceedings of the National Academy of Sciences*, 106(47):20069–20074, 2009.
- [59] M. J. McKeown and T. J. Sejnowski. Independent component analysis of fMRI data: examining the assumptions. *Hum Brain Mapp*, 6(5-6):368–372, 1998.
- [60] V. Menon and L. Q. Uddin. Saliency, switching, attention and control: a network model of insula function. *Brain Struct Funct*, 214(5-6):655–667, Jun 2010.
- [61] S. A. Nastase, V. Gazzola, U. Hasson, and C. Keysers. Measuring shared responses across subjects using intersubject correlation. *Soc Cogn Affect Neurosci*, 14(6):667–685, 08 2019.
- [62] Fabian Pedregosa, Gaël Varoquaux, Alexandre Gramfort, Vincent Michel, Bertrand Thirion, Olivier Grisel, Mathieu Blondel, Peter Prettenhofer, Ron Weiss, Vincent Dubourg, Jake Vanderplas, Alexandre Passos, David Cournapeau, Matthieu Brucher, Matthieu Perrot, and Édouard Duchesnay. Scikit-learn: Machine learning in python. *J. Mach. Learn. Res.*, 12(null):2825–2830, November 2011.
- [63] J. D. Power, K. A. Barnes, A. Z. Snyder, B. L. Schlaggar, and S. E. Petersen. Spurious but systematic correlations in functional connectivity MRI networks arise from subject motion. *Neuroimage*, 59(3):2142–2154, Feb 2012.

- [64] J. M. Reinen, O. Y. Chen, R. M. Hutchison, B. T. T. Yeo, K. M. Anderson, M. R. Sabuncu, J. L. Roffman, J. W. Smoller, J. T. Baker, and A. J. Holmes. The human cortex possesses a reconfigurable dynamic network architecture that is disrupted in psychosis. *Nat Commun*, 9(1):1157, 03 2018.
- [65] U. Sakoglu, G. D. Pearlson, K. A. Kiehl, Y. M. Wang, A. M. Michael, and V. D. Calhoun. A method for evaluating dynamic functional network connectivity and task-modulation: application to schizophrenia. *MAGMA*, 23(5-6):351–366, Dec 2010.
- [66] Roser Sala-Llonch, Stephen M. Smith, Mark Woolrich, and Eugene P. Duff. Spatial parcellations, spectral filtering, and connectivity measures in fmri: Optimizing for discrimination. *Human Brain Mapping*, 40(2):407–419, 2019.
- [67] Mehroze Salehi, Abigail S. Greene, Amin Karbasi, Xilin Shen, Dustin Scheinost, and R. Todd Constable. There is no single functional atlas even for a single individual: Functional parcel definitions change with task. *NeuroImage*, 208:116366, 2020.
- [68] Mehroze Salehi, Abigail S. Greene, Amin Karbasi, Xilin Shen, Dustin Scheinost, and R. Todd Constable. There is no single functional atlas even for a single individual: Functional parcel definitions change with task. *NeuroImage*, 208:116366, 2020.
- [69] S. M. Smith, K. L. Miller, S. Moeller, J. Xu, E. J. Auerbach, M. W. Woolrich, C. F. Beckmann, M. Jenkinson, J. Andersson, M. F. Glasser, D. C. Van Essen, D. A. Feinberg, E. S. Yacoub, and K. Ugurbil. Temporally-independent functional modes of spontaneous brain activity. *Proc. Natl. Acad. Sci. U.S.A.*, 109(8):3131–3136, Feb 2012.
- [70] Sphinx. Nilearn, 2010-2015. <http://nilearn.github.io/>, Accessed on July 29, 2016.
- [71] Olaf Sporns. *Networks of the Brain*. MIT press, 2010.
- [72] Olaf Sporns. *Discovering the human connectome*. MIT press, 2012.
- [73] C. Sripada, M. Angstadt, S. Rutherford, D. Kessler, Y. Kim, M. Yee, and E. Levina. Basic Units of Inter-Individual Variation in Resting State Connectomes. *Sci Rep*, 9(1):1900, 02 2019.
- [74] Bertrand Thirion, Gaël Varoquaux, Elvis Dohmatob, and Jean-Baptiste Poline. Which fmri clustering gives good brain parcellations? *Frontiers in neuroscience*, 8(167):13, 2014.
- [75] ucsf. Federal government expenditures and number of affected people with alzheimer’s disease, 2009. <https://ind.ucsf.edu/>, Accessed on July 09, 2016.
- [76] Sebastian Urchs, Jonathan Armoza, Yassine Benhajali, Jolène St-Aubin, Pierre Orban, and Pierre Bellec. Mist: A multi-resolution parcellation of functional brain networks. *MNI Open Research*, 1:3, 12 2017.
- [77] John Darrell Van Horn and Arthur W Toga. Human neuroimaging as a ‘big data’ science. *Brain imaging and behavior*, 2014.
- [78] Zhanxiong Wu, Dong Xu, Thomas Potter, Yingchun Zhang, and The Alzheimer’s Disease Neuroimaging Initiative . Effects of brain parcellation on the characterization of topological deterioration in alzheimer’s disease. *Frontiers in Aging Neuroscience*, 11:113, 2019.
- [79] M. Yaesoubi, T. Adal, and V. D. Calhoun. A window-less approach for capturing time-varying connectivity in fMRI data reveals the presence of states with variable rates of change. *Hum Brain Mapp*, 39(4):1626–1636, 04 2018.
- [80] T. Yarkoni, R. A. Poldrack, T. E. Nichols, D. C. Van Essen, and T. D. Wager. Large-scale automated synthesis of human functional neuroimaging data. *Nat. Methods*, 8(8):665–670, Jun 2011.
- [81] B. T. Yeo, F. M. Krienen, M. W. Chee, and R. L. Buckner. Estimates of segregation and overlap of functional connectivity networks in the human cerebral cortex. *Neuroimage*, 88:212–227, 03 2014.

- [82] BT Thomas Yeo, Fenna M Krienen, Jorge Sepulcre, Mert R Sabuncu, Danial Lashkari, Marisa Hollinshead, Joshua L Roffman, Jordan W Smoller, Lilla Zöllei, Jonathan R Polimeni, et al. The organization of the human cerebral cortex estimated by intrinsic functional connectivity. *Journal of neurophysiology*, 106(3):1125–1165, 2011.
- [83] Q. Yu, Y. Du, J. Chen, H. He, J. Sui, G. Pearlson, and V. D. Calhoun. Comparing brain graphs in which nodes are regions of interest or independent components: A simulation study. *J. Neurosci. Methods*, 291:61–68, 11 2017.
- [84] X. N. Zuo, C. Kelly, J. S. Adelstein, D. F. Klein, F. X. Castellanos, and M. P. Milham. Reliable intrinsic connectivity networks: test-retest evaluation using ICA and dual regression approach. *Neuroimage*, 49(3):2163–2177, Feb 2010.

Chapter 3

Supplementary materials of the first article

Second Article.

Supplementary Materials: Unraveling reproducible dynamic states of individual brain functional parcellation

by

Amal Boukhdhir¹, Yu Zhang², Max Mignotte³, and Pierre Bellec⁴

- (¹) Centre de recherche de l'institut universitaire de gériatrie de Montréal, Montréal, Québec, Canada
Département d'informatique et de recherche opérationnelle, Université de Montréal, Montréal, Québec, Canada
- (²) Centre de recherche de l'institut universitaire de gériatrie de Montréal, Montréal, Québec, Canada
- (³) Département d'informatique et de recherche opérationnelle, Université de Montréal, Montréal, Québec, Canada
- (⁴) Département de psychologie, Université de Montréal, Montréal, Québec, Canada

This article was submitted in Network Neuroscience.

1. Introduction

Functional brain parcellation has been a very active topic of investigation for the past two decades, yet there was no evidence to date of reproducible results at the individual level. In the previous chapter, our cluster temporal analysis showed the existence of "dynamic parcellation states" with highly homogeneous parcellations within a state, and highly dissimilar parcellations across states. We also demonstrated that these dynamic states of parcellations were highly reproducible at the within-subject level.

This chapter is supplementary materials for chapter 2 in which we address different research questions around our proposed dynamic approach. First, our objective is to investigate the hypothesis of the inexistence of a clear structured state in the whole brain parcellation. The validity of this hypothesis shows the importance of applying the seed-based parcellations in our dynamic parcellation approach. We investigate the similarity scores between the whole brain parcellations and the seed-based parcellations associated with three seed subnetworks. We also aim to extend the Dypac algorithm by considering the spatially connected dynamic states instead of the spatially distributed dynamic states. We then replicate all the experiments of Chapter 2 to verify the sensitivity of the parcellation algorithm to its different parameters including the number of clusters, the window length, the cluster size threshold, the smoothing kernels, seed coordinates and the number of replications of the seed-based parcellations. Additionally, we investigate the within-sessions versus the between sessions effect across days on the identified dynamic states. Also, we aim to quantify the synchrony between the dynamics of the different states of parcellations. We generate these dynamic states for the ten subjects of the Midnight scan club (MSC) resting-state dataset.

2. Whole brain parcellations had no clear structured states

We aimed to test the existence of structured states within the whole brain reconfiguration. To this end, we proposed a whole brain parcellation approach across sliding windows. First, we generated several whole brain k-Means parcellations across sliding windows. Then, we computed the adjusted rand index similarity matrix between all pairs of sliding window parcellations. Our results showed very low similarity scores between pairs of k-Means parcellations and no clear structure was detected from the whole brain parcellation. For instance, the adjusted rand index similarity matrix for subject MSC01 did not show any groups of homogeneous sliding window parcellations (See left side Fig. 1). Also, the distribution of the similarity scores between sliding window parcellations were very low; i.e. adjusted rand

index scores < 0.01 (See Fig. right side 1). This clearly showed that, although individual brain subnetworks follow reproducible "states", there was no strong coupling across different brain subnetworks which would lead to full-brain parcellation states.

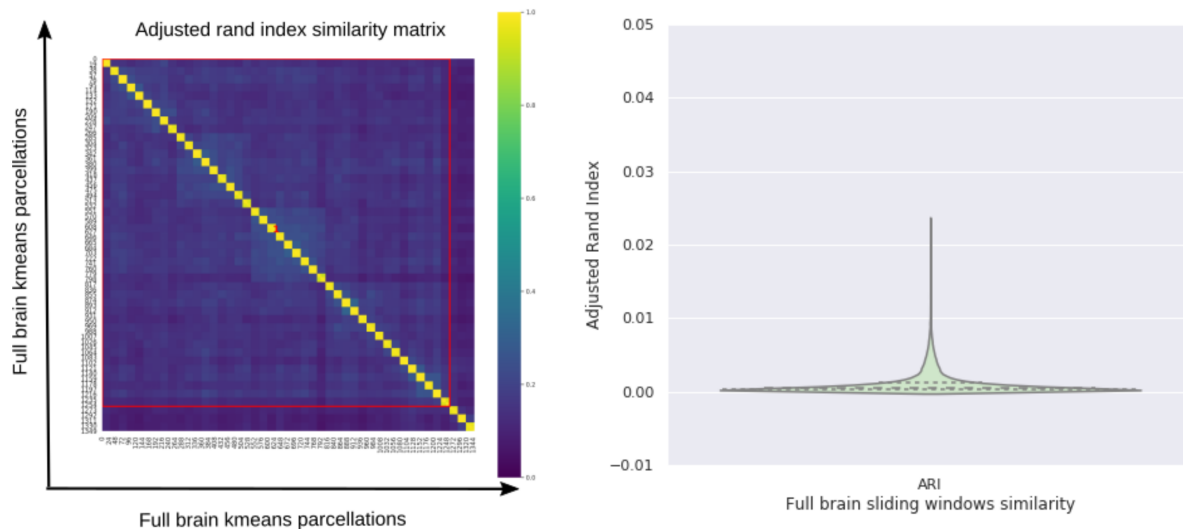


Fig. 1. Similarity between full brain parcellations.

(A) The similarity matrix of the full brain parcellations were dissimilar across sliding windows in the case of subject MSC01. (B) Distribution of the adjusted rand index scores across subjects. The number of timepoints in the window length = 100. The number of sliding window replications = 30. A total of 1349 brain parcellations were included across five sessions. Three subjects of the Midnight scan club dataset were included (MSC01, MSC02, MSC03).

3. Dynamic states can be identified for spatially contiguous regions

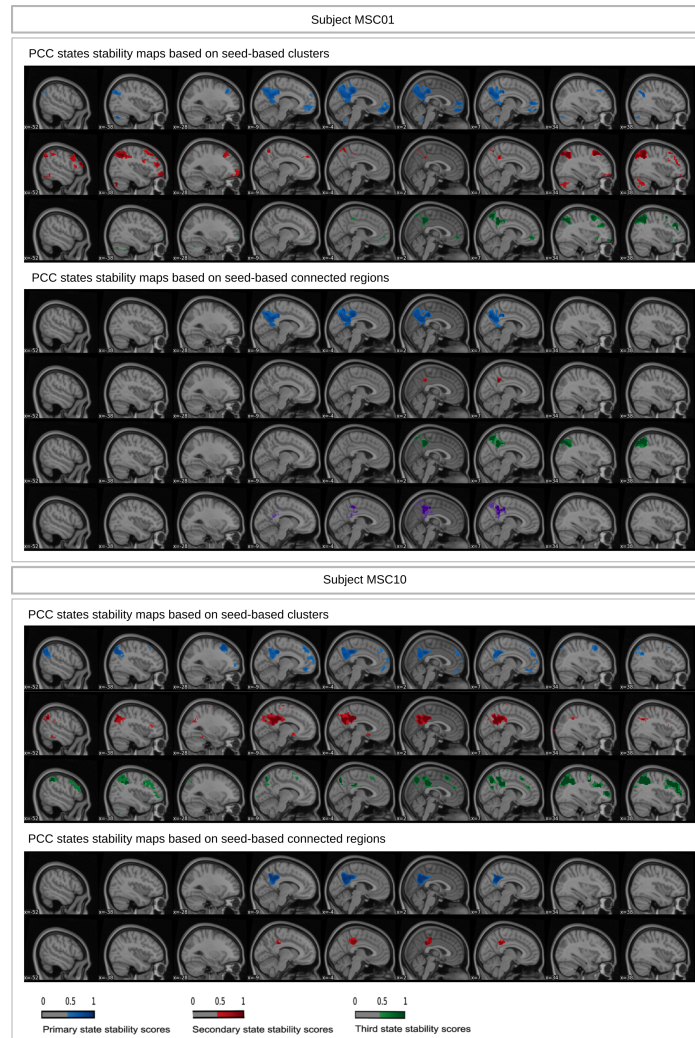


Fig. 2. The spatially contiguous regions were overlapping with the spatially distributed parcels surrounding the seed in the state stability maps of the dACC seed.

The minimum size of regions in the spatially contiguous regions was fixed to 50 voxels. The number of replications of seed-based parcellations = 30. The cluster size threshold = 5%. The seed-based parcellations were clustered into 12 clusters. The smoothing kernel = 6 mm, the cluster size threshold = 10%, the Dice threshold = 0.3, the number of timepoints in the window length = 100. Subject MSC01 and Subject MSC10 of the Midnight scan club dataset were included.

Our dynamic states of parcellations were generated by aggregating several seed-based parcellations distributed over the brain. Many parcellation algorithms proposed in the past have enforced the parcels to be spatially contiguous. In order to make our method

more directly comparable to these prior works, we also implemented an extension in which each distributed parcel was subdivided into spatially contiguous regions. To this end, we extracted the regions having a minimum of 50 voxels. For the dACC and PCC seed voxels, we reported, side-by-side, both the state stability maps associated with the spatially contiguous regions and the distributed regions throughout the brain (see Fig. 2 and Fig. 3). Our results showed a good consistency between the distributed spatial parcels (or clusters) surrounding the seed and the spatially contiguous regions. For instance, the dACC primary state and subject MSC01 had a high overlap between the dACC distributed parcel and the dACC contiguous regions (See Fig. 2, X=4). Also, the distributed dACC parcel of the secondary state and subject MSC10 had a high overlap with the spatially contiguous dACC region of the primary state (See Fig. 2, X=4). In the case of the PCC, the primary states of subject MSC01 were highly overlapping for both the spatially distributed parcel surrounding the seed and the contiguous region (See Fig. 3, X=4).

The aggregation of seed-based contiguous regions suppressed the distributed regions, by construction. For instance, in the primary state and subject MSC10, the sACC region only occurred in the state map of the spatially distributed regions (See Fig. 2, X=4). Also, in the case of subject MSC10 and the third state of the PCC seed, the dorsal attentional regions only occurred in the case of the spatially distributed regions (See Fig. 3, X=38).

Overall, these findings strongly support the existence of multiple states either in the case of the spatially distributed parcels or the case of spatially contiguous regions.

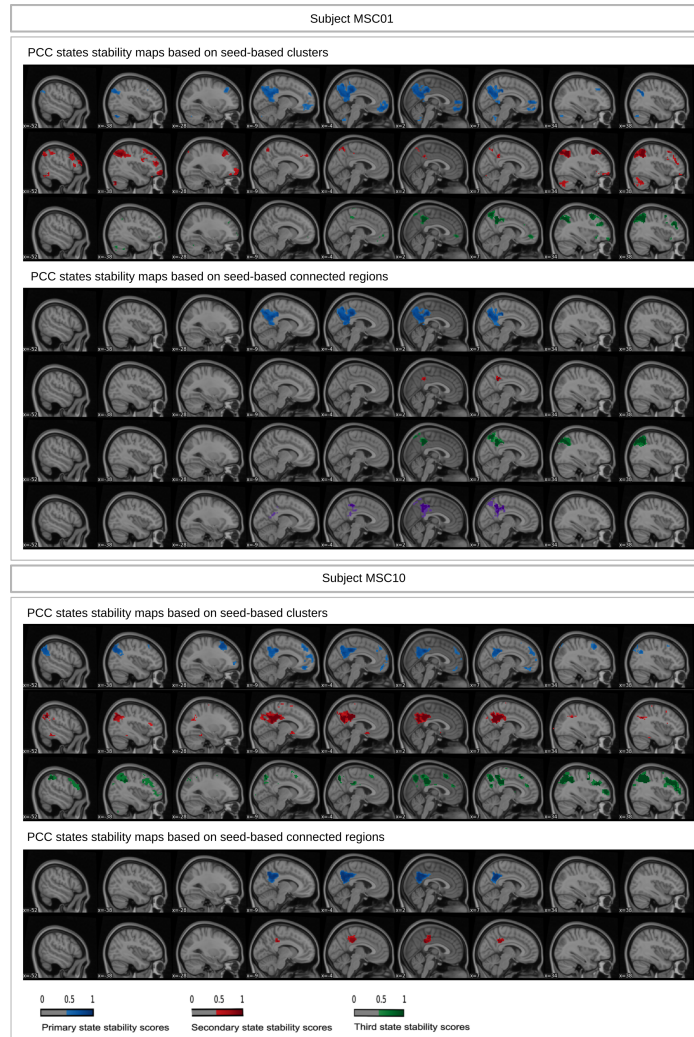


Fig. 3. The spatially contiguous regions were overlapping with the spatially distributed parcels surrounding the seed in the state stability maps of the PCC seed.

The minimum size of regions in the spatially contiguous regions was fixed to 50 voxels. The number of replications of the seed-based parcellations = 30. The cluster size threshold = 5%. The seed-based parcellations were clustered into 12 and 50 clusters. The smoothing kernel = 6 mm, the cluster size threshold = 10%, the Dice threshold = 0.3, the number of timepoints in the window length = 100. Subject MSC01 and Subject MSC10 of the Midnight scan club dataset were included.

4. Spatial similarity of the seed-based parcellations

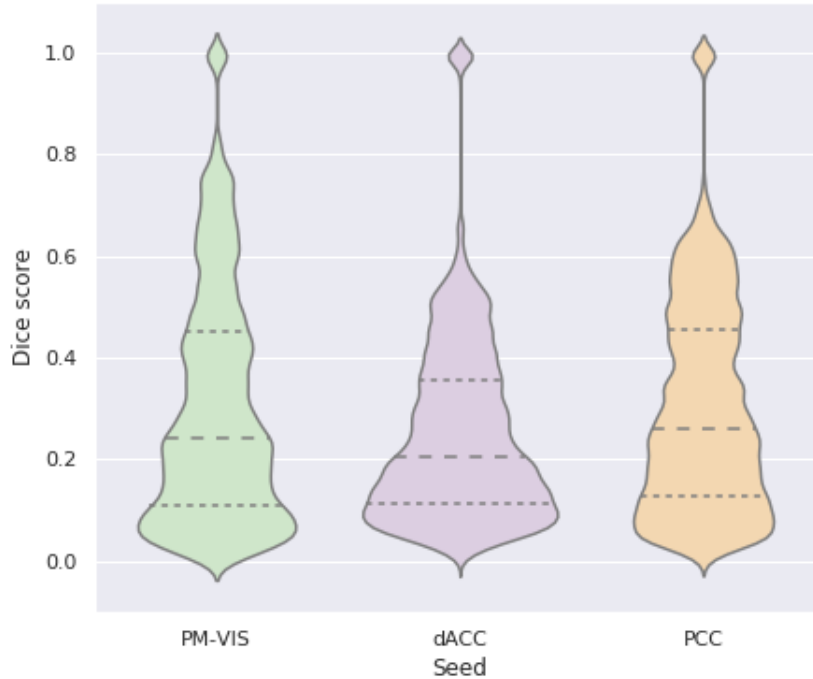


Fig. 4. Spatial similarity between seed-based parcellations in terms of Dice scores.

We included the Dice scores associated with seed-based parcellations. We studied three seed voxels from the PM-VIS, dACC and PCC subnetworks. The smoothing kernel = 6 mm. Number of timepoints in the window length = 100. Ten subjects from the Midnight scan club dataset were included.

We aimed to investigate the spatial similarity of the seed-based parcellations used to generate the dynamic state stability maps. To this end, we reported the Dice scores between pairs of seed-based parcellations across seeds and subjects. Three seed voxels were investigated including PM-VIS, dACC and PCC. Our results showed that some seed-based parcellations were very highly correlated with near perfect Dice scores (around 1) and that Dice scores were around the median 0.23 for the PM-VIS and the PCC seeds while the dACC had a lower median with Dice score = 0.2 (See Fig. 4).

5. The dynamic parcellation approach results are robust to its parameters

5.1. Reproducibility of our dynamic states of parcellations was insensitive to resolution, yet some spatial states were consistent for some subjects and variable for others

We aimed to investigate the effect of the resolution; i.e. the number of clusters, in the seed-based parcellations on the reproducibility of dynamic states of parcellations. To this end, we computed the within- and the between-subject reproducibility. Our results showed that the within-subject reproducibility of the dynamic states of parcellations was higher than the between-subject reproducibility both in the cases of 12 and 50 clusters (See Fig. 5). For instance, the PCC median of the within-subject reproducibility was about 0.9 in both 12 and 50 cluster cases. Moreover, the between-subject reproducibility distributions were highly overlapping across the three seeds.

We also observed that the 50 cluster-based states had overlapping regions with the 12 cluster-based states at the level of voxels surrounding the seed for some subjects and states. For instance, subject MSC01 and the dACC primary states overlapped for the dACC regions surrounding the seed with a larger spatial distribution in the case of the 12 clusters (Fig. 6, X=2). Similarly, the secondary dACC states and subject MSC03 had some overlap in the dACC regions surrounding the seed even though the 12 clusters regions were more lateralized toward the motor regions (See Fig. 7, X=2). Moreover, we observed that the 50 cluster-based states had an overlap with the 12 cluster-based states at the level of the distributed regions throughout the brain. For instance, the dACC primary states and subject MSC01 had an overlap at the level of the insular regions (See Fig. 6, X=38). Similarly, both the dACC secondary states of subject MSC06 involved the insular regions (See Fig. 7, X=38).

Conversely, some subjects and states had either a negligible overlap, inconsistencies in the regions or absence of the 12 clusters based-states. For instance, the 50-clusters primary state in the case of the dACC and subject MSC07 had a very small dACC region compared to the 12-clusters primary state (see Fig. 6, X=4). Also, the 12-clusters secondary state and subject MSC08 had lateralized dACC regions towards the motor regions while the 50-clusters secondary state involved regions from the visual cortex (See Fig. 7, X=4). Also, most states of the third states were inconsistent across scales (See Fig. 8).

Overall, the reproducibility of our dynamic states of parcellations was insensitive to

the scale, yet spatial states were consistent for some states and subjects and variable across others.

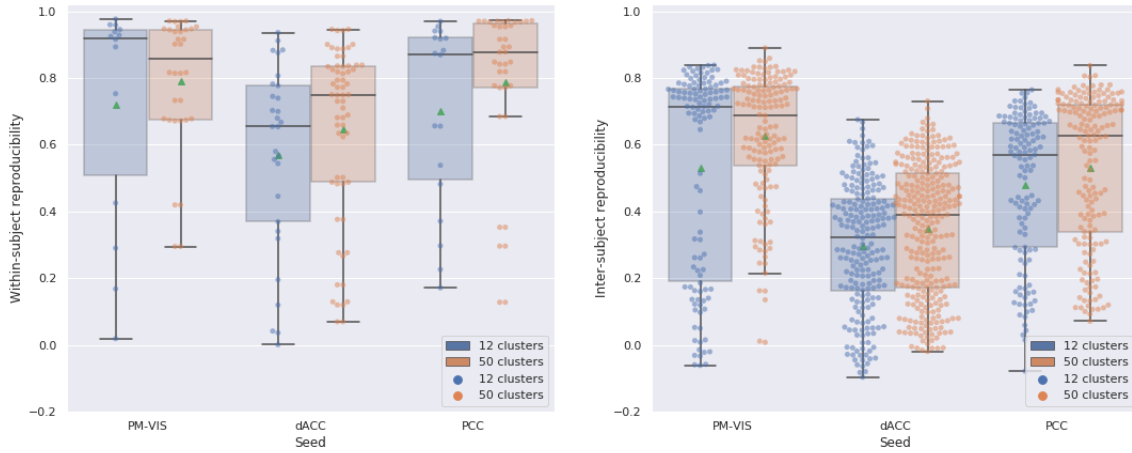


Fig. 5. Within-subject reproducibility of dynamic states was higher at the within-subject level than the between-subject level across scales.

We studied three seed voxels: PM-VIS, dACC and PCC. The number of replications of our Dypac algorithm replications with different seeds = 30. Number of replications of seed-based parcellations = 30. The cluster size threshold = 5%. The seed-based parcellations were clustered into 12 and 50 clusters. The smoothing kernel = 6 mm, the Dice threshold = 0.3. The number of timepoints in the window length = 100. Ten subjects of the Midnight scan club dataset were included.

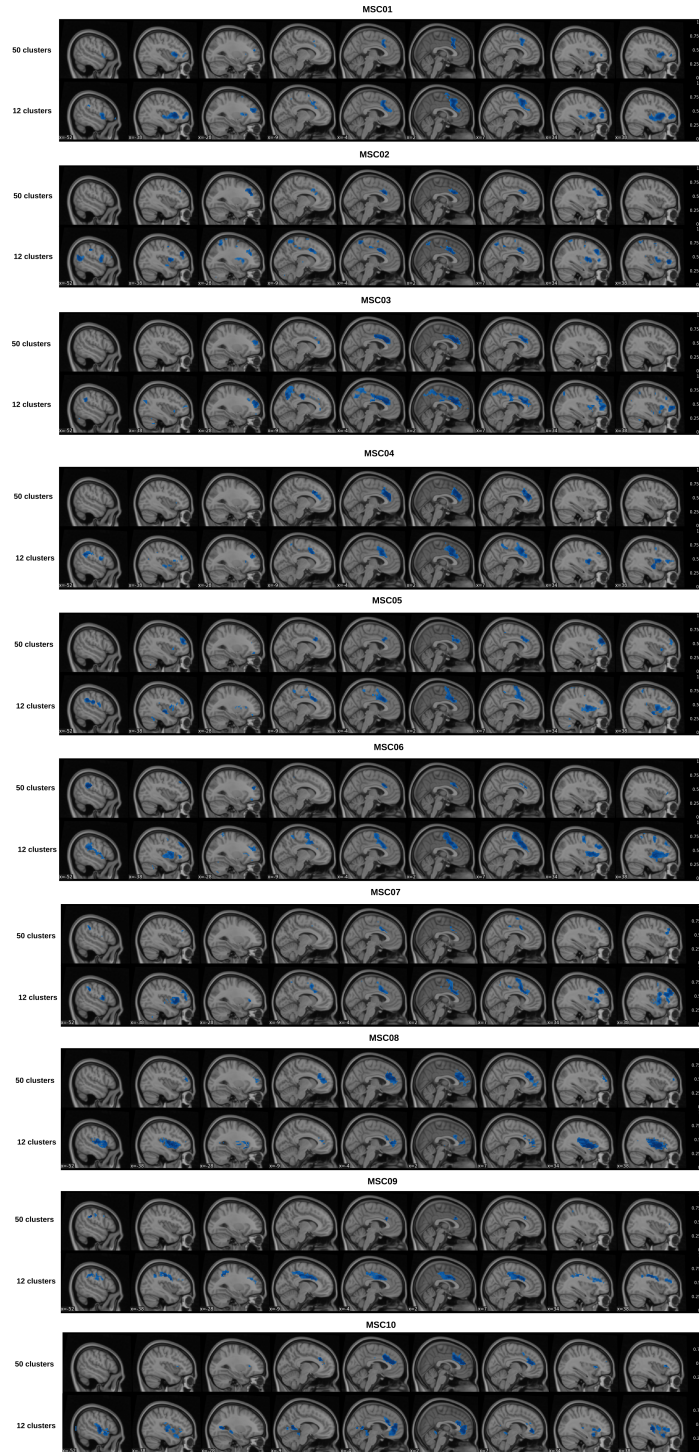


Fig. 6. Primary states were overlapping across scales for some subjects in the case of the dACC seed.

We studied three seed voxels: PM-VIS, dACC and PCC. The number of replications of our Dypac algorithm replications with different seeds = 30. The number of replications of the seed-based parcellations for each replication = 30. The cluster size threshold = 5%. The seed-based parcellations were clustered into 12 and 50 clusters. The smoothing kernel = 6 mm, the Dice threshold = 0.3. The number of timepoints in the window length = 100. Ten subjects of the Midnight scan club dataset were included.

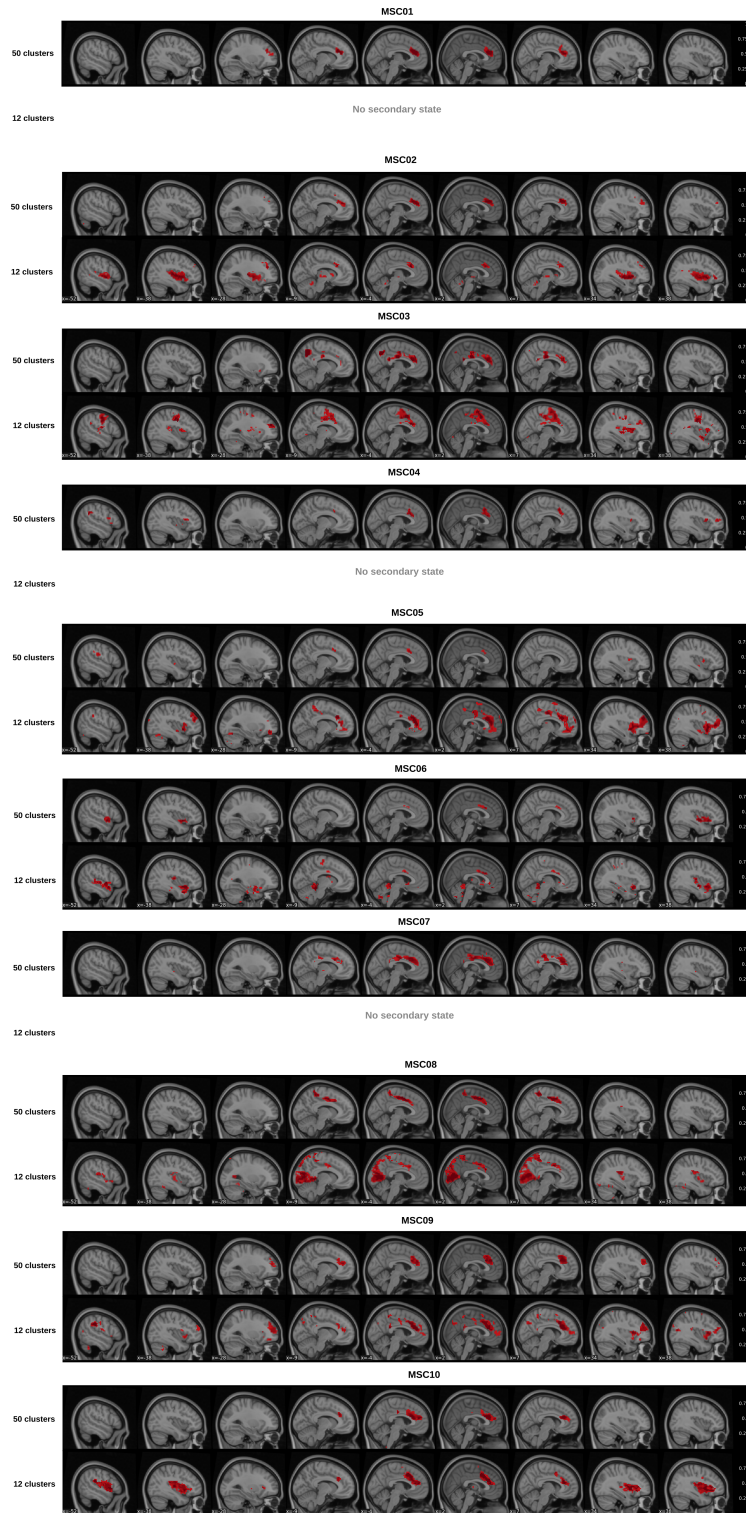


Fig. 7. Secondary states were overlapping across scales for some subjects and states and variable across others in the case of the dACC seed.

We studied three seed voxels: PM-VIS, dACC and PCC. The number of replications of the seed-based parcellations for each replication = 30. The cluster size threshold = 5%. The seed-based parcellations were clustered into 12 and 50 clusters. The smoothing kernel = 6 mm, the Dice threshold = 0.3. The number of timepoints in the window length = 100. Ten subjects of the Midnight scan club dataset were included.

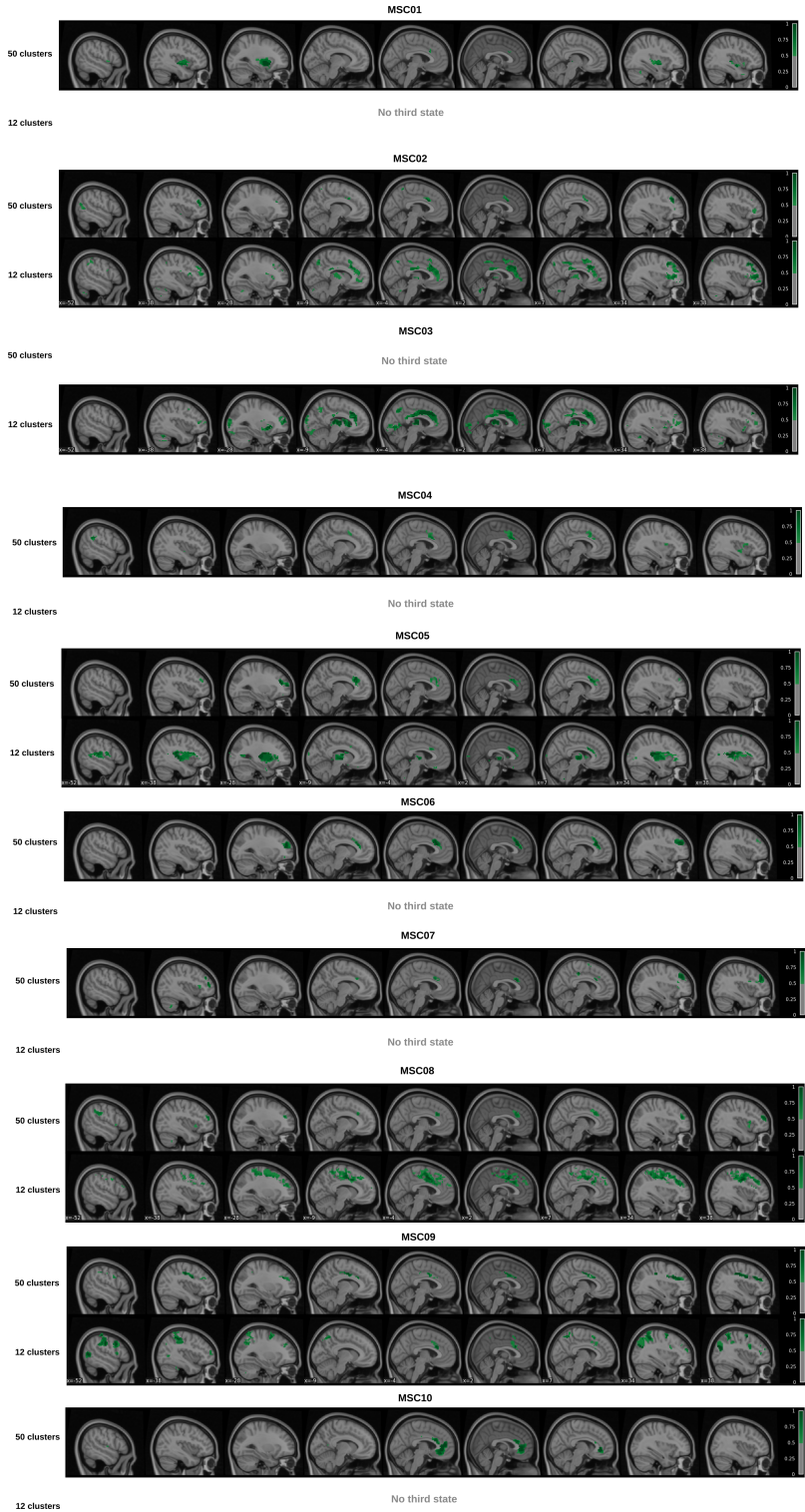


Fig. 8. Third dACC dynamic states were inconsistent across scales. We studied three seed voxels: PM-VIS, dACC and PCC. The number of replications of our Dypac algorithm replications with different seeds = 30. The number of replications of the seed-based parcellations for each replication = 30. The cluster size threshold = 5%. The seed-based parcellations were clustered into 12 and 50 clusters. The smoothing kernel = 6 mm, the Dice threshold = 0.3. The number of timepoints in the window length = 100 timepoints. Ten subjects of the Midnight scan club dataset were included.

5.2. Dynamic states can be identified at different time scales

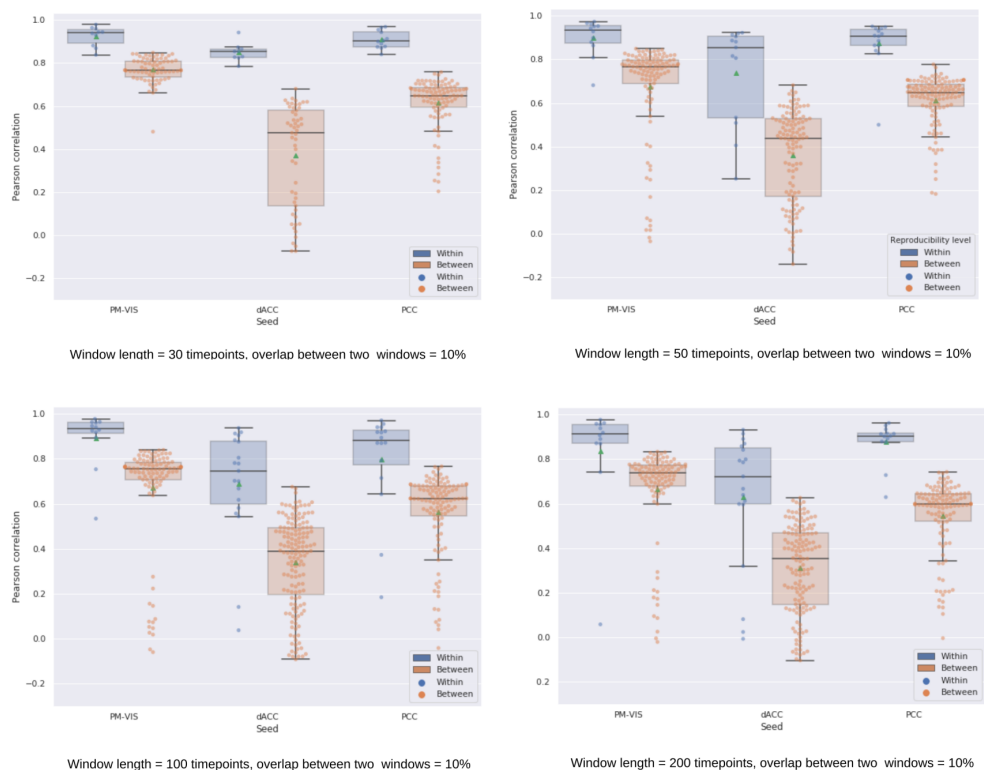


Fig. 9. Within-subject reproducibility scores were higher than between-subject reproducibility scores for most dynamic states of parcellations.

In the case of 30 timepoints, some subjects did not capture any state. We studied three seed voxels: PM-VIS, dACC and PCC. The number of replications of seed-based parcellations = 30. The seed-based parcellations were clustered into 12 clusters. The smoothing kernel = 6 mm, the cluster size threshold = 10%, the Dice threshold = 0.3. Ten subjects of the Midnight scan club dataset were included.

We aimed to investigate the effect of the window length on the reproducibility of the dynamic states of parcellations. Thus, we computed the within- and the between-subject reproducibility for different window lengths; i.e. the number of timepoints = 30, 50, 100, 200 in window lengths for the ten subjects of the Midnight scan club dataset. Our results showed that within-subject reproducibility was higher than between-subjects reproducibility for all window length values (see Fig. 9). For instance, in the case of 50 timepoints, within-subject reproducibility scores had a Pearson correlation median > 0.83 across seeds. However, between-subjects reproducibility scores had a correlation median < 0.78 across seeds (See Fig. 9). Similarly, in the case of 200 timepoints, within-subject reproducibility scores had a Pearson correlation score > 0.7 , however, between-subjects reproducibility scores had a median correlation score < 0.7 (See Fig. 9).

For different number of timepoints in the sliding windows, the studied subnetworks were multistate in the case of the dACC and the PCC seeds while the PM-VIS was monostate for most subjects and at multiple time scales. However, we observed the absence of states for some subjects in the case of 30 timepoints. The sensitivity of the k-Means algorithm to local minima due to few time samples may be at the origin of this limitation.

5.3. Subnetworks were multistate with a dominant primary state for different window lengths

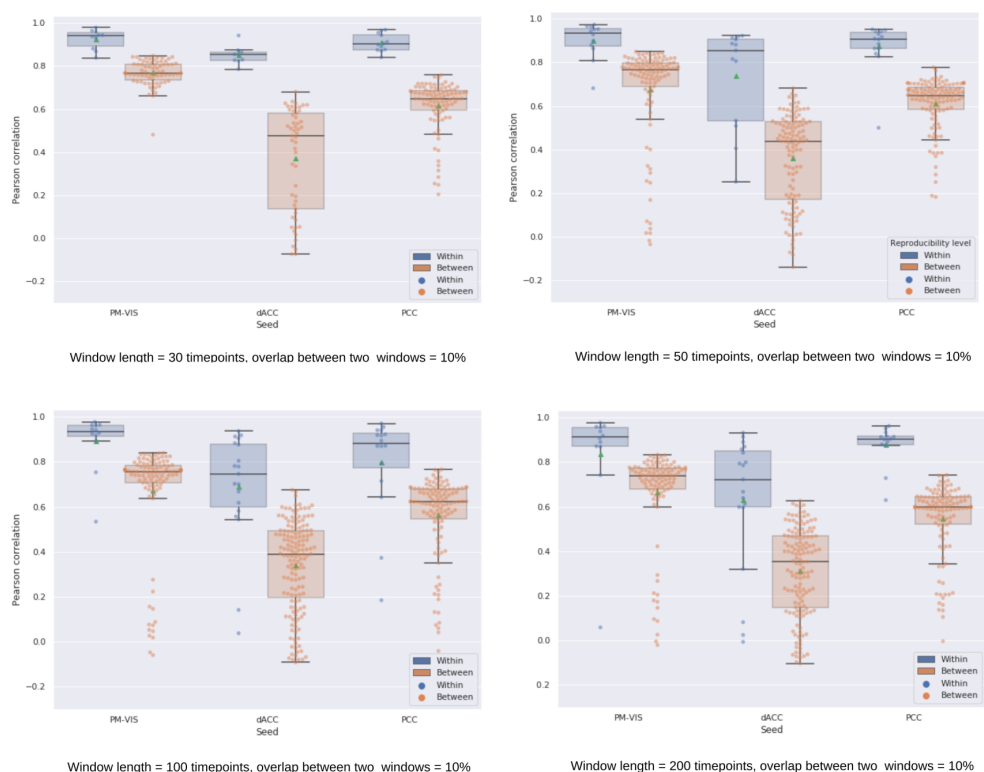


Fig. 10. The number of dynamic states and their dwell time was insensitive to different window lengths.

We reported the dwell time from both sets of independent sessions. We studied three seed voxels including the PM-VIS, the dACC and the PCC. The number of replications of seed-based parcellations = 30. The seed-based parcellations were clustered into 12 clusters. The smoothing kernel = 6 mm, the cluster size threshold = 10%, the Dice threshold = 0.3. Ten subjects of the Midnight scan club dataset were included.

We investigated the distribution of the states dwell time for different number of timepoints per window; i.e., number of timepoints = 30, 50, 100, 200. Three seeds from the PM-VIS, the dACC and the PCC subnetworks were investigated. Our results showed that the dACC

and the PCC seeds were multistate for different number of timepoints in a single window. For instance, the dwell time of the dACC seed had a maximum of three states in the case of 30 time points, three states in the case of 50 timepoints, five states in the case of 100 time points and four states in the case of 200 time points. Moreover, the primary state was always a dominant state with an important difference between its dwell time and the dwell time of the secondary state. For instance, in the case of 50 time points and the dACC seed, the primary state had a dominant dwell time with a median = 38% over a median dwell time equal to 11% in the case of the secondary state. Similarly, the dwell time of the PCC seed had a maximum of three, four, four and three states, respectively for the 30, 50, 100 and 200 timepoints. The dominant primary state in the case of 50 timepoints and the PCC seed had a median dwell time = 42% over a median dwell time = 11% in the case of its secondary state. Unlike the dACC and the PCC, the PM-VIS seed was monostate for most subjects and up to three states for few subjects. Its secondary and third states had very low dwell time (around 10%) compared to the primary state (See Fig. 10). Altogether, these results suggested that the dynamic states of parcellations were multistate for the dACC and the PCC seeds and mono-state for the PM-VIS seed for most subjects and multistate for few subjects, regardless of the window time length.

5.4. Dynamic states reproducibility was insensitive to low cluster size thresholds

We aimed to investigate the impact of different cluster size thresholds on the reproducibility of dynamic states of parcellations. Thus, we reported the within- and between-subjects reproducibility for different cluster size thresholds as the percentage of the seed-based parcellations included in a given state over their total number. The results of the lowest cluster size threshold; i.e. score = 5%, showed large distribution of reproducibility scores both at the within- and the between-subjects levels compared to higher cluster size thresholds; i.e. score > 10%. Still, the median of the within-subject reproducibility was higher than the between-subject reproducibility for all cluster size thresholds and all seeds (See Fig. 11). These results demonstrated the insensitivity of the reproducibility of the dynamic states of parcellations to the cluster size threshold.

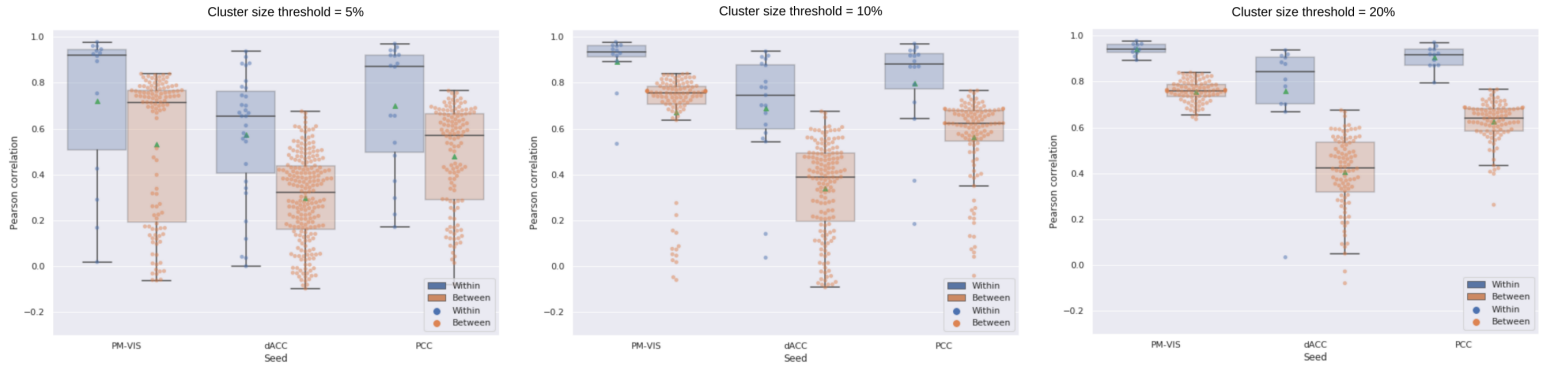


Fig. 11. Dynamic states reproducibility was insensitive to cluster size threshold. We studied three seed voxels including the PM-VIS, the dACC and the PCC. The number of replications of seed-based parcellations = 30. The seed-based parcellations were clustered into 12 clusters, the smoothing kernel = 6 mm, the Dice score threshold = 0.3. The number of timepoints per window = 100. Ten subjects of the Midnight scan club dataset were included.

5.5. The PCC and the dACC subnetworks were multistate and the PM-VIS was monostate for most subjects across different cluster size thresholds

We investigated the distribution of the states dwell time for different values of cluster size thresholds = 5%, 10%, 20%. Three seeds from the PM-VIS, the dACC and the PCC subnetworks were investigated. Our results showed that the dACC and the PCC seeds were multistate across cluster size thresholds. For instance, the dwell time of the dACC seed had a maximum of five states in some subjects when the cluster size thresholds were equal to 5% and 10% while it had only up to three states in the case of 20% cluster size threshold. Moreover, the primary state was always a dominant state with an important difference between its dwell time and the dwell time of the secondary state of all the values of cluster size thresholds. For instance, in the case of a cluster size threshold equal to 5%, the dACC seed and the primary state had a dominant dwell time with a median = 43% over a median dwell time = 13% in the case of the secondary state (See Fig. 12). Altogether, these results suggested that the dynamic states of parcellations were multistate for the dACC and the PCC seeds. Dynamic states of parcellations were mono-state in the case of the PM-VIS seed for most subjects and multistate for few subjects, regardless of the cluster size threshold.

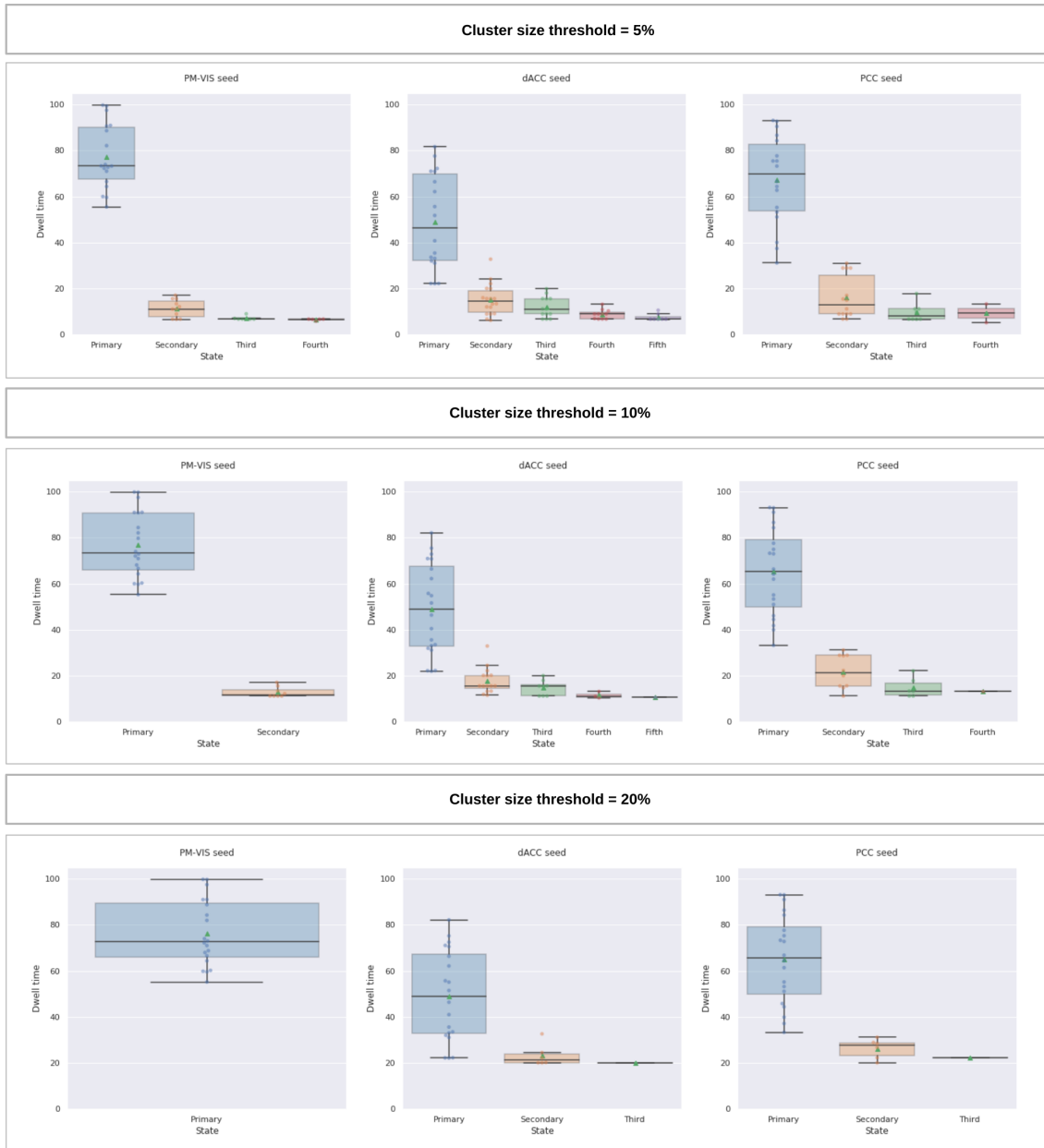


Fig. 12. The number of dynamic states and their dwell time was insensitive to different cluster size thresholds.

We studied three seed voxels including the PM-VIS, the dACC and the PCC. The number of replications of the seed-based parcellations = 30. The seed-based parcellations were clustered into 12 clusters. The smoothing kernel size = 6 mm, the Dice score threshold = 0.3. The number of timepoints per window = 100. Ten subjects of the Midnight scan club dataset were included.

5.6. Reproducibility of dynamic states of parcellations in the case of different smoothing kernels

We aimed to investigate the impact of the spatial smoothing on the spatial state maps. Thus, we generated the dynamic states of parcellations for different smoothing kernels; i.e., 4mm, 6mm and 8mm, and we reported the within- and between-subjects reproducibility. Our results showed that all within-subjects reproducibility were higher than between-subjects reproducibility. For instance, the median of within-subject reproducibility scores were higher than 0.8 Pearson correlation for all seeds across different smoothing kernels while the between-subjects reproducibility were lower than 0.8 Pearson correlation for all seeds and all smoothing kernels (See Fig. 13). These findings suggested the insensitivity of our dynamic states of parcellations to the kernel size.

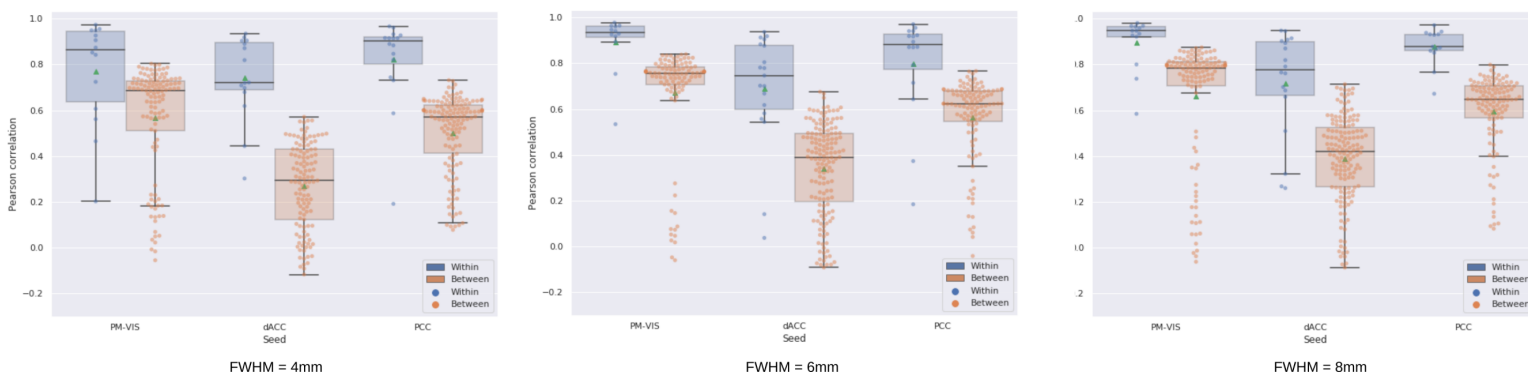


Fig. 13. The within- and between-subjects reproducibility of our dynamic states of parcellations were insensitive to the smoothing kernel size.

We studied three seed voxels: PM-VIS, dACC and PCC. The number of replications of seed-based parcellations for each replication=30. The seed-based parcellations were clustered into 12 clusters, the cluster size threshold = 10%, the Dice threshold = 0.3. The number of timepoints per window = 100. Ten subjects of the Midnight scan club dataset were included.

5.7. The PCC and the dACC subnetworks were multistate for different smoothing kernels and the PM-VIS was mono-state for most subjects

We aimed to get a better understanding of the dwell time distribution of the dynamic states of parcellations for different smoothing kernels. Our results showed the existence of many states across the three studied subnetworks; i.e. dACC, PCC and PM-VIS seeds. For instance, the PM-VIS had three, two and three states, respectively for 4mm, 6mm and 8mm smoothing kernels. However, the dwell times of the secondary and the third states of the

PM-VIS subnetwork occurred for a few subjects and their dwell time was very low; i.e. dwell time 10%. That suggested the PM-VIS was mono-state for most subjects and multistate for some subjects with a dominant primary state. Conversely, the dACC and the PCC secondary states had much lower dwell time than the primary state; i.e. dwell time $> 10\%$, for different smoothing kernels. These findings suggested the PCC and the dACC subnetworks were multistate while the PM-VIS was mono-state for different smoothing kernels (See Fig. 14).

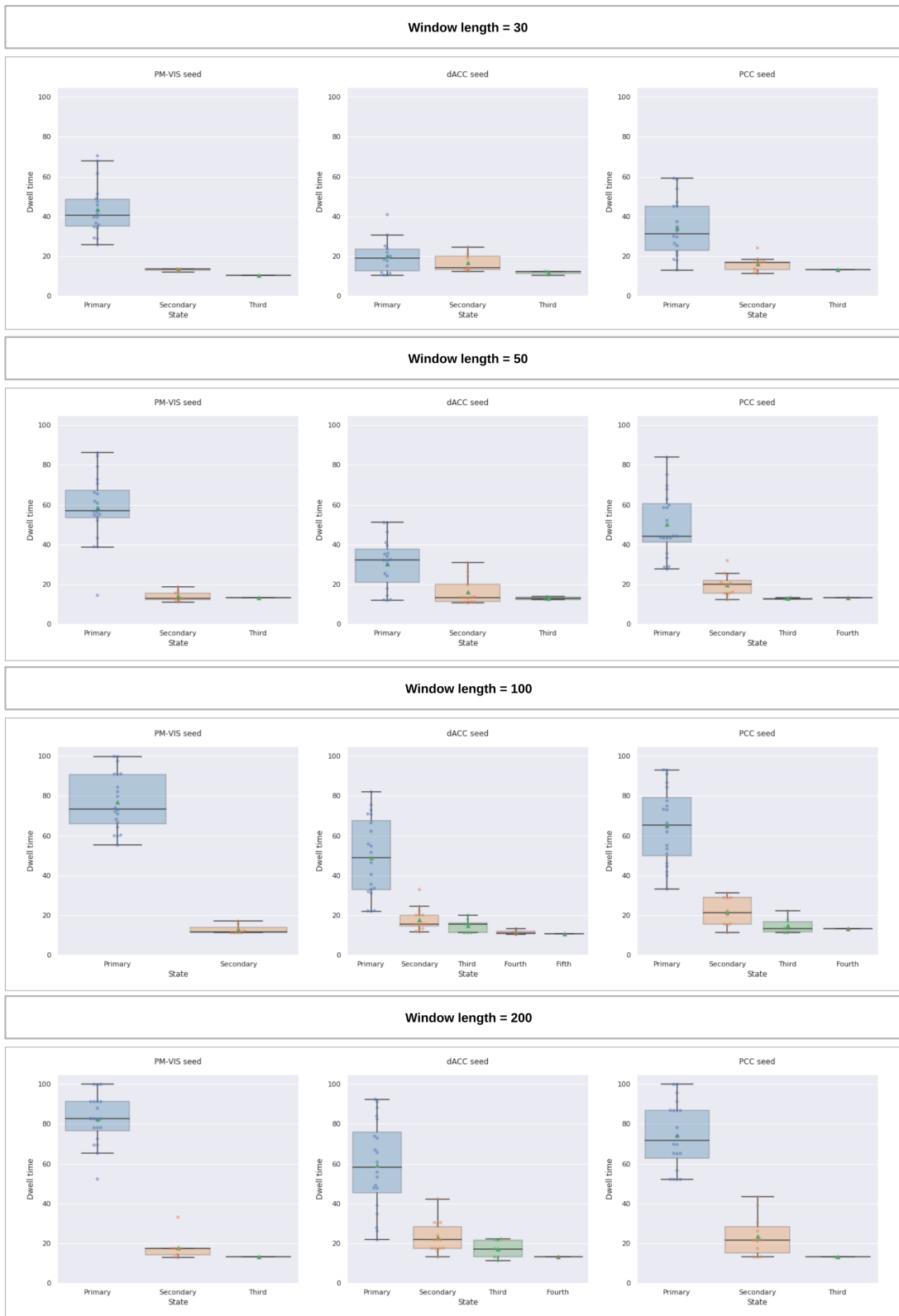


Fig. 14. The number of dynamic states and their dwell time was insensitive to the smoothing kernel.

We studied three seed voxels including the PM-VIS, the dACC and the PCC. The number of replications of seed-based parcellations = 30. The cluster size threshold = 10%. The seed-based parcellations were clustered into 12 clusters, the Dice threshold = 0.3, the number of timepoints per window = 100. Ten subjects of the Midnight scan club dataset were included.

5.8. The reproducibility of the dynamic states of parcellations was not sensitive to changes in the seeds coordinates

We aimed to investigate the reproducibility of many seed voxels from the visual, the dACC and the PCC subnetworks to verify the generalizability of the conclusions associated with the studied subnetworks. We manually picked 15 different seeds from each subnetwork including boundaries (See MNI coordinates of the chosen seeds in table 1). We computed their within-subject and between-subjects reproducibility scores. Our results showed that within-subject reproducibility outperformed the between-subjects reproducibility scores in terms of the Pearson correlation. For instance, the within-subjects reproducibility scores had a median correlation > 0.9 in the case of the PCC seed while all between-subjects reproducibility scores had a median correlation < 0.79 (See Fig. 15). These results suggested that within-subjects reproducibility of our dynamic states of parcellations was higher than between-subjects reproducibility for all the studied seeds from the PM-VIS, the dACC and the PCC subnetworks.

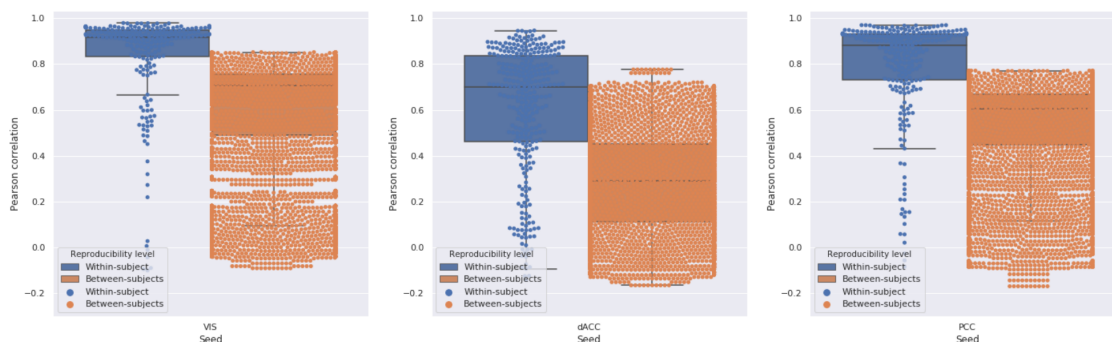


Fig. 15. Within- and between-subjects reproducibility of our dynamic states of parcellations for 15 seeds per subnetwork.

We studied three seed voxels including the PM-VIS, the dACC and the PCC. The number of replications of the seed-based parcellations was equal to five. The seed-based parcellations were clustered into 12 clusters. The smoothing kernel size = 6 mm, the cluster size threshold = 10%, the Dice threshold = 0.3, the number of timepoints per window = 100. Ten subjects of the Midnight scan club dataset were included.

5.9. Within-subjects reproducibility was insensitive to the number of replications of the seed-based parcellations

To evaluate the impact of the number of replications of the seed-based parcellations, we computed the within-subjects reproducibility of the dynamic states of parcellations in the case of 1, 5 and 30 seed-based parcellations. Different initializations of the random number generator were used for different k-Means parcellations. Our results showed very similar distributions across replications. For instance, the within-subjects reproducibility medians

were all aligned to very close scores for all seeds (See Fig. 16). These findings suggested that the variability across seeds in the k-Means parcellations were negligible in the context of our Dypac algorithm.

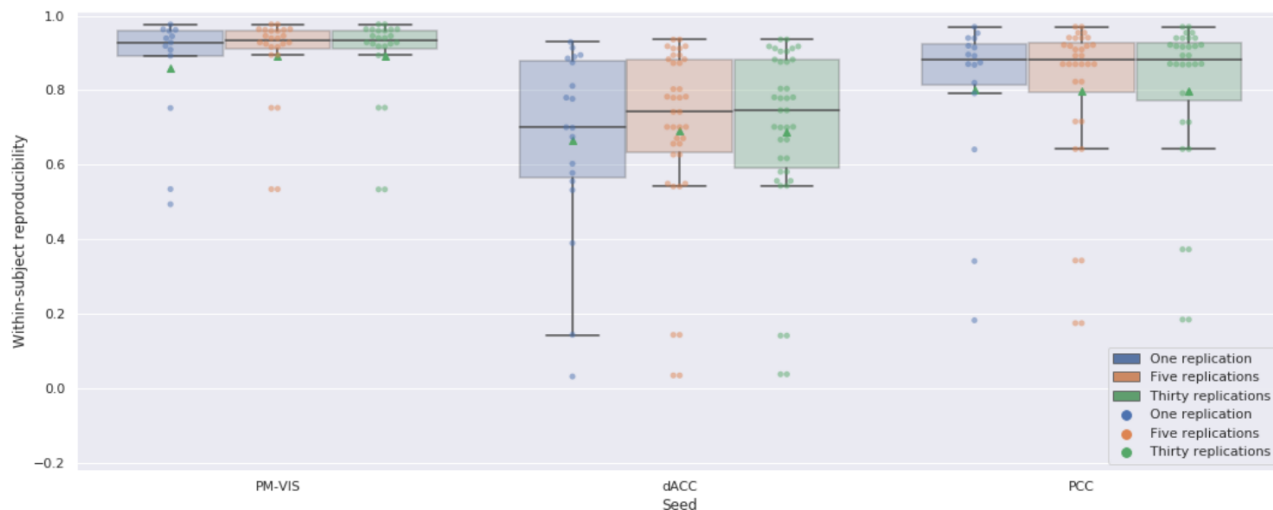


Fig. 16. The within-subject reproducibility of our dynamic states of parcellations was insensitive to the number of replications of the seed-based k-Means parcellations.

We studied three seed voxels including the PM-VIS, the dACC and the PCC. The seed-based parcellations were clustered into 12 clusters. The smoothing kernel = 6 mm, the cluster size threshold = 10%, the Dice threshold = 0.3, the number of timepoints per window = 100. Ten subjects of the Midnight scan club dataset were included.

6. Dynamic states suppressed differences within-sessions versus across days in the case of resting state functional MRI data

We aimed to investigate the within-sessions versus the between sessions effect across days on the identified dynamic states. To this end, we computed the probability of a given state to be associated with two sliding windows either from the same session or from different sessions (across days). Our results showed highly overlapping probability distributions for the sliding windows of the same state to fall into the same session or different sessions (See Fig. 17). Thus, there was no substantial impact of the differences in the brain activity across sessions on the identified dynamic states.

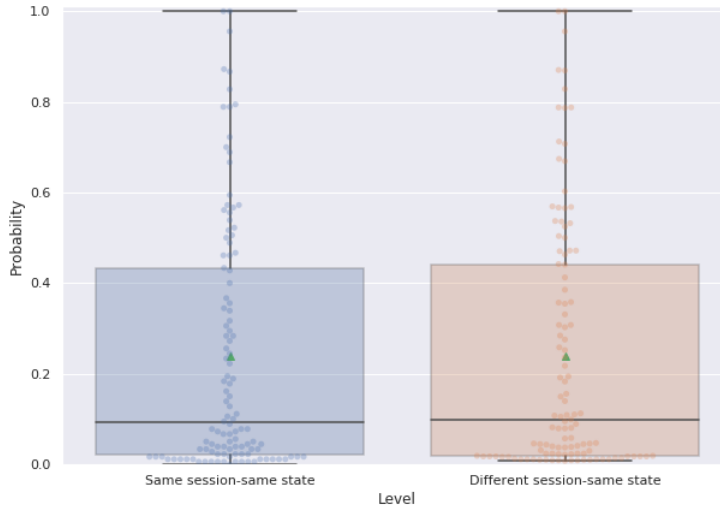


Fig. 17. Dynamic states occurred with the same probability either across days or across sessions.

For each state, we computed the probability of two sliding windows to be in the same session or in different sessions. We studied three seed voxels including the PM-VIS, the dACC and the PCC. The number of seed-based parcellations = 5. Ten subjects of the Midnight scan club dataset were included.

7. Different dynamic states had different temporal dynamics

We aimed to quantify the synchrony between the dynamics of the different states of parcellations, from different seeds and over time. To this end, we computed the Adjusted Rand Index (ARI) similarity scores between one-hot encoding of states associated with seed-based parcellations (over sliding windows) as a measure of the synchrony between spatial states over time. The sliding windows were ordered chronologically. The seed-based one-hot parcellation dynamics was the binary representation in which 1 value indicated the sliding window was included in the state and 0 otherwise, for a given sliding window. We computed the ARI between one-hot temporal dynamics associated with different seeds for five sets of sessions (within-set) and between two sets of five independent sessions (between-sets). This allowed us to quantify to which extent the spatial spatial patterns (states) associated with different seed subnetworks were involved, at the same time (over sliding windows) both within- and between-sets. No substantial association between sets was expected, as these sessions were acquired independently making inter-set synchronization unlikely, with the possible exception of habituation, fatigue or stress effects accruing systematically at the beginning or the end of a session. The low ARI scores within- and between-sets showed there

was no synchrony between the states of different pairs of seeds both at the within-set and between-sets. That is, the states associated with one seed did not occur at the same time as the states of another seed. Also, we observed that the within-set scores were slightly higher than between-sets scores in the case of the PCC/PM-VIS pair. For instance, for the three pairs of seeds (i.e. dACC/PCC, dACC/PM-VIS, PCC/PM-VIS), the average ARI score 0.02. However, The PCC/PM-VIS pair had an average ARI of 0.05 (See Fig. 18). These findings demonstrated the existence of different temporal dynamics for the states associated with different seed subnetworks.

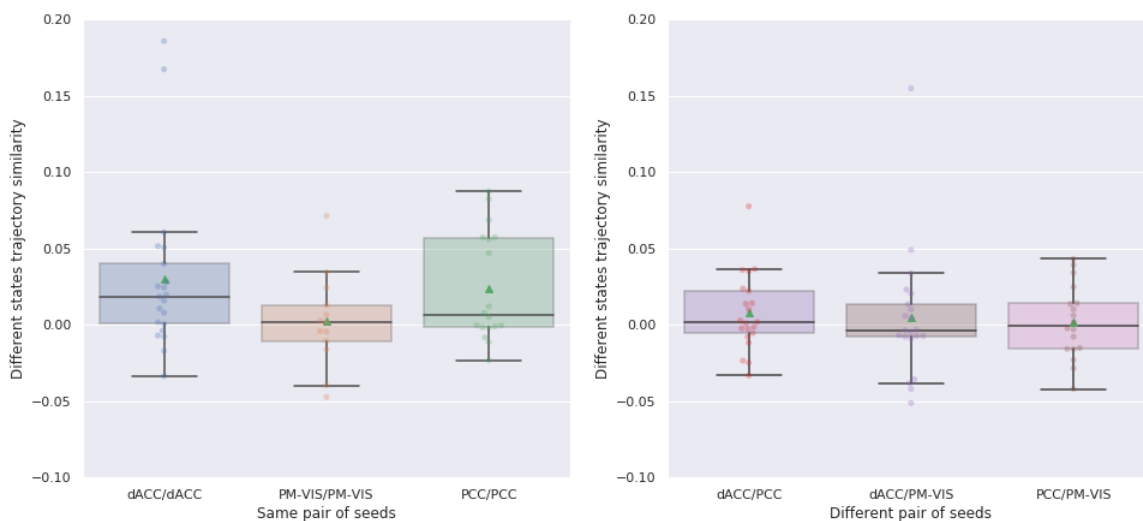


Fig. 18. Dynamic states of parcellations had different temporal dynamics.

The ARI similarity scores were computed between the seed-based parcellations associated with different pairs of seed subnetworks. Each seed-based parcellation was a chronologically ordered sliding window parcellation from the MSC sessions. We computed the ARI either between the states from at the within-set level or at the between-sets level. We maximized the ARI scores between two distinct states associated with two different seed subnetworks (i.e. dACC/PCC, dACC/PM-VIS, PCC/PM-VIS). We replicated the Dypac algorithm 30 times. The number of seed-based parcellations = 5. The seed-based parcellations were clustered into 12 clusters. The smoothing kernel = 6 mm, the cluster size threshold = 10%, the Dice threshold = 0.3, the number of timepoints per window = 100. Ten subjects of the Midnight scan club dataset were included.

8. Conclusion

To summarize, we show our dynamic parcellation algorithm had robust findings across different parameters in the context of resting state functional MRI and long hours acquisitions. These findings gave evidence of the reliability of our dynamic parcellation approach and a proof of concept that motivates to conduct further research to extend it at the full

brain level. This is a challenging area of research since more than two decades even in the case of static parcellations due to the large dimensionality of the functional MRI data especially at a scanning high resolution. Another interesting area of research is the application of the dynamic states of parcellation to reduce the functional MRI data with a minimized information loss and use these reduced data for clinical applications including the prediction of neurological disorders.

Chapter 4

Second Article

Third Article.

A scalable dynamic parcellation algorithm for the compression of individual fMRI data

by

Amal Boukhdhir¹, Hanad Sharmarke², Yu Zhang², Basile
Pinsard², Julie Boyle², Max Mignotte³, and Pierre Bellec⁴

- (¹) Centre de recherche de l'institut universitaire de gériatrie de Montréal, Montréal, Québec, Canada
Département d'informatique et de recherche opérationnelle, Université de Montréal, Montréal, Québec, Canada
- (²) Centre de recherche de l'institut universitaire de gériatrie de Montréal, Montréal, Québec, Canada
- (³) Département d'informatique et de recherche opérationnelle, Université de Montréal, Montréal, Québec, Canada
- (⁴) Département de psychologie, Université de Montréal, Montréal, Québec, Canada

This article was submitted in To be determined.

ABSTRACT. Functional brain parcellations are intensively used to reduce the high dimensionality of functional MRI data into more compact representations. In the literature, there exists no consensus regarding the best approach to parcellate individual brain parcellations, despite more than two decades of investigation. The main limitation of previous approaches was that functional parcellations were not highly reproducible and there was loss of information between the original signal and the reduced data. Neglecting the dynamic reconstructions of these brain regions was among the main reasons for this poor performance in some brain regions including, the heteromodal cortices. Some individual parcellation approaches have recently proposed to improve these performance measures. Still, these approaches were either not scalable enough to replicate on large longitudinal datasets, or it required terabytes of functional MRI data to generate brain parcels. In our previous work, we formalized the parcellation problem as a dynamic approach that identified different spatial reconstructions or ‘dynamic states of parcellations’ for a given seed subnetwork called DYPAC 1.0. The scalability of this cluster aggregation approach motivated us to extend it to a full brain implementation called DYPAC 2.0. We used ten hours per subject of training and test data from the cneuromod movie10 dataset. We found low information loss between the reduced and the original data throughout the cerebral cortices, i.e. only 20% information loss. We also found that average within-subject reproducibility reached high scores for many dynamic states throughout the brain (over .9 training-test spatial correlation). This work opens new research directions to studying the brain dynamics often neglected by previous methods based on static parcellations, and may therefore improve the new clinical applications studying differences in brain interactions in both healthy brains and disease.

Keywords: Full brain parcellation, dynamic parcellation, dynamic states, cognitive states, cluster aggregation, soft parcellation

1. Introduction

Brain parcellation can be viewed and understood as a tool for compressing functional MRI data. The main objective is to reduce the dimensionality of brain functional organization with a high fidelity. Functional brain parcellations are very useful and intensively applied in the neuroscience field, and specifically network neuroscience. For instance, different studies reported better accuracy in the prediction of mental states, neurological disorders, etc., depending on the choice of a brain parcellation [?, 36]. Traditional static brain parcellations subdivided the cerebral cortex into a single fixed parcellation composed of “hard” binary assignment of voxels to a given parcel with well-defined boundaries [?]. Even though there existed several static functional approaches in the literature, there was no consensus on which approach better reduce the high dimensionality of the functional data [6]. That is, the compression rate of static parcellations seem to reflect primarily the size of parcels (resolution), and state-of-the-art algorithms offer little to no advantage compared to random brain parcellation (see Fig 7 of [76]). Additionally, the evaluation of the goodness of functional parcellations was evaluated using reproducibility on test-retest datasets. However, these reproducibility scores did not reach high scores

at the individual level and it plateaued at 0.7 dice score even in the context of over 30 minutes of resting state data [39]. Researchers associated this mainly, to within-subject or between-subjects fMRI variability [19, 61, 73]. For instance, a recent study investigated the variability in spatial functional boundaries of regions associated with different human adults' lifespan (20-93). Here, the authors explained the differences in parcellation boundaries by differences in cortical thickness and anatomical alignment due to age differences [40].

Another research direction formalized the parcellation problem as a space-time decomposition using soft and dynamic parcellations. Soft parcellation meant that a given voxel was attributed a weight of appartenance to a given parcel, e.g. a probability score [?]. Dynamic parcellation meant that different parcels could overlap, and the strength of expression of a given parcel may vary over time. An important difference between static and dynamic parcellations was how fMRI data were compressed in parcels. In the case of a static parcellation, the compression was univariate. Each parcel represented the average functional activity at a specific spatial location in the cerebral cortex. An average signal was generated for each parcel, or a principal component analysis was applied to the signal inside the parcel [?]. In the case of dynamic parcellations, the compression was multivariate as the parcels (or spatial modes of decomposition) were used altogether using a multivariate regression analysis to fit a full brain activity volumes over time [22] resulting in spatially overlapping parcels, i.e., the same voxel was involved with different states. This approach was applied by the Independent component analysis ICA for more than a decade. Recently, some researchers showed the application of a dynamic approach improved the fidelity of the compressed data to the actual neurobiological changes over time in space. For instance, Dadi and colleagues used the spatial sparsity constraint to generate dynamic brain parcels [?]. Authors showed the compression of activation maps was improved using soft and dynamic parcellations over a range of classic static parcellations [?]. Here, authors showed the existence of variability in temporal features that were not confounded with spatial features [41]. Despite the existence of different attempts to apply the space-time decomposition of fMRI data, there are still two main limitations of previous approaches. First, the lack of scalability to the high dimensionality of functional MRI data (e.g., ICA approach). This motivated the introduction of PROFUMO [17], a matrix factorisation model that identified subject-specific spatial maps using a variational Bayesian approach with spatiotemporal priors instead of ICA dual regression. Other previous approaches required terabytes of functional data to converge to good quality solutions [?]. That could be problematic, especially in the case of the clinical datasets; e.g. Alzheimer disease datasets. Our previous seed-based implementation of DYPAC1.0 was based on a simple and scalable cluster aggregation. This motivated us to see if it could be extended to a scalable full brain analysis. We also wanted to see if we can reduce the information loss between the

original and the reduced functional data using full brain state stability maps.

The main finding of DYPAC1.0 was the existence of high spatial reproducibility at the within-subject level (between test-retest datasets) in short time series (about 3 minutes) and using a very basic clustering algorithm. Across states, there existed different spatial reconfigurations within the same subject, especially in the cases of the dACC and PCC seed subnetworks. That is, there were some differences locally, at the level of a region surrounding the seed subnetwork for some states. There were also differences in spatial states involving multiple regions distributed throughout the brain. Similar local and distributed variations were observed with the PCC seed subnetwork, which had up to three states. In the literature, there existed a spatial overlapping pattern between space-time decompositions generated by the ICA and the DYPAC1.0 approach even though the underlying formalism was different. That spatial overlap was identified in the case of the visual network, the default mode network, the MPFC regions and regions of the dorsal attentional subnetwork [18, 30, 84].

In this paper, we build upon the findings of Boukhdhir and colleagues and we extend the dynamic parcellation approach to extract full brain dynamic states of functional parcellations at the individual level [18]. We define a dynamic state of parcellation as the time-space decomposition that occurs for short time durations in the resting state condition. This approach is based on aggregating sliding-window parcellations for a given region to obtain stability maps of the different dynamic states of parcellations. We generate these dynamic states for the six subjects of the Courtois Neuromod dataset and we aim to evaluate the compression quality of the state stability maps at the full brain level. We also aim to study similarities and variations within-subject (between sets of independent data for the same subject) and across subjects.

2. Methods

2.1. DYPAC2.0

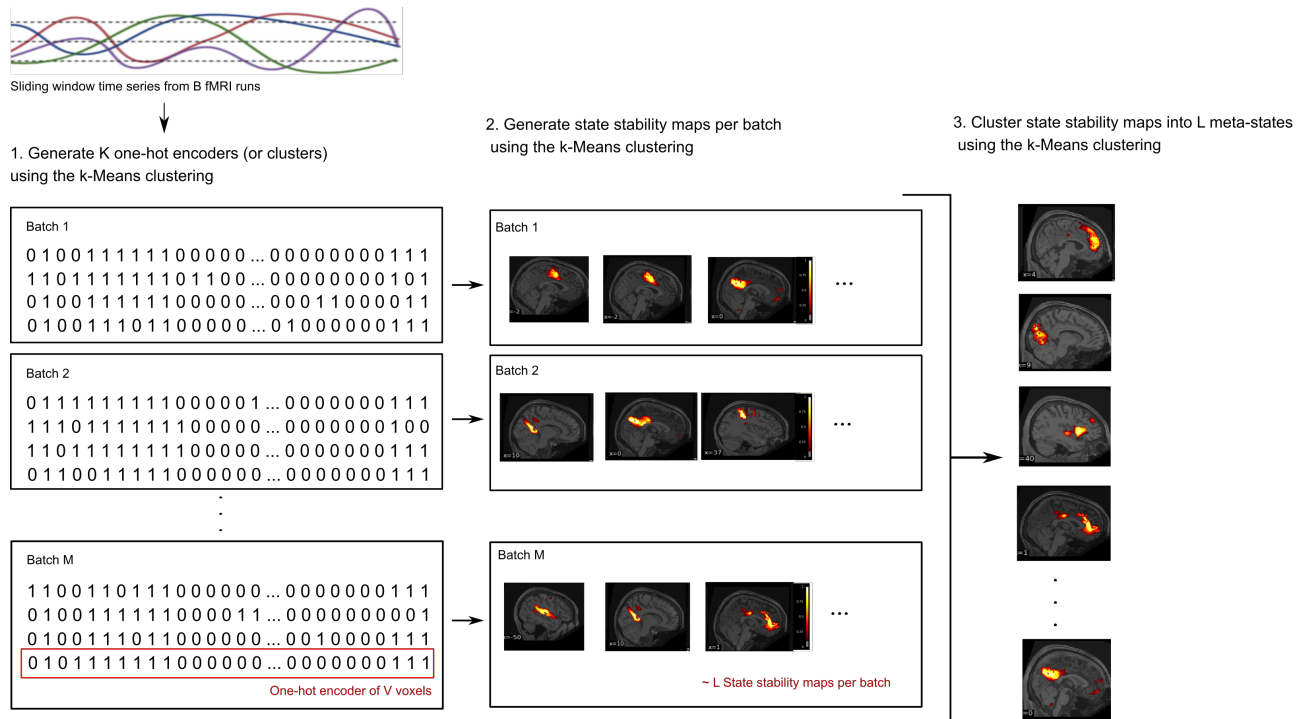


Fig. 1. Subject-specific dynamic parcellation approach at the full brain level (DYPAC2.0).

The first step consists of running k-Means directly on the time series. Here, we generate a family of parcels represented with one-hot encoders. The second-step aggregation clustering procedure generates a set of state stability maps at the full brain level. The third step consisted of clustering the state stability maps of the previous step into L clusters.

2.1.1. Overview. We implemented a new algorithm which identifies individual dynamic states of brain parcellation at the full brain, using a multi-level ensemble clustering approach. This algorithm is an extension of the Dynamic Parcel Aggregation with Clustering (DYPAC2.0) algorithm proposed by Boukhdhir and colleagues [18]. DYPAC2.0 uses a simple two level clustering, one on sliding time windows, and one-hot encoders aggregated over many windows. A one-hot encoder is a binary vector of length V (number of voxels in a brain mask), in which each voxel has a value one if it is included in a given cluster, and zero otherwise.

2.1.2. First-level cluster analysis. The first level clustering consists of replicating a k-Means analysis on R sliding windows of fixed size, uniformly distributed in a given fMRI time series. The k-Means algorithm has a parameter K which sets the number of clusters (parcels) in the brain. We generate an array of parcels represented with K one-hot encoders.

K one-hot encoders of length V are generated for each sliding window, and one-hot vectors are aggregated over R replications, as well as B fMRI datasets (or runs) collected on the same individual (see Fig. 1).

2.1.3. Second-level cluster analysis. The second-level aggregation clustering procedure groups the one-hot encoders into states. A traditional k-Means clustering with L states is again applied at this step. Note that this parameter is set globally, i.e. it indicates the overall number of possible states across all brain parcels. For each state cluster, the average of all one-hot encoders in that state is generated, producing a state stability map. Stability scores range from 0 to 1, with 0 indicating a voxel which was never associated with a brain parcel in that state, and 1 indicating a voxel always included in the parcels of that state (see Fig. 1).

2.1.4. State trimming. Because we had observed in DYPAC1.0 that many dynamic states are noisy, and should not be included in a state, each state cluster is further "trimmed" using the following approach. For each one-hot vector in a state cluster, the average value of the stability map of that cluster is generated, over the voxels in the one-hot vector. Only one-hot vectors which achieve an average stability over a threshold $t=0.3$ are assigned to a state cluster. Final stability maps are generated after this trimming procedure, on the remaining one-hot vectors. Some state clusters may end up empty because of the trimming procedure, and will be excluded from further analysis, which means that the effective number of states after trimming may be less than the specified L.

2.1.5. Memory requirements. Models were run using the following parameters: K=50 brain clusters, L=150 dynamic states and R=100 replications. Note that with the dataset we used, V 150k and B 60. In total, the array of one-hot encoders can reach a very large size, $V \times (K.R.B)$, but is tractable in memory because it is represented as a sparse boolean array. As K one-hot encoders coding for a given brain parcel have exactly V non-zero elements, the aggregated one-hot encoders use $V.R.B$ bits of memory (independent of the number of clusters K). With the values listed above, the aggregated one-hot encoder array will have $150k.100.60=900M$ non-zero elements, which easily fits in memory even on commodity hardware.

2.1.6. Processing time. We used the k-Means implementation of scikit-learn <https://scikit-learn.org/stable/modules/generated/sklearn.cluster.KMeans.html> for both the first-level and second-level cluster analysis. This particular implementation supports sparse data, so the large number of features (V 150k) is handled efficiently, as each one-hot vector is very sparse, and the memory requirements are kept to a low level, as outlined in the preceding paragraph. This implementation still has a quadratic run-time complexity as a function of the number of measures to be clustered, which is here very large $K.R.B=300k$.

In order to limit this computation time, we also implemented a version of DYPAC2.0 that relies on batches of fMRI data. Additionally, we used the latest release of the k-Means implementation in scikit-learn which runs this algorithm in parallel on multiple cores. This further improves scalability on multiple cores. We rely on the parallel grid computing of compute canada which allows us to allocate up to 32 cores per node ¹.

2.1.7. Batch processing. To accommodate the large number of one-hot encoders size across multiple states at the full brain level, we subdivided the overall one-hot encoders into M batches (or subgroups) of one-hot encoders. Stability maps are generated independently in each batch, and then aggregated into an array of size $V \times (M.L)$ ². This array is entered into a third-level cluster analysis that groups the state stability maps into meta-states clusters. stability maps within a given meta-state are averaged to produce final stability maps. The batch size directly impacts the reliability of the estimation of the state stability maps. Therefore, there should be a compromise between the computational cost and the number of one-hot encoders. The higher the number of one-hot encoders are within the same batch, the better the state stability maps are. The lower the number of one-hot encoders is, the lower the computational cost is. In the application proposed here, as each subject had a large number of fMRI runs available (B 60), we used M=10.

2.1.8. Code implementation. The code for DYPAC2.0 is available via github³. The application program interface is inherited from the base linear decomposition class of the nilearn library [70], and is using nilearn tools for loading preprocessed fMRIprep data and generating a brain mask. The codebase includes unit testing covering all key methods, and separates the ensemble clustering tools (bascpp.py), the fMRI interface (dypac.py) from the temporal embeddings tools (embeddings.py, see section on fMRI compression below). Nilearn and matplotlib were also used to generate all the figures in this paper.

2.2. Dataset and preprocessing

The cneuromod movie10 dataset included about ten hours of functional data per participant. Six participants were included (female=3, male=3, their age ranges between 31-47 years old. Informed consent was obtained from all participants [28]. Each participant watched four different movies in the MRI scanner, including Bourne supremacy movie (100 minutes duration), Wolf of wall street movie (170 minutes duration), Hidden figures movie (120 minutes duration, presented twice) and Life movie (100 minutes duration, presented twice). Each movie was cut into roughly ten minute segments presented in a

¹<https://docs.computecanada.ca/wiki/Cedar>

²Strictly speaking, the second dimension of this array may be smaller than M.L, as some states are empty following the trimming procedure.

³<https://github.com/courtois-neuromod/dypac>

separate run. Exact cutting points were manually selected to not interrupt the narrative flow. The cneuromod movie10 dataset included about ten hours of functional data per participant. Six participants were included (female=3, male=3, their age ranges between 31-47 years old. Informed consent was obtained from all participants [28]. Each participant watched four different movies in the MRI scanner, including Bourne supremacy movie (100 minutes duration), Wolf of wall street movie (170 minutes duration), Hidden figures movie (120 minutes duration, presented twice) and Life movie (100 minutes duration, presented twice). Each movie was cut into roughly ten minute segments presented in a separate run. The sequence is available on the Siemens PRISMA scanner at UNF through a concept to production agreement, and was used with the following parameters:slice acceleration factor=4, TR=1.49s, TE=37ms, flip angle=52 degrees, voxel size= 2mmX2mmX2mm, 60 slices, acquisition matrix 96X96. Exact cutting points were manually selected to not interrupt the narrative flow.

For each functional MRI run, different steps of the fMRIPrep v20.1.1 preprocessing pipeline were applied [2]. First, a reference volume and its skull-stripped version were generated. To correct for susceptibility distortions, a deformation field was estimated using 3dQwarp AFNI [2]. Using the susceptibility distortion, an unwarped functional MRI reference run was computed to have a better co-registration with the anatomical reference. The functional MRI reference run was then co-registered to the T1w reference using flirt (i.e.; FSL 5.0.9). To correct the remaining distortions in the functional MRI reference runs, we configured co-registration with nine degrees of freedom. Head-motion parameters were also estimated before spatiotemporal filtering using mcflirt (i.e.; FSL 5.0.9, [2]). Each functional MRI run was resampled into standard space, to generate a preprocessed functional BOLD signal the *MNI152NLin2009cAsym* space. We adapted the P24 denoising strategy of [25] which included six motion parameters (i.e., six degrees of freedom), six temporal derivatives, six quadratic terms, and six quadratic expansions of the derivatives of motion estimates for a total 24 regressors [27]. We excluded the frames that exceeded a threshold of 0.5 mm FD or 1.5 standardised DVARS. Volumetric resamplings were performed using antsApplyTransforms (ANTs), configured with Lanczos interpolation to minimize the smoothing effects of other kernels [52].

We used a reasonable preprocessing strategy that allowed us to capture clean well-known dynamic states in the literature without aggressively removing neurobiological signals. So it is important that a tradeoff is made, therefore, we intend to analyse the effect of different denoising strategies to evaluate the impact of the preprocessing on the performance measures in the case of brain parcellation.

The load-confounds library is used to import confound factors generated by fmriprep in Nilearn. These confounds were regressed out of individual fMRI time series, which were further standardized to a zero mean and unit variance and spatially smoothed with an 8 mm smoothing kernel using Nilearn MultiNiftiMasker method. Dypac2.0 analyses were restricted to an individual-specific segmentation of the grey matter generated using freesurfer as part of the fmriprep preprocessing pipeline.

2.3. Functional MRI loss of information analysis after compression

We aimed to quantify the quality of the compressed functional MRI data and whether it was representative of these raw data. We separated the cineuro mod movie10 into training and test sets. The training set was composed of 44 runs (10 minutes each) from four different movies, including Life (5 runs), Bourne supremacy (10 runs), Hidden figures (12 runs), Wolf of wall street (17 runs). The test set was composed of only 17 runs (10 minutes each) from two different movies, including Life (5 runs) and Hidden figures (12 runs). We generated subject-specific parcellations on the training set, and then evaluated compression quality on the test set. To quantify the compression quality of the functional MRI, we computed the R-squared measure between the preprocessed time series at each voxel, and the compressed time series using the DYPAC2.0 stability maps. Specifically, the fMRI time series were projected in the vector basis of stability maps using an ordinary least-squares linear projection. This resulted into a reduced set of time series, one per stability map. Then, the reduced time series were multiplied with the stability maps, in order to generate a linear mixture of parcels with same dimensionality as the original time series. The R-squared coefficient expressed the percentage of variance of the original time series effectively captured by the compressed time series. Note that the compression factor is very high (approximately 1000), as there are originally about 150k voxels, which get projected into a space of dimension lower than $L=150$ (the number of stability maps generated by DYPAC2.0). A higher R-squared score indicated a better explained variance in the functional MRI signal, or in other words lower information loss between the original signal and the compressed state stability map. We compared the R-squared measure both at the within- and the between-subjects level. At the within-subjects level, we computed the R-squared scores between each functional MRI run and all its corresponding state stability maps from the same subject. At the between-subjects level, the functional MRI runs were compressed using state stability maps associated with different subjects. We reported the results in Fig. 2 and Fig. 3.

2.4. Reproducibility analysis

We also aimed to evaluate the reproducibility of the dynamic states of parcellations at the full brain level. To this end, we conducted a quantitative consistency analysis both at

the within- and the between-subject levels in the context of movie data. This allowed us to quantify and identify similarities and variations in the spatial reconfigurations of the dynamic states. We compared the spatial reproducibility at the within-subjects and the between-subjects levels in terms of the Pearson correlation measure of spatial stability maps. We matched the training set maps to the maps from the second set using the Hungarian method [51]. A higher correlation showed a stronger linear relationship between two state stability maps. This indicated high spatial consistency between the dynamic states of parcellations from the two sets of independent data. We repeated these analyses at the full brain level (here, 150 states) and the six subjects of the cneuromod movie10 dataset.

3. Results

3.1. State stability maps led to better compression within-subject than between-subject

To evaluate the compression quality of the state stability maps, we quantified the information loss between the original functional MRI signal and the state stability maps using the R-squared measure. This measure could be perceived as the space-time decomposition analogue of parcel homogeneity. We compared the within-subjects scores (individual time series are compressed with state stability maps generated on the same subject) with the between-subjects scores (individual time series are compressed with state stability maps generated on a different subject). Our results demonstrated that within-subjects R-squared scores outperformed the between-subjects R-squared scores. For instance, the average R-squared median was 0.68 at the within-subjects level compared to 0.55 at the between-subjects level (See Fig. 2). We reported the average R-squared maps scores both at the within- and the between-subjects levels (See Fig. 3). We observed that the average R-squared map generated from the same subjects states and runs (row=1 and column=1 in Fig. 3) had brighter colors than all the others maps generated from different subjects' runs and states (row=2 and row=3 in Fig 3). We also noticed that subcortical regions had low R-squared scores for all maps with red colors (See Fig. 3).

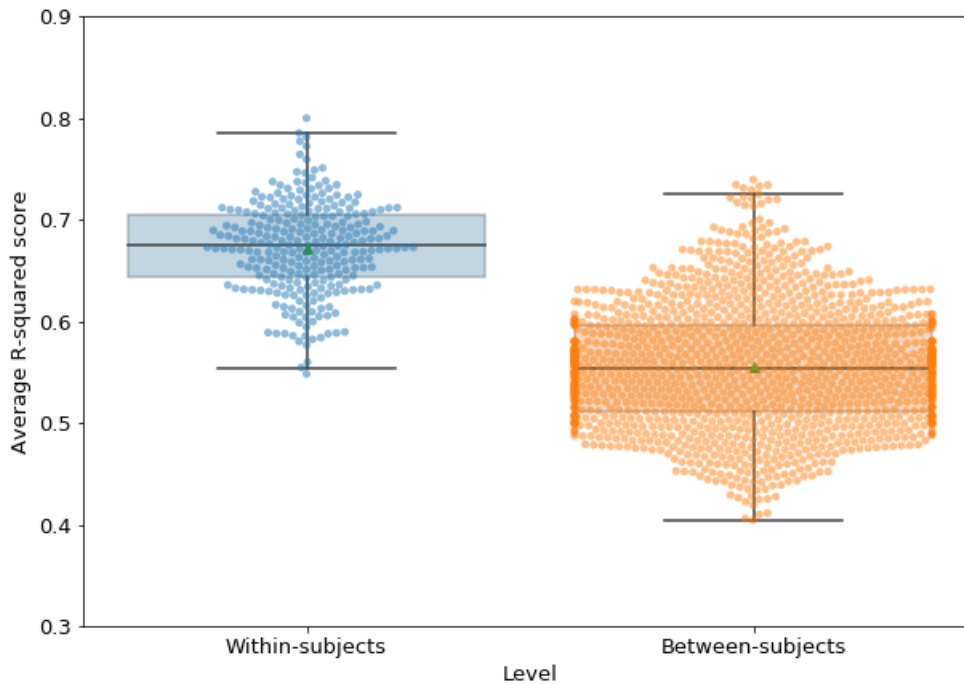


Fig. 2. The functional MRI signal compression quality was higher within-subject than between-subjects.

The average R-squared scores were computed between the functional MRI signal for each run and the state stability maps at the full brain level. Higher R-squared scores revealed that the loss between the real and the compressed data was minimized (e.g., If R-squared score = 1, that showed there was no information loss in the compressed state map). At the within-subjects level (blue), we computed the average R-squared score for each functional MRI run such that the state stability maps and the fMRI signals were associated with the same subject. At the between-subjects level (orange), we computed the average R-squared score for each run such that the state stability map and the fMRI signal were associated with different subjects. Six subjects from the *cneuromod movie10* dataset were included. Each subject had 150 state stability maps at the full brain level. 44 functional MRI runs were used to compute the R-squared scores from different four movies, including *Life* (5 runs), *Bourne supremacy* (10 runs), *Hidden figures* (12 runs), *Wolf of wall street* (17 runs).

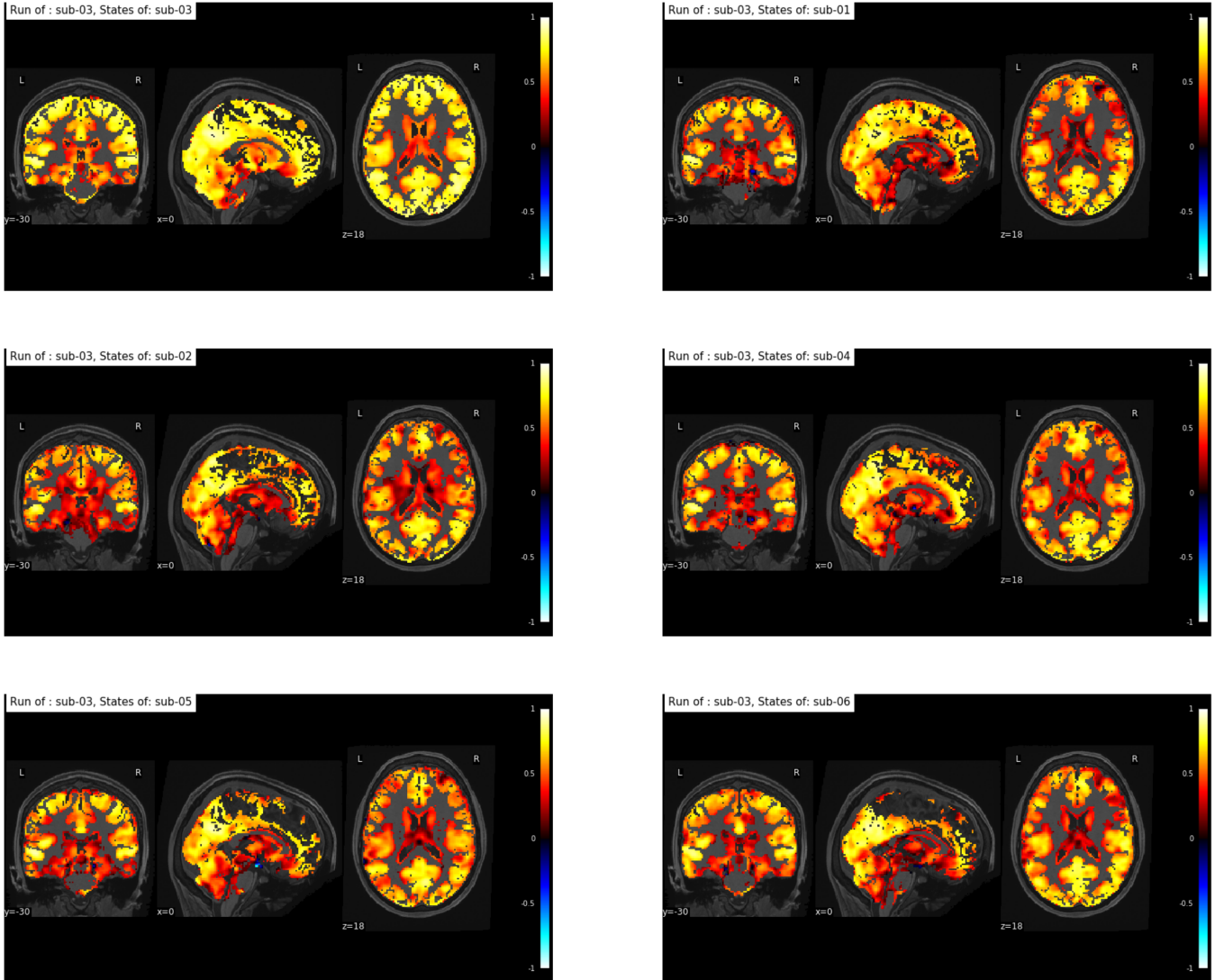


Fig. 3. The state stability maps had lower information loss when used for functional MRI compression at the within-subject level compared to the between-subject level.

We computed the average R-squared maps associated with the functional MRI runs of the Hidden figures movie. The first (row,column) corresponded to the average R-squared map of subject sub-03. This map was computed by averaging the 12 R-squared maps associated with 12 functional runs and 150 state stability maps. The functional runs and the state maps belong to the same subject sub-03 (within-subject level). The rest of the maps, in this figure, were generated such that the functional data was associated with subject sub-03 and the state stability maps were associated with the other five subjects from the cneuromod movie10 dataset. Each subject had 12 functional MRI runs from the Hidden figures movie and 150 dynamic states of parcellations at the full brain level.

3.2. Within-subjects reproducibility was higher than between-subjects, with some overlap in distribution

To assess the reproducibility of parcellations, we generated the dynamic states of parcellations based on two sets of independent data, for each subject. This allowed us to quantify and identify similarities and variations in the spatial reconfigurations of the dynamic states. Our results showed that within-subjects reproducibility distribution highly overlapped with between-subjects reproducibility distribution. There existed 75% overlap in the within-subjects distribution such that the scores ranged between 0 and 0.87 (See Fig. 4). However, the within-subjects median outperformed the between-subjects median with, respectively 0.68 and 0.37 scores (See Fig. 4).

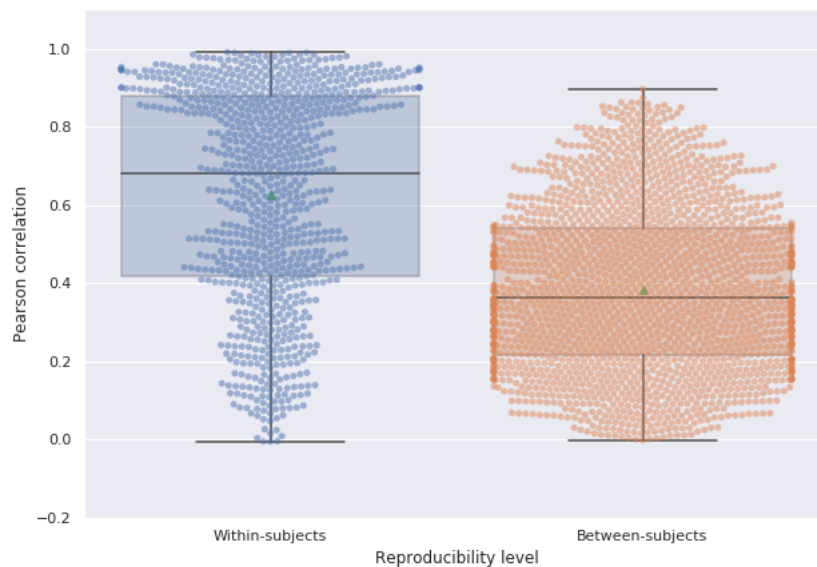


Fig. 4. Within-subjects reproducibility distribution was highly overlapping with the between-subjects reproducibility distribution in the case of movie data.

At the within-subjects level, we computed the Pearson correlation between the state stability maps of the same subject and matched between the two independent sets; i.e. training set and the test set. The training set was composed of 44 runs (10 minutes each) from four different movies, including Life (5 runs), bourne supremacy (10 runs), Hidden figures (12 runs), Wolf of wall street (17 runs). The test set was composed of only 17 runs from two different movies, including Life (5 runs) and Hidden figures (12 runs). A complete matching between states was applied using the Hungarian method by maximizing the Pearson correlation between pairwise maps. 150 dynamic states of parcellations were generated at the full brain level. Six subjects were investigated from the cneuromod movie10 dataset.

3.3. Dynamic states of parcellations were reproducible for some regions in the brain and inconsistent for others across the full brain in the context of the movie data

3.3.1. Within-subject reproducibility. We aimed to compare the similarities and variations of the dynamic states of parcellations between the training and the test sets at the within-subjects level. We classified the state stability maps according to their reproducibility levels. To better organize the dynamic states of parcellations, we distinguished three groups according to their reproducibility level: (1) high reproducibility level (Pearson correlation coefficients > 0.7), (2) average reproducibility level (Pearson correlation coefficients ≤ 0.7 and Pearson correlation coefficients ≥ 0.5) and (3) low reproducibility level (Pearson correlation coefficients < 0.5 and Pearson correlation coefficients ≥ 0.3).

In the case of the high reproducibility level, we observed a high consistency between the state stability maps of the training and the test sets associated with different regions in the brain. For instance, the posterior cingulate cortex (PCC) regions had high similarity between the state stability maps of the two sets (Fig. 5, map E versus map E'). Similarly, the state stability maps of the visual network were very similar with higher stability scores in the case of the test set with near perfect stability scores (Fig. 5, map I versus map I'). Similarly, we observed a high consistency between the visual regions located between the parietal and the occipital lobes (See Fig. 5, map K versus map K'). Cerebellar regions had also very consistent state stability maps across the two independent sets (Fig. 5, map H versus map H'). Moreover, the state stability maps associated with the insular regions were very consistent across the two sets of independent data with high stability scores for most voxels; i.e. stability scores > 0.75 (See Fig. 5, maps B versus map B' and map D versus map D'). The motor regions were also among the most reproducible regions across the two sets of independent data (Fig. 5, map G versus map G'). Compared to other regions throughout the brain, its state stability maps showed lower stability scores with less than 0.5 values for most voxels. Overall, many distributed dynamic states of parcellations had a high level of reproducibility across the training and the test sets in the context of movie data. Most voxels within these states were also highly stable with, at least 0.75 stability score for most voxels.

In the case of the average reproducibility, we observed that most state stability maps had remarkable spatial overlap in the maps of the training and the test sets. For instance, the state stability maps of the visual regions were spatially overlapping across the two sets (See Fig. 6, map = A versus map A'). Also, the state stability map C' of the test set in Fig. 6 showed that the dorsal anterior cingulate cortex regions (dACC) overlapped with the

dACC of map C associated with the training set (See Fig. 6). It also extended towards the frontoparietal regions. Within the same group of maps, we observed that some regions of the default mode network (DMN) had average stability scores; i.e. scores > 0.25 , including the frontoparietal regions (See Fig. 6, map F versus map F'). The dorsal attentional regions appeared also in the averagely reproducible state maps (See Fig. 6, map I versus map I' and map K versus map K'). Most voxels in those regions had average stability scores both in the training and test sets. Overall, different maps across the full brain had average reproducibility scores; i.e., reproducibility scores were superior to 0.5 and inferior to 0.7. At the voxel level, most stability scores within regions had average stability scores; i.e. stability scores were around 0.5.

Added to the highly and averagely reproducible state maps, we also observed that some states had low reproducibility from different regions in the brain. We reported the three map views such that the selected coordinates corresponded to the most stable regions in the state map. For instance, we found very low reproducibility between the insular regions in map C and the regions in map C'. Also, we observed low stability scores across voxels in the state maps. These voxels corresponded most likely to noise patterns. For instance, F and K maps corresponded clearly to noise. Even though some other state maps were not reproducible, we recognized some well-known regions including the insular regions in maps C, the dorsal attentional regions in map E (See Fig. 7).

Overall, we observed that different reproducible regions were identified in the state stability maps, at the full brain level. These regions had higher to low stability scores. Highly reproducible maps were more likely to include mostly stable voxels. Conversely, the state maps associated with poor reproducibility had very noisy and low stability scores.

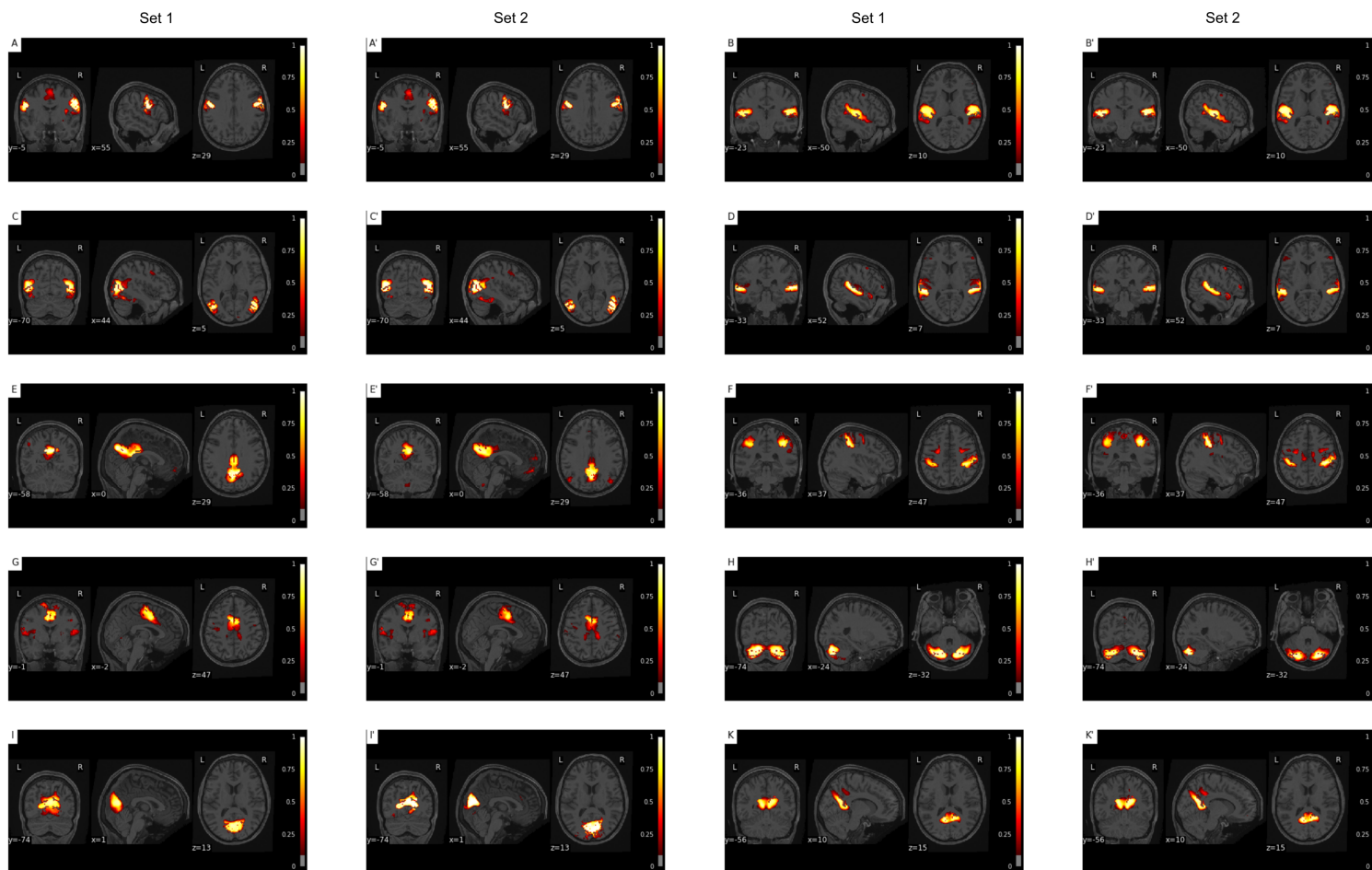


Fig. 5. Highly reproducible state stability maps across the training and the test data at the within-subjects level and across the whole brain.

We showed few state stability maps of subject sub-03 among the maps that were classified as highly reproducible with a reproducibility score threshold > 0.7 . The first and third columns were associated with the training set maps and the second and fourth columns were associated with the test set maps. The color bars showed the stability scores ranging between 0.1 and 1 values.

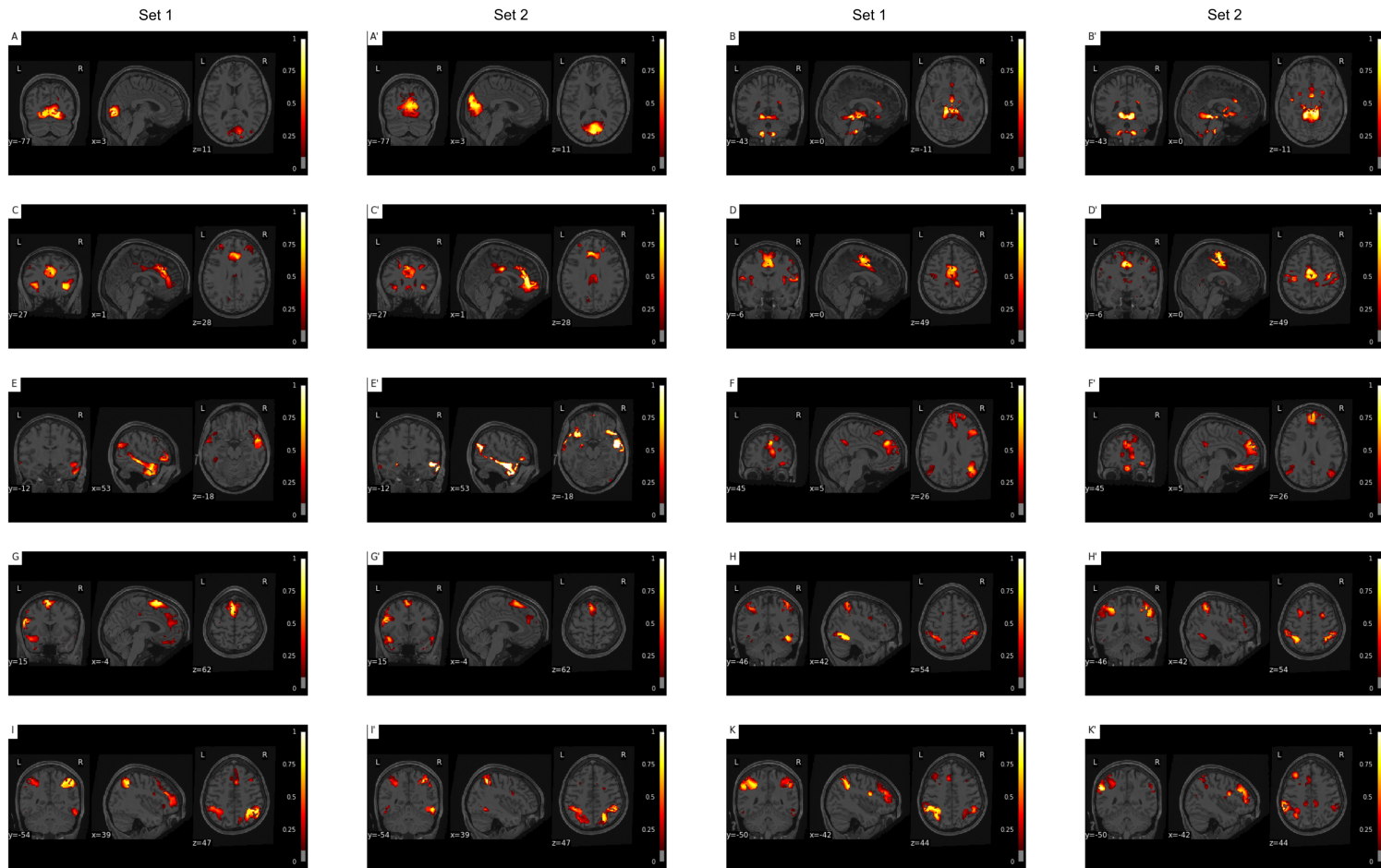


Fig. 6. Averagely reproducible state stability maps across the training and the test data at the within-subjects level and across the whole brain in the context of movie data.

We showed a few state stability maps of subject sub-03 among the maps that were classified among the maps having reproducibility score thresholds within $[0.5 \dots 0.7]$ scores. The first and third columns were associated with the training set maps and the second and fourth columns were associated with the test set maps. The color bars showed the stability scores ranging between 0.1 and 1 values.

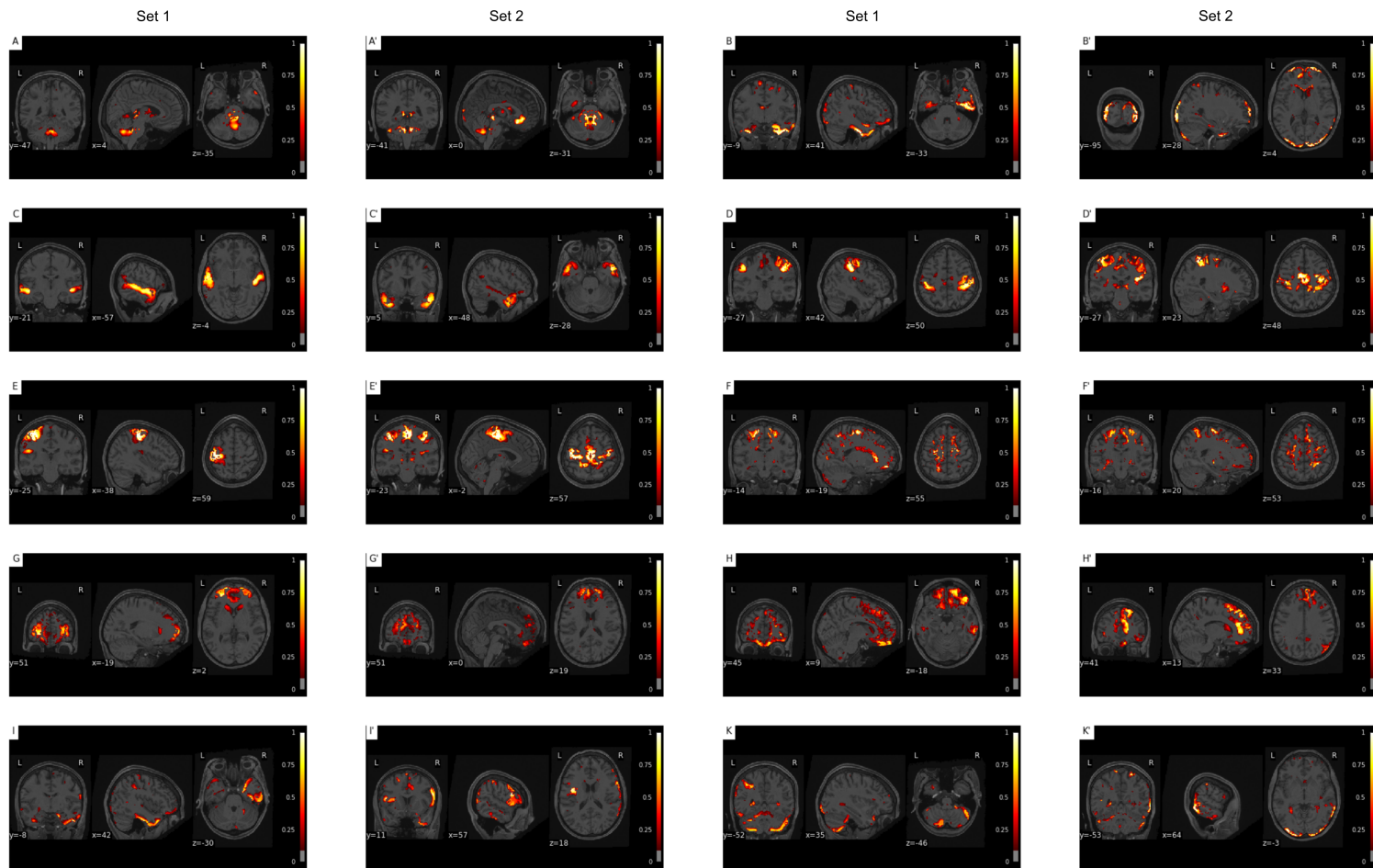


Fig. 7. Some state stability maps had low reproducibility across the training and the test data at the within-subjects level and across the whole brain.

A complete matching of the state maps from the training and the test data was applied using the Hungarian method by maximizing the Pearson correlation between the maps of the same subject (here, subject sub-03). We only showed a few state stability maps among the maps that were classified among the maps having reproducibility score thresholds within $[0.3 \dots 0.49]$ scores. The first and third columns were associated with the training set maps and the second and fourth columns were associated with the test set maps. The color bars showed the stability scores ranging between 0.1 and 1 values.

3.3.2. Between-subjects reproducibility. We aimed to visually compare the similarities and the differences between the dynamic states of parcellations between two subjects in the context of the movie data. This allowed us to identify the spatial overlap between the state stability maps across subjects. We distinguished between three groups of maps according to their reproducibility scores across the two sets; i.e. training and test data. In the case of highly reproducible maps, we observed a high spatial overlap between the state stability maps of subjects for different regions in the brain and the movie data. For instance, the insular regions were highly overlapping between the two subjects sub-02 and sub-03 (See Fig. 8, map C versus map C'). Additionally, we found a very high spatial consistency in the state stability maps of visual regions between subjects sub-02 and sub-03 (See Fig. 8, map E versus map E' and map F versus map F'). The cerebellum had also highly reproducible state stability maps across subjects sub-02 and sub-03 and it involved different regions from the cerebellum (See Fig. 8, map G versus map G' and map I versus map I').

Likewise the highly reproducible maps, we also observed that some regions overlapped between the state stability maps of different subjects. We found that these maps had some overlapping regions between two different subjects. For instance, the state stability map associated with the DMN and subject sub-02 overlapped with the DMN of subject sub-03 (See Fig. 9, map C versus map C'). In this case, map C' of subject sub-03 had more stable PCC voxels as part of the DMN compared to the PCC of subject sub-02 in map C (See Fig. 9). The dorsal attentional network regions were also involved in the averagely reproducible state maps between the two subjects sub-02 and sub-03 (See Fig. 9, map F versus map F'). Even though the stability of voxels in map F and subject sub-02 were higher than those in map F' and subject sub-03, their spatial coverage had an important overlap.

Conversely to the previous reproducibility levels, in the group of poorly reproducible state stability maps, we found mostly inconsistent regions in the state stability maps of two different subjects. For instance, the PCC of subject sub-02 and map E had a slight overlap with the PCC of subject sub-03 and map E'. Also, subcortical regions of subject sub-02 and map H had a very poor overlap with the spatial regions of subject sub-03 and map H' (See Fig. 10).

Overall, we found that dynamic states of parcellations had different levels of reproducibility ranging from high to low reproducibility at the between-subjects level in the context of movie data. We also observed that some well-known networks had different dynamic states of parcellations involving overlapping regions that were associated with more than one level of reproducibility at the between-subjects level (e.g., the visual regions).

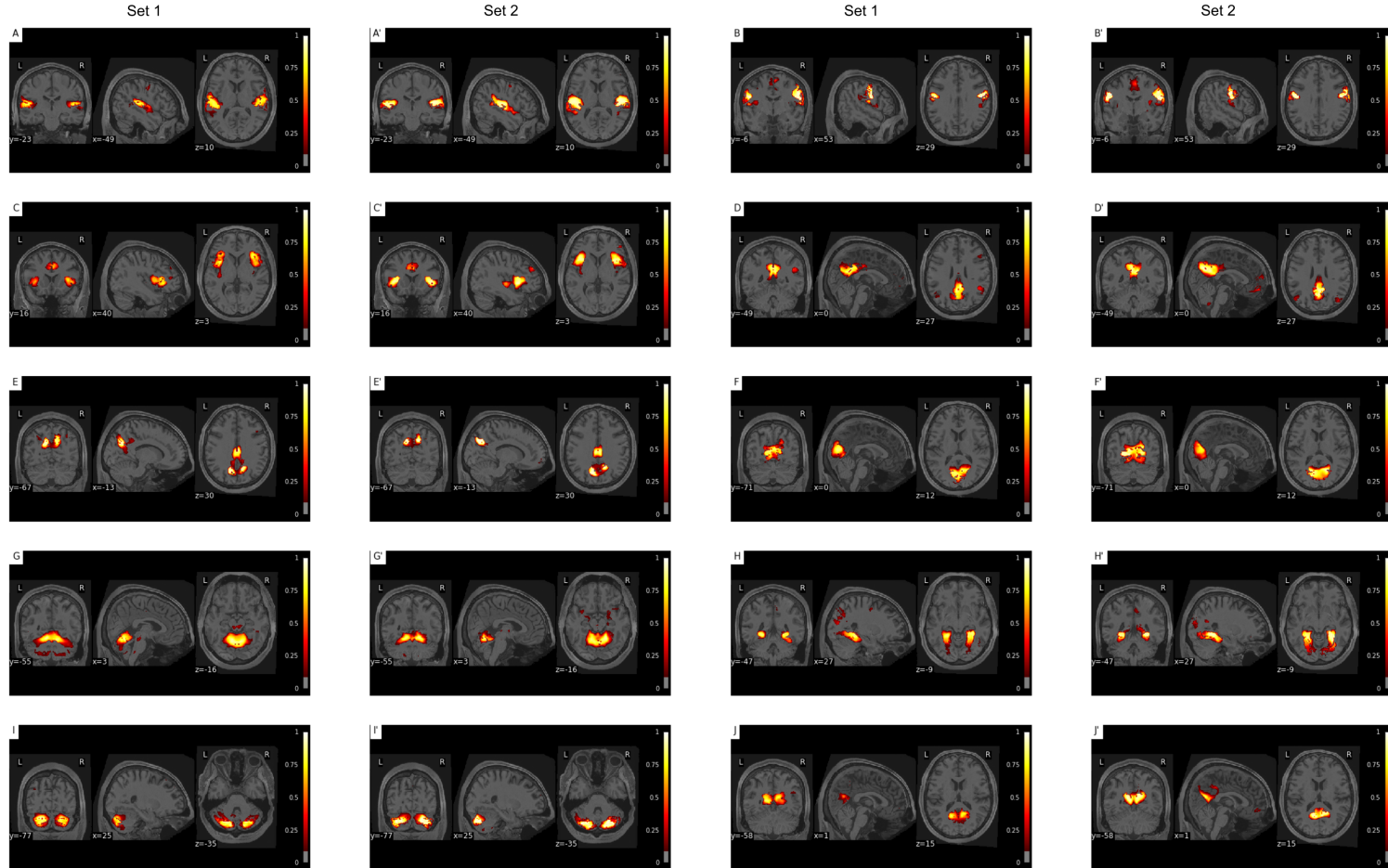


Fig. 8. Highly reproducible state stability maps across the training and the test data at the between-subjects level and the movie data.

A complete matching of the state maps from the training and the test data was applied using the Hungarian method by maximizing the Pearson correlation between the state stability maps of the same subject (here, subject sub-02 and sub-03). That is, each subject state from the training set was matched to its most similar state in the test set. The matched states were associated with different subjects. The first and third columns were associated with subject sub-02 and the second and fourth columns were associated with subject sub-03. A threshold was applied to keep only stability scores over 0.7. The color bars showed the stability scores ranging between 0.1 and 1 values.

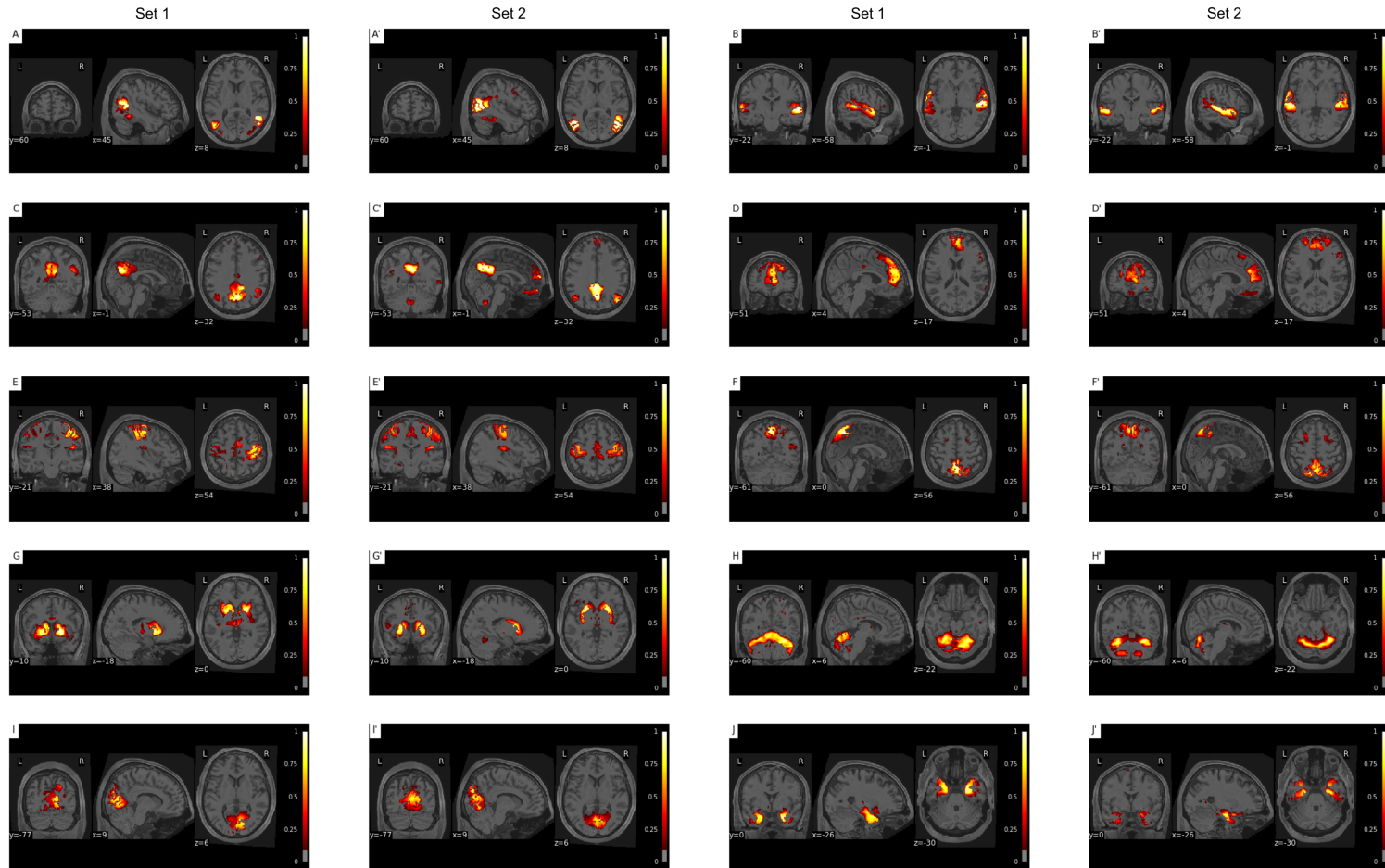


Fig. 9. Averagely reproducible state stability maps across the training and the test data at the between-subjects level in the context of movie data.

The first and third columns were associated with subject sub-02 and the second and fourth columns were associated with subject sub-03. A threshold was applied to keep only stability scores ≥ 0.5 and stability scores ≤ 0.7 . The color bars showed the stability scores ranging between 0.1 and 1 values.

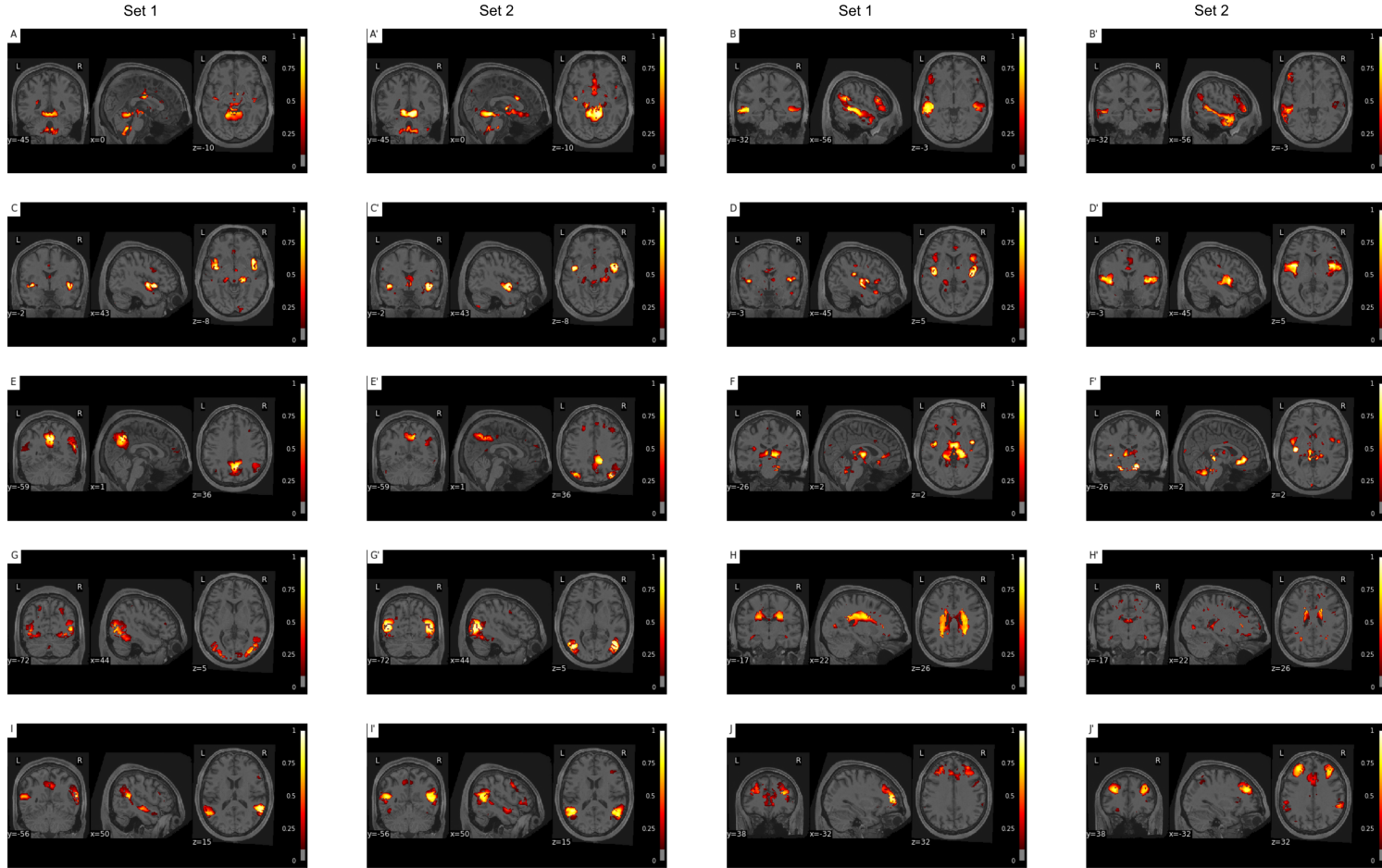


Fig. 10. Some state stability maps had low reproducibility scores at the between-subject level.

The first and third columns were associated with subject sub-02 and the second and fourth columns were associated with subject sub-03. A threshold was applied to keep only stability scores ≥ 0.3 and stability scores < 0.5 . The color bars showed the stability scores ranging between 0.1 and 1 values.

4. Discussion

In this work, we aimed to generalize the identification of dynamic states of brain parcellations at the full brain level for individuals. Our first main finding was the existence of different dynamic states of parcellations across the brain. We also found its state stability maps had promising compression quality of the reduced data. Some dynamic states were markedly different in terms of the brain regions involved and some states were spatially overlapping despite being derived from the same subject in the context of movie data. We also distinguished three different levels of spatial reproducibility among the identified dynamic states of parcellations, i.e. high, medium and low reproducibility both at the within-subject level (between the two independent sets) and the between-subjects levels. We also found better compression quality at the within-subject level compared to the between-subject level. Another main finding of this paper was the existence of very high spatial reproducibility for some state stability maps both at the within-between subjects level; i.e. Pearson correlation > 0.7 . Still, we found the reproducibility at the within-subjects level outperformed the reproducibility at the between-subject level.

In the literature of brain parcellation, both our approach and Dadi and colleagues 2020 showed the existence of different modes of variations at the full brain level [?]. Also, both approaches reported promising results by identifying different modes of variations of the cerebral cortex [?, 18]. The main difference with our work was that Dadi and colleagues used a collection of brain atlases with different resolutions; i.e. 64 to 1024 static brain parcels to extract soft parcels. These parcels were identified using a huge dataset of 2.4TB. However, in our approach, few hours of data were enough to identify time-space decomposition at the full brain level based simply on aggregating k-Means one-hot encoders. These one-hot encoders were generated in short windows using functional signals. Salehi and colleagues also shared with us their consistent theoretical formalization of brain parcellations [67]. That is, authors suggested brain parcellation was not fixed and showed the existence of parcellations for different cognitive states, including the motor task, the working memory task and the resting state task [67]. The main difference with our approach was the generation of static parcellation per task using several minutes of fMRI data per parcellation [Salehi et al., 2018]. Before these approaches, many researchers studied the rich dynamic architecture of brain networks using the dynamic functional connectivity [44, 43, 1, 4, 33, 50]. These researchers suggested the neuroscience community needed new computational methods to unravel the repetitive spatial patterns over time and develop new methods for simplified representations in the context of complex and high-dimensional feature space of dynamic fMRI data [25]. These methods would facilitate the analysis of the individual differences in internal cognitive states over short time scales [25].

To evaluate the quality of the space-time decomposition of the cerebral cortex into dynamic states of parcellations, we evaluated the compression quality of the real functional signal both at the within-subject and the between-subjects levels. We found that the within-subject compression scores outperformed the between-subjects compression scores. For instance, we observed some state stability maps had near perfect R-squared scores as a compression measure (with an average R-squared score of 0.63), while between-subject state stability maps had 0.39 average R-squared score (See Fig. 2). In the literature, the compression quality scores were lower than our scores in terms of R-squares scores (with an average R-squared measure of 0.55 in the case of 512 states), however, a direct comparison is still required between our approach and state of the art approaches [?]. We also observed that most voxels throughout the brain had high R-squared scores at the within-subject level as shown in the R-squared map in Fig. 3 (Row=1, column=1). Only subcortical regions had lower compression quality with lower R-squared scores. In the literature, for instance the subcortical regions had challenging issues in fMRI scans, including the physiological noise and the spatial resolution [48]. Therefore, we observed higher information loss (or lower R-squared scores with around 0.5 scores, See Fig. 3) in the subcortical regions voxels compared to the rest of the cerebral cortex (most voxels had > 0.7 R-squared measures). Overall, promising findings showed that our approach generated a good representation of fMRI data with high fidelity to the original signal and a lower loss of information in the reduced version.

We also conducted a reproducibility analysis to evaluate the goodness of the generated dynamic states of parcellations. We found different levels of reproducibility scores going from high scores to low scores. We found that the average reproducibility scores at the within-subject level (average score=0.62, See Fig. 4). In our previous work, we reported higher average reproducibility scores associated with three seed subnetworks in a resting state condition, including the PM-VIS, the dACC and the PCC with respectively 0.97, 0.82 and 0.9 average reproducibility scores. The differences in the average reproducibility scores could be explained by the differences in reproducibility for different regions of the brain. We distinguished three groups of state stability maps associated with different regions according to their reproducibility scores. The visual maps showed different subnetworks could be included in different groups, including the PCC regions, the visual regions and the salience network regions. The existence of different levels of reproducibility could be associated with the differences in the cognitive states of a given subject during the movie watching and between the two replicated sets. Also, some dynamic states of parcellations had very poor reproducibility with noisy state stability maps (scores > 0.5). In the future, we are planning to provide further analysis to identify noisy patterns among other neurobiological

meaningful state stability maps. Still, these findings were consistent with ICA- based components which in part were associated with noise patterns in fMRI data [10, 30, 84]. Another important finding in this work was that our within-subject reproducibility scores distribution had a high overlap with the between-subjects reproducibility scores (only 25% of within-subject reproducibility scores exceeded the between-subject reproducibility). In a previous work, we showed there were two disjoint distributions between within- and between-subject reproducibility scores in the case of three subnetworks and resting state data [18]. Even though the theoretical basis was the same, the differences in reproducibility distributions at the within- and the between-subjects levels differed in the cases of the resting state and the movie data. These findings could be associated with the movie watching fMRI. That is, the cognitive engagement of subnetworks across subjects was more consistent due to the same stimuli in the movie which was not the case in the random fluctuations of resting state data. Future interesting research directions could be to study the differences in the spatial changes in dynamic states of parcellations across time and in the context of movie data to quantify the alignment of spatial maps over time.

In the future, we are planning to compare the compression quality of our approach with other existing approaches both in the cases of static and soft parcellations, including the ICA and DIFUMO. This would allow us to position our contribution with respect to other approaches to identify when it performed better and its limitations. We also aim to generalize our approach to different datasets; i.e. hcprtr dataset, and generate performance measures; i.e. the reproducibility and the compression quality. That would allow us to see whether we still have the same performance results on other datasets in different contexts; i.e., task state, resting state. Also, an interesting research area to investigate is to study differences in state stability maps between healthy controls and psychiatric disorders. This helps to isolate the specific changes in brain dynamics reflected on brain parcels over time in both cases.

Neuroimaging research datasets were dramatically increasing in size during the past five years. Additionally, there was an emergent trend of the application of deep learning models in the neuroscience field. However, there were few guidelines in the literature on how to handle the high dimensionality of neuroimaging data. In the field of brain parcellation, few approaches suggested scalable algorithms to parcellate the brain. Thus, the replication of brain parcellations on different datasets has been challenging for the past two decades. For instance, Nilearn platform hosted several brain atlases, including BASC [15], Yeo’s atlas [82] to facilitate their use by other researchers. Most of these atlases were generated at the group level. Altogether, this motivated neuroscientist researchers to have practical guidelines to replicate parcellations at the subject level regardless of the dataset

size. Therefore, we are planning to provide a technical report that describes our algorithm implementation added to memory and time profiling to show its scalability and ease to run on custom datasets.

5. Conclusion

In this work we used a simple clustering technique such as k-Means to identify highly reproducible functional parcellation at the full brain level, even when applied on short fMRI time series (a few minutes). We extended the DYPAC method to identify the main states of these dynamic parcellations, and demonstrated that their spatial distributions had high compression quality between the reduced and the raw signal. We also found different groups of dynamic states grouped by their reproducibility. The formalization of the parcellation problem as a dynamic problem would have further implications on the neuroimaging analyses, including many graph-based neuroimaging analyses. This opens new research directions to explore after replacing the static parcellations by the dynamic parcellations. Also, these parcellations would help studying the rich dynamic interactions between functional brain networks.

6. Acknowledgment

The Courtois project on neural modelling was made possible by a generous donation from the Courtois foundation, administered by the Fondation Institut Gériatrie Montréal at CIUSSS du Centre-Sud-de-l'île-de-Montréal and University of Montreal. The Courtois NeuroMod team is based at "Centre de Recherche de l'Institut Universitaire de Gériatrie de Montréal", with several other institutions involved. See the cneuromod documentation for an up-to-date list of contributors ⁴.

⁴<https://docs.cneuromod.ca>

Chapter 5

Discussion

5.1. Contributions

In this thesis, I developed a new method that accurately estimates individual dynamic brain parcellation and that may help the neuroimaging community better understand the rich dynamic interactions between brain subnetworks. The cornerstone of our method is the existence of highly similar seed-based parcellations extracted (or one-hot encoders) from short time windows, sometimes separated by several days. This was the key to generating stable dynamic brain parcellations which challenged the notion of a fixed, static brain parcellation estimated from a very long time series. We used a simple cluster aggregation method that generated seed based parcels over multiple time windows. Our results showed that dynamic states of parcellations were subject-specific, highly reproducible, and reliable enough to successfully differentiate subjects in a fingerprinting experiment with high accuracy. We investigated the sensitivity of the DYPAC1.0 algorithm to different parameters and we found its robustness to these parameters. We then extend our original method to work on the full brain, the DYPAC2.0 algorithm, and found that the resulting parcels allowed to compress individual fMRI time series in very low dimension (from over 100k voxels down to 150 parcels), with high fidelity.

Recent approaches in the parcellation field questioned the idea of a fixed functional organization of the human brain. The idea of space-time decomposition itself was applied for more than two decades using ICA. Still, our approach was, to our knowledge, the first attempt to shed light on this individual dynamic brain organization using a simpler, hard clustering technique. Our work also considered a fine temporal scale (in the order of a few minutes) and a voxel level of resolution (i.e. without reducing the dimensionality in a fine-grain parcellation), which is not common in cluster-based analysis typically applied on “super-voxels”. Also, we were the first to provide dynamic parcellations at the individual level and to compare their state stability maps within- and between-subjects, extending the

individual static parcellation work of Gordon et al. (2017). In the first two chapters of this work, we run our analysis on long scanning acquisitions from ten subjects of the resting state data of the Midnight Scan club dataset. We found for each subject a rich repertoire of dynamic states (up to three states) per subject, especially in the case of heteromodal cortices, i.e. the PCC and the dACC subnetworks. The identified regions in the state stability maps were reported by previous studies as biologically valid neural cognitive states (e.g., high stability was observed around the motor and premotor regions of the dACC maps was explained in the literature by the existence of a functional coupling between the AI and the dACC that facilitates a rapid access to the motor system [3]). Also, we run reproducibility analysis and the performance measures were consistent with the previous results. I published this work in Network Neuroscience journal, that represented a key proof of concept for a dynamic parcellation approach.

Overall, our visual and quantitative analysis showed promising results with potential areas of improvements. First, DYPAC1.0 generated dynamic parcels for specific seed subnetworks without scaling at the full brain level or Gigabytes of memory were required to iterate over several seeds throughout the brain. Second, there were no guidelines on how to evaluate the homogeneity of the dynamic parcels. The cluster aggregation method used as a basis of DYPAC1.0 was simple and could be modified to scale to the high dimensionality of the full brain level. This motivated us to extend the seed-based parcellation method DYPAC1.0 to DYPAC2.0 as a full brain parcellation method, keeping the idea of an ensemble clustering method building on top of a fast and scalable algorithm (K-means).

Due to the high increasing demand of the neuroimaging data (to Terabytes), we expect DYPAC2.0 tool to be highly in demand for dimensionality reduction by the neuroimaging community as an open-source and scalable tool. We run all our analysis on the cneuromod movie10 dataset, providing several hours of high-resolution (in time and space) functional MRI acquisitions. Up to date, we were using the movie data for six subjects but we are planning to extend this to task data from the same subjects. To evaluate DYPAC2.0, we evaluated the compression quality of the dynamic states at the voxel level as a homogeneity measure. Our results showed that the state stability maps generated by DYPAC2.0 led to better compression within-subject than between-subject. This validated again dynamic parcels are subject specific. Also, we replicated the reproducibility analysis of the first paper. Consistently to the results of DYPAC1.0 and resting state data, we found the within-subject reproducibility scores were higher than the between-subject's reproducibility scores. Still, it is important to mention that the nature of the used functional signal impacted the reproducibility scores. That is, we found a higher overlap between the within- and the between-subjects distributions in the case of the movie data compared to the

resting state data. This opened new research directions for investigation, in the future to understand the differences in dynamic states underlying the differences in cognitive states in resting state and movie signals. This may also be due to differences in acquisition parameters between the cneuromod and midnight brain scan datasets, and our choices of preprocessing strategies. These avenues need to be investigated further.

In both rest and movie data, the rich repertoire of dynamic states characterized the heterogeneity of cognitive states in functional data. Investigating the association of these dynamic states to their cognitive states could help a better understanding of how the human brain reconfigures its subnetworks both in the cases of movie and rest signals. It is also interesting to compare whether the same movie stimuli triggers the same dynamic states between subjects. In our first paper, we ran a temporal analysis that confirmed the non existence of temporal consistency in the dynamic states at rest. In the context of task stimuli, we hypothesize the existence of temporal synchrony of dynamic states over time, at the within-subject and the between-subject levels. It is therefore important to run a temporal analysis in the case of the movie and task data to validate our hypothesis.

Another important future work would be to characterize the dynamic states throughout the brain by differentiating which states were associated with neural cognitive processes and which states were just noisy patterns, including the physiological noise. We are also planning to investigate to which extent do the DYPAC2.0 states differ from ICA and DIFUMO components (another scalable soft parcellation method proposed recently) ? and whether DYPAC2.0 dynamic states offered important gains in reproducibility and compression scores compared to DIFUMO and ICA.

Most importantly, we intend to show the usefulness of the generated state stability maps in neuroimaging research as part of the cneuromod projects. For instance, we want to know whether the dynamic states could be used to define the nodes of the artificial neural networks and help to improve the training and the prediction of cognitive tasks using artificial neural networks based on recordings of the activity of biological neural networks. Another application of the dynamic states would be to generate connectome-based models to accurately decode cognitive states. In this context, group dynamic states could be identified as spatial and overlapping patterns across subjects. These states could be used, for example, as subtypes to characterize groups of healthy subjects or groups of people with neurological disorders.

In the litterature, different brain parcellation schemes was developed to identify the nodes of the structural connectivity networks. The objective was to describe the Alzheimer

disease related deterioration of structural connectivity networks. The results showed that the topological examination of structural networks with different parcellation schemes can provide important complementary Alzheimer disease related information and thus contribute to a more accurate and earlier diagnosis [78]. In the context of the dynamic states of parcellations, we found better performance measures in comparison with the static brain parcellations and we hypothesize that the use of our parcels would improve the identification of the disease.

Another interesting extension of our work is to look at the generalizability of the compression quality of dynamic states with new datasets including the cneuromod movies (with about 30 hours of data per subject for six subjects) and the cneuromod HCP test-retest dataset (with 7 tasks including working memory, visual task, etc.). Also, it would be interesting to evaluate to which extent our DYPAC states improves quality metrics compared to group atlases, widely used in the literature.

5.2. Conclusion

The objective of this thesis was the generation of a new scalable tool to parcellate the brain into dynamic states of parcellations DYPAC. We proceeded on stepwise contributions. First, we presented DYPAC1.0, a seed-based parcellation method at the individual level, as a proof of concept to show the dynamic parcellations represent an interesting tool to better reduce the dimensionality of the brain compared to static parcellations. Our visual and quantitative analysis showed promising results which encouraged us to extend this method to the full brain. Second, we carefully investigated the impact of hyper-parameters on the outputs of DYPAC1.0. Third, we proposed a scalable open-source dynamic parcellation at the full brain and at the individual level called DYPAC2.0. We reported promising results in terms of the reproducibility and the compression quality of functional signals. We expect this tool to be widely used for the dimensionality reduction of big functional data in the future and it opens new potential research directions in neuroimaging research.

Supplementary Materials

.1. Supplement 1: The Dice score coefficient

$$\text{Dice score} = \frac{2 \times \sum_{x1==1} \text{Part1}(x1) \sum_{x2==1} \text{Part2}(x2)}{\sum_{x1} \text{Part1}(x1) + \sum_{x2} \text{Part2}(x2)} \quad (.1.1)$$

We used the Dice score coefficient [32] to quantify the similarity between two seed-based parcellations. The Dice score formula is illustrated in Eq. .1.1. *Part1* and *Part2* represent the two seed-based parcellations. *x1* and *x2* variables represent the voxels in, respectively *Part1* and *Part2*. This score ranges between 0 and 1. The higher this score is, the more similar the two parcellations are.

.2. Supplement 2: The Adjusted Rand Index

$$\text{rand index} = \frac{a + b}{a + b + c + d} \quad (.2.1)$$

$$\text{adjusted rand index} = \frac{(\text{rand index} - \text{expected rand index})}{(\text{max}(\text{rand index}) - \text{expected rand index})} \quad (.2.2)$$

We used the Adjusted Rand Index (ARI) as a temporal similarity measure between two seed-based parcellations by considering all pairs of voxels and counting pairs that are assigned or not in a state associated with a given time point in two different seed-based parcellations. *a* and *b* represent the voxels falling in the state, at the same time points, for two different seed-based parcellations. *c* and *d* represent the voxels not in the state, at the same time points, for two different seed-based parcellations (See Eq. .2.1).

The adjusted Rand index is thus ensured to have a value close to 0.0 for random labeling independently of the number of clusters and samples and exactly 1.0 when the seed-based parcellations are identical (up to a permutation) (See Eq. .2.2).

.3. Supplement 3: The Hungarian algorithm

Algorithm 1 Hungarian algorithm

```

1: procedure MATCH(maps1, maps2)
2:   Init states1 ▷ Number of state stability maps in set1
3:   Init states2 ▷ Number of state stability maps in set2
4:   for s1 in states1 do
5:     for s2 in states2 do
6:       dist = pearsonr(maps1(s1), maps2(s2))
7:       costs(s1, s2) = (1 - dist)
8:       distances(s1, s2) = dist
9:       row_id, col_id = linear_sum_assignment(costs)
10:    for s in max(states1, states2) do
11:      distances_matched_maps(s) = distances(row_id(s), col_id(s))
12:      matched_state_maps(s) = (row_id(s), col_id(s))
13:   Return distances_matched_maps
14:   Return matched_state_maps

```

Prior to quantifying the spatial reproducibility, we used the Hungarian method algorithm to match the state stability maps both at the within- and the between-subjects levels [51]. We used this algorithm because it solved for us the assignment problem of state stability maps in polynomial time. The MATCH procedure illustrated the Hungarian algorithm in Alg. 1. In lines [4..8], we iterated over all pairs of state stability maps in set 1 (represented by *maps1*) and set 2 (represented by *maps2*). We used the Pearson correlation score to quantify the spatial similarity distance *dist* between a pair of maps (See line 6). The cost associated with a pair of map was computed in line 7. Then, we used the linear sum assignment function to match state stability maps.

The linear sum assignment problem is also known as minimum weight matching in bipartite graphs. A problem instance is described by a matrix *C*, where each *costs*(*s1*, *s2*) is the cost of matching the state stability map *s1* of the first set (considered to be the "workers") and the state stability map *s2* of the second set (considered to be the "jobs"). The goal was to find a complete assignment of the workers to jobs of minimal cost s.t. each row is assigned to at most one column *col_id*, and each column to at most one row *row_id*. Formally, let *X* be a boolean matrix where $X[s1, s2] = 1$. if row *s1* is assigned to column *s2*. Then the optimal assignment has *cost* as computed in Eq. .3.1.

$$\text{cost} = \min \left(\sum_{s1} s2 \sum_{s2} \text{costs}(s1), s2 X_{s1}, s2 \right) \quad (.3.1)$$

References

- [1]
- [2]
- [3] Salience network.
- [4] E. A. Allen, E. Damaraju, S. M. Plis, E. B. Erhardt, T. Eichele, and V. D. Calhoun. Tracking whole-brain connectivity dynamics in the resting state. *Cereb. Cortex*, 24(3):663–676, Mar 2014.
- [5] S. Arslan, S. I. Ktena, A. Makropoulos, E. C. Robinson, D. Rueckert, and S. Parisot. Human brain mapping: A systematic comparison of parcellation methods for the human cerebral cortex. *Neuroimage*, 170:5–30, 04 2018.
- [6] Salim Arslan and Daniel Rueckert. Multi-level parcellation of the cerebral cortex using resting-state fmri. In *International Conference on Medical Image Computing and Computer-Assisted Intervention*, pages 47–54. Springer, 2015.
- [7] David Arthur and Sergei Vassilvitskii. How slow is the k-means method? In *Proceedings of the Twenty-Second Annual Symposium on Computational Geometry, SCG '06*, page 144–153, New York, NY, USA, 2006. Association for Computing Machinery.
- [8] A. Badhwar, Y. Collin-Verreault, D. Lussier, H. Sharmarke, P. Orban, S. Urchs, I. Chouinard, J. Vogel, O. Potvin, S. Duchesne, and P. Bellec. A dataset of long-term consistency values of resting-state fMRI connectivity maps in a single individual derived at multiple sites and vendors using the Canadian Dementia Imaging Protocol. *Data Brief*, 31:105699, Aug 2020.
- [9] D. S. Bassett, N. F. Wymbs, M. A. Porter, P. J. Mucha, J. M. Carlson, and S. T. Grafton. Dynamic reconfiguration of human brain networks during learning. *Proc. Natl. Acad. Sci. U.S.A.*, 108(18):7641–7646, May 2011.
- [10] C. F. Beckmann, M. DeLuca, J. T. Devlin, and S. M. Smith. Investigations into resting-state connectivity using independent component analysis. *Philos. Trans. R. Soc. Lond., B, Biol. Sci.*, 360(1457):1001–1013, May 2005.
- [11] Christian F. Beckmann. Modelling with independent components. *NeuroImage*, 62(2):891 – 901, 2012. 20 YEARS OF fMRI.
- [12] P. Bellec, S. Lavoie-Courchesne, P. Dickinson, J. P. Lerch, A. P. Zijdenbos, and A. C. Evans. The pipeline system for Octave and Matlab (PSOM): a lightweight scripting framework and execution engine for scientific workflows. *Front Neuroinform*, 6:7, 2012.
- [13] Pierre Bellec, Y Benhajali, Felix Carbonell, C Dansereau, G Albouy, M Pelland, C Craddock, O Collignon, J Doyon, E Stip, et al. Multiscale statistical testing for connectome-wide association studies in fmri. *arXiv preprint arXiv*, 2014.

- [14] Pierre Bellec, Vincent Perlbarg, Saâd Jbabdi, Mélanie Pélégrini-Issac, Jean-Luc Anton, Julien Doyon, and Habib Benali. Identification of large-scale networks in the brain using fmri. *Neuroimage*, 29(4):1231–1243, 2006.
- [15] Pierre Bellec, Pedro Rosa-Neto, Oliver C Lyttelton, Habib Benali, and Alan C Evans. Multi-level bootstrap analysis of stable clusters in resting-state fmri. *Neuroimage*, 51(3):1126–1139, 2010.
- [16] R. F. Betzel, M. A. Bertolero, E. M. Gordon, C. Gratton, N. U. F. Dosenbach, and D. S. Bassett. The community structure of functional brain networks exhibits scale-specific patterns of inter- and intra-subject variability. *Neuroimage*, 202:115990, 11 2019.
- [17] Woolrich M. W. Glasser M. F. Robinson E. C. Beckmann C. F. Van Essen D. C. Harrison S. J. Bijsterbosch, J. D. and S. M. Smith. The relationship between spatial configuration and functional connectivity of brain regions. 2018.
- [18] Amal Boukhdhir, Yu Zhang, Max Mignotte, and Pierre Bellec. Unraveling reproducible dynamic states of individual brain functional parcellation. *Network Neuroscience journal*, 2020.
- [19] R. M. Braga and R. L. Buckner. Parallel Interdigitated Distributed Networks within the Individual Estimated by Intrinsic Functional Connectivity. *Neuron*, 95(2):457–471, Jul 2017.
- [20] U. Braun, A. Schfer, D. S. Bassett, F. Rausch, J. I. Schweiger, E. Bilek, S. Erk, N. Romanczuk-Seiferth, O. Grimm, L. S. Geiger, L. Haddad, K. Otto, S. Mohnke, A. Heinz, M. Zink, H. Walter, E. Schwarz, A. Meyer-Lindenberg, and H. Tost. Dynamic brain network reconfiguration as a potential schizophrenia genetic risk mechanism modulated by NMDA receptor function. *Proc. Natl. Acad. Sci. U.S.A.*, 113(44):12568–12573, 11 2016.
- [21] B. R. Buchsbaum, S. Greer, W. L. Chang, and K. F. Berman. Meta-analysis of neuroimaging studies of the Wisconsin card-sorting task and component processes. *Hum Brain Mapp*, 25(1):35–45, May 2005.
- [22] V. D. Calhoun, T. Adali, G. D. Pearlson, and J. J. Pekar. Spatial and temporal independent component analysis of functional mri data containing a pair of task-related waveforms. *Hum Brain Mapp*, 13(1):43–53, May 2001.
- [23] J. Casorso, X. Kong, W. Chi, D. Van De Ville, B. T. T. Yeo, and R. Li?geois. Dynamic mode decomposition of resting-state and task fMRI. *Neuroimage*, 194:42–54, 07 2019.
- [24] J. E. Chen, C. Chang, M. D. Greicius, and G. H. Glover. Introducing co-activation pattern metrics to quantify spontaneous brain network dynamics. *Neuroimage*, 111:476–488, May 2015.
- [25] J. E. Chen, M. Rubinov, and C. Chang. Methods and Considerations for Dynamic Analysis of Functional MR Imaging Data. *Neuroimaging Clin. N. Am.*, 27(4):547–560, Nov 2017.
- [26] W. Chiong, S. M. Wilson, M. D’Esposito, A. S. Kayser, S. N. Grossman, P. Poorzand, W. W. Seeley, B. L. Miller, and K. P. Rankin. The salience network causally influences default mode network activity during moral reasoning. *Brain*, 136(Pt 6):1929–1941, Jun 2013.
- [27] Wolf D. H. Power J. D. Roalf D. R. Baum G. L. Ruparel K. Shinohara R. T. Elliott M. A. Eickhoff S. B. Davatzikos C. Gur R. C. Gur R. E. Bassett D. S. Ciric, R. and T. D. Satterthwaite. Benchmarking of participant-level confound regression strategies for the control of motion artifact in studies of functional connectivity. *NeuroImage*, (154):174–187, March 2017.
- [28] cneuromod. cneuromod, 2018-2020. <https://www.cneuromod.ca/>, Accessed on July 29, 2020.
- [29] K. Dadi, G. Varoquaux, A. Machlouzarides-Shalit, K. J. Gorgolewski, D. Wassermann, B. Thirion, and A. Mensch. Fine-grain atlases of functional modes for fMRI analysis. *Neuroimage*, 221:117126, Jul 2020.
- [30] J. S. Damoiseaux, S. A. Rombouts, F. Barkhof, P. Scheltens, C. J. Stam, S. M. Smith, and C. F. Beckmann. Consistent resting-state networks across healthy subjects. *Proc. Natl. Acad. Sci. U.S.A.*, 103(37):13848–13853, Sep 2006.

- [31] christian Dansereau, Pierre Orban, and Pierre Bellec. Functional subtypes for prediction in schizophrenia. 2016.
- [32] Lee R. Dice. Measures of the amount of ecologic association between species. *Ecology*, 26(3):297–302, 1945.
- [33] P. Donnelly-Kehoe, V. M. Saenger, N. Lisofsky, S. Kohn, M. L. Kringelbach, J. Schwarzbach, U. Lindenberger, and G. Deco. Reliable local dynamics in the brain across sessions are revealed by whole-brain modeling of resting state activity. *Hum Brain Mapp*, 40(10):2967–2980, 07 2019.
- [34] S. B. Eickhoff, B. T. T. Yeo, and S. Genon. Imaging-based parcellations of the human brain. *Nat. Rev. Neurosci.*, 19(11):672–686, 11 2018.
- [35] E. S. Finn, X. Shen, D. Scheinost, M. D. Rosenberg, J. Huang, M. M. Chun, X. Papademetris, and R. T. Constable. Functional connectome fingerprinting: identifying individuals using patterns of brain connectivity. *Nat. Neurosci.*, 18(11):1664–1671, Nov 2015.
- [36] Alex Fornito, Andrew Zalesky, and Edward Bullmore. *Fundamentals of Brain Network Analysis*. Academic Press, 2016.
- [37] J. Gonzalez-Castillo, C. W. Hoy, D. A. Handwerker, M. E. Robinson, L. C. Buchanan, Z. S. Saad, and P. A. Bandettini. Tracking ongoing cognition in individuals using brief, whole-brain functional connectivity patterns. *Proc. Natl. Acad. Sci. U.S.A.*, 112(28):8762–8767, Jul 2015.
- [38] E. M. Gordon, T. O. Laumann, B. Adeyemo, J. F. Huckins, W. M. Kelley, and S. E. Petersen. Generation and Evaluation of a Cortical Area Parcellation from Resting-State Correlations. *Cereb. Cortex*, 26(1):288–303, Jan 2016.
- [39] E. M. Gordon, T. O. Laumann, B. Adeyemo, and S. E. Petersen. Individual Variability of the System-Level Organization of the Human Brain. *Cereb. Cortex*, 27(1):386–399, 01 2017.
- [40] Liang Han, Neil K Savalia, Micaela Y Chan, Phillip F Agres, Anupama S Nair, and Gagan S Wig. Functional parcellation of the cerebral cortex across the human adult lifespan. *Cerebral Cortex*, 28(12):4403–4423, 10 2018.
- [41] Samuel J. Harrison, Janine D. Bijsterbosch, Andrew R. Segerdahl, Sean P. Fitzgibbon, Seyedeh-Rezvan Farahibozorg, Eugene P. Duff, Stephen M. Smith, and Mark W. Woolrich. Modelling subject variability in the spatial and temporal characteristics of functional modes. *NeuroImage*, 222:117226, 2020.
- [42] HCP. Hcp data releases, 2012-2015. <http://www.humanconnectome.org/>, Accessed on July 12, 2016.
- [43] R Matthew Hutchison, Thilo Womelsdorf, Elena A Allen, Peter A Bandettini, Vince D Calhoun, Maurizio Corbetta, Stefania Della Penna, Jeff H Duyn, Gary H Glover, Javier Gonzalez-Castillo, et al. Dynamic functional connectivity: promise, issues, and interpretations. *Neuroimage*, 80:360–378, 2013.
- [44] A. Iraj, T. P. Deramus, N. Lewis, M. Yaesoubi, J. M. Stephen, E. Erhardt, A. Belger, J. M. Ford, S. McEwen, D. H. Mathalon, B. A. Mueller, G. D. Pearlson, S. G. Potkin, A. Preda, J. A. Turner, J. G. Vaidya, T. G. M. van Erp, and V. D. Calhoun. The spatial chronnectome reveals a dynamic interplay between functional segregation and integration. *Hum Brain Mapp*, 40(10):3058–3077, 07 2019.
- [45] Estrid Jakobsen, Joachim Boettger, Pierre Bellec, Stefan Geyer, Rudolf Ruebsamen, Michael Petrides, and Daniel S Margulies. Subdivision of broca’s region based on individual-level functional connectivity. *European Journal of Neuroscience*, 43(4):561–571, 2016.
- [46] S. R. Jilka, G. Scott, T. Ham, A. Pickering, V. Bonnelle, R. M. Braga, R. Leech, and D. J. Sharp. Damage to the Salience Network and interactions with the Default Mode Network. *J. Neurosci.*, 34(33):10798–10807, Aug 2014.
- [47] Michio Kaku. *The future of the mind: The scientific quest to understand, enhance, and empower the mind*. Doubleday, 2014.

- [48] S. Katyal, Clint Greene, and D. Ress. High-resolution functional magnetic resonance imaging methods for human midbrain. *Journal of visualized experiments : JoVE*, 63:e3746, 2012.
- [49] R. Kong, J. Li, C. Orban, M. R. Sabuncu, H. Liu, A. Schaefer, N. Sun, X. N. Zuo, A. J. Holmes, S. B. Eickhoff, and B. T. T. Yeo. Spatial Topography of Individual-Specific Cortical Networks Predicts Human Cognition, Personality, and Emotion. *Cereb. Cortex*, 29(6):2533–2551, 06 2019.
- [50] O. Korhonen, H. Saarimaki, E. Glerean, M. Sams, and J. Saramaki. Consistency of Regions of Interest as nodes of fMRI functional brain networks. *Netw Neurosci*, 1(3):254–274, Oct 2017.
- [51] H. Kuhn. The hungarian method for the assignment problem. *Naval Research Logistic Quarterly*, 2, 05 2012.
- [52] C. Lanczos. Evaluation of Noisy Data. *Journal of the Society for Industrial and Applied Mathematics Series B Numerical Analysis*, (1):76–85, 1964.
- [53] R. Leech and D. J. Sharp. The role of the posterior cingulate cortex in cognition and disease. *Brain*, 137(Pt 1):12–32, Jan 2014.
- [54] J. Liu, X. Liao, M. Xia, and Y. He. Chronnectome fingerprinting: Identifying individuals and predicting higher cognitive functions using dynamic brain connectivity patterns. *Hum Brain Mapp*, 39(2):902–915, 02 2018.
- [55] X. Liu and J. H. Duyn. Time-varying functional network information extracted from brief instances of spontaneous brain activity. *Proc. Natl. Acad. Sci. U.S.A.*, 110(11):4392–4397, Mar 2013.
- [56] J. MacQueen. Some methods for classification and analysis of multivariate observations. In *Proceedings of the Fifth Berkeley Symposium on Mathematical Statistics and Probability, Volume 1: Statistics*, pages 281–297, Berkeley, Calif., 1967. University of California Press.
- [57] D. S. Margulies, S. S. Ghosh, A. Goulas, M. Falkiewicz, J. M. Huntenburg, G. Langs, G. Bezgin, S. B. Eickhoff, F. X. Castellanos, M. Petrides, E. Jefferies, and J. Smallwood. Situating the default-mode network along a principal gradient of macroscale cortical organization. *Proc. Natl. Acad. Sci. U.S.A.*, 113(44):12574–12579, 11 2016.
- [58] Daniel S Margulies, Justin L Vincent, Clare Kelly, Gabriele Lohmann, Lucina Q Uddin, Bharat B Biswal, Arno Villringer, F Xavier Castellanos, Michael P Milham, and Michael Petrides. Precuneus shares intrinsic functional architecture in humans and monkeys. *Proceedings of the National Academy of Sciences*, 106(47):20069–20074, 2009.
- [59] M. J. McKeown and T. J. Sejnowski. Independent component analysis of fMRI data: examining the assumptions. *Hum Brain Mapp*, 6(5-6):368–372, 1998.
- [60] V. Menon and L. Q. Uddin. Saliency, switching, attention and control: a network model of insula function. *Brain Struct Funct*, 214(5-6):655–667, Jun 2010.
- [61] S. A. Nastase, V. Gazzola, U. Hasson, and C. Keysers. Measuring shared responses across subjects using intersubject correlation. *Soc Cogn Affect Neurosci*, 14(6):667–685, 08 2019.
- [62] Fabian Pedregosa, Gaël Varoquaux, Alexandre Gramfort, Vincent Michel, Bertrand Thirion, Olivier Grisel, Mathieu Blondel, Peter Prettenhofer, Ron Weiss, Vincent Dubourg, Jake Vanderplas, Alexandre Passos, David Cournapeau, Matthieu Brucher, Matthieu Perrot, and Édouard Duchesnay. Scikit-learn: Machine learning in python. *J. Mach. Learn. Res.*, 12(null):2825–2830, November 2011.
- [63] J. D. Power, K. A. Barnes, A. Z. Snyder, B. L. Schlaggar, and S. E. Petersen. Spurious but systematic correlations in functional connectivity MRI networks arise from subject motion. *Neuroimage*, 59(3):2142–2154, Feb 2012.

- [64] J. M. Reinen, O. Y. Chen, R. M. Hutchison, B. T. T. Yeo, K. M. Anderson, M. R. Sabuncu, J. L. Roffman, J. W. Smoller, J. T. Baker, and A. J. Holmes. The human cortex possesses a reconfigurable dynamic network architecture that is disrupted in psychosis. *Nat Commun*, 9(1):1157, 03 2018.
- [65] U. Sakoglu, G. D. Pearlson, K. A. Kiehl, Y. M. Wang, A. M. Michael, and V. D. Calhoun. A method for evaluating dynamic functional network connectivity and task-modulation: application to schizophrenia. *MAGMA*, 23(5-6):351–366, Dec 2010.
- [66] Roser Sala-Llonch, Stephen M. Smith, Mark Woolrich, and Eugene P. Duff. Spatial parcellations, spectral filtering, and connectivity measures in fmri: Optimizing for discrimination. *Human Brain Mapping*, 40(2):407–419, 2019.
- [67] Mehroo Salehi, Abigail S. Greene, Amin Karbasi, Xilin Shen, Dustin Scheinost, and R. Todd Constable. There is no single functional atlas even for a single individual: Functional parcel definitions change with task. *NeuroImage*, 208:116366, 2020.
- [68] Mehroo Salehi, Abigail S. Greene, Amin Karbasi, Xilin Shen, Dustin Scheinost, and R. Todd Constable. There is no single functional atlas even for a single individual: Functional parcel definitions change with task. *NeuroImage*, 208:116366, 2020.
- [69] S. M. Smith, K. L. Miller, S. Moeller, J. Xu, E. J. Auerbach, M. W. Woolrich, C. F. Beckmann, M. Jenkinson, J. Andersson, M. F. Glasser, D. C. Van Essen, D. A. Feinberg, E. S. Yacoub, and K. Ugurbil. Temporally-independent functional modes of spontaneous brain activity. *Proc. Natl. Acad. Sci. U.S.A.*, 109(8):3131–3136, Feb 2012.
- [70] Sphinx. Nilearn, 2010-2015. <http://nilearn.github.io/>, Accessed on July 29, 2016.
- [71] Olaf Sporns. *Networks of the Brain*. MIT press, 2010.
- [72] Olaf Sporns. *Discovering the human connectome*. MIT press, 2012.
- [73] C. Sripada, M. Angstadt, S. Rutherford, D. Kessler, Y. Kim, M. Yee, and E. Levina. Basic Units of Inter-Individual Variation in Resting State Connectomes. *Sci Rep*, 9(1):1900, 02 2019.
- [74] Bertrand Thirion, Gaël Varoquaux, Elvis Dohmatob, and Jean-Baptiste Poline. Which fmri clustering gives good brain parcellations? *Frontiers in neuroscience*, 8(167):13, 2014.
- [75] ucsf. Federal government expenditures and number of affected people with alzheimer’s disease, 2009. <https://ind.ucsf.edu/>, Accessed on July 09, 2016.
- [76] Sebastian Urchs, Jonathan Armoza, Yassine Benhajali, Jolène St-Aubin, Pierre Orban, and Pierre Bellec. Mist: A multi-resolution parcellation of functional brain networks. *MNI Open Research*, 1:3, 12 2017.
- [77] John Darrell Van Horn and Arthur W Toga. Human neuroimaging as a ‘big data’ science. *Brain imaging and behavior*, 2014.
- [78] Zhanxiong Wu, Dong Xu, Thomas Potter, Yingchun Zhang, and The Alzheimer’s Disease Neuroimaging Initiative . Effects of brain parcellation on the characterization of topological deterioration in alzheimer’s disease. *Frontiers in Aging Neuroscience*, 11:113, 2019.
- [79] M. Yaesoubi, T. Adal, and V. D. Calhoun. A window-less approach for capturing time-varying connectivity in fMRI data reveals the presence of states with variable rates of change. *Hum Brain Mapp*, 39(4):1626–1636, 04 2018.
- [80] T. Yarkoni, R. A. Poldrack, T. E. Nichols, D. C. Van Essen, and T. D. Wager. Large-scale automated synthesis of human functional neuroimaging data. *Nat. Methods*, 8(8):665–670, Jun 2011.
- [81] B. T. Yeo, F. M. Krienen, M. W. Chee, and R. L. Buckner. Estimates of segregation and overlap of functional connectivity networks in the human cerebral cortex. *Neuroimage*, 88:212–227, 03 2014.

- [82] BT Thomas Yeo, Fenna M Krienen, Jorge Sepulcre, Mert R Sabuncu, Danial Lashkari, Marisa Hollinshead, Joshua L Roffman, Jordan W Smoller, Lilla Zöllei, Jonathan R Polimeni, et al. The organization of the human cerebral cortex estimated by intrinsic functional connectivity. *Journal of neurophysiology*, 106(3):1125–1165, 2011.
- [83] Q. Yu, Y. Du, J. Chen, H. He, J. Sui, G. Pearlson, and V. D. Calhoun. Comparing brain graphs in which nodes are regions of interest or independent components: A simulation study. *J. Neurosci. Methods*, 291:61–68, 11 2017.
- [84] X. N. Zuo, C. Kelly, J. S. Adelstein, D. F. Klein, F. X. Castellanos, and M. P. Milham. Reliable intrinsic connectivity networks: test-retest evaluation using ICA and dual regression approach. *Neuroimage*, 49(3):2163–2177, Feb 2010.